

TALLINN UNIVERSITY OF TECHNOLOGY  
DOCTORAL THESIS  
60/2019

# **Adaptive Wear Mechanisms of Diamond Coatings at Room and Elevated Temperatures**

MAXIM YASHIN



TALLINN UNIVERSITY OF TECHNOLOGY

School of Engineering

Department of Mechanical and Industrial Engineering

This dissertation was accepted for the defence of the degree 15/10/2019

**Supervisor:**

Senior Research Scientist Vitali Podgurski  
School of Engineering  
Tallinn University of Technology  
Tallinn, Estonia

**Opponents:**

Assoc. Prof František Lofaj  
Department of Ceramics  
Institute of Materials Research of SAS, Slovakia

Senior Research Scientist Sergei Vlassov  
Material Science  
Laboratory of Low Temperatures  
University of Tartu, Estonia

**Defence of the thesis:** 17/12/2019, Tallinn

**Declaration:**

Hereby I declare that this doctoral thesis, my original investigation and achievement, submitted for the doctoral degree at Tallinn University of Technology has not been submitted for doctoral or equivalent academic degree.

Maxim Yashin

-----  
signature



European Union  
European Regional  
Development Fund



Investing  
in your future

Copyright: Maxim Yashin, 2019

ISSN 2585-6898 (publication)

ISBN 978-9949-83-496-9 (publication)

ISSN 2585-6901 (PDF)

ISBN 978-9949-83-497-6 (PDF)

TALLINNA TEHNIKAÜLIKOOL  
DOKTORITÖÖ  
60/2019

**Teemantpinnete adaptiivkulumise  
mehhanismid toa- ja kõrgendatud  
temperatuuridel**

MAXIM YASHIN

**TAL  
TECH**  
KIRJASTUS



# Contents

List of Publications .....	6
Author's Contribution to the Publications .....	7
Other author's publications .....	8
Introduction .....	9
Abbreviations .....	10
Symbols .....	11
1 Theoretical background .....	12
1.1 Properties and application of diamond.....	12
1.2 Classification of diamond coatings.....	13
1.3 Tribological mechanisms of the wear of diamond coatings.....	14
1.3.1 Surface roughness.....	14
1.3.2 Tribological layer .....	14
1.3.3 Ripple patterns.....	17
1.3.4 Plastic deformation within coating/substrate system .....	17
1.4 Goals of thesis .....	19
2 Materials and methods .....	21
2.1 Method of deposition of diamond coatings.....	21
2.2 Sliding tests .....	23
2.3 Methods of structural study .....	23
3 Results and discussion.....	25
3.1 Structure of the investigated diamond coatings and DLC.....	25
3.2 Wear behavior of diamond coatings.....	30
3.2.1 Theory of self-organization for diamond coating/ substrate tribological system..	30
3.2.2 Self-organization and wear types of diamond coating .....	33
3.2.3 Analysis of tribological behavior of NCD-1 and NCD-2 coatings .....	35
3.2.4 Investigation of deflection of diamond coatings.....	43
3.2.5 Analysis of tribological behavior of diamond coatings at high temperature .....	49
3.2.6 Protection of diamond coatings against oxidation attack at high temperature ....	53
3.2.7 Summary of comparison of tribology behavior of MCD, NCD and DLC coatings...	53
4 Conclusions .....	55
References .....	57
Acknowledgements.....	64
Abstract.....	65
Lühikokkuvõte.....	66
Appendix .....	67
Curriculum vitae.....	108
Elulookirjeldus.....	109

## List of Publications

The list of author's publications, on the basis of which the thesis has been prepared:

- Publication I. V. Podgursky; A. Bogatov; **M. Yashin**; S. Sobolev; J. S. Gershman, Relation between Self-Organization and Wear Mechanisms of Diamond Films. *Entropy*, 2018, 20 (4), 279-295.
- Publication II. **M. Yashin**; A. Bogatov; V. Podgurski, Comparative Analysis of Wear Rates of Microcrystalline Diamond and Diamond-Like Carbon Coatings Deposited on WC-Co Substrates. *Key Engineering Materials*, 2016, 721, 436–440.
- Publication III. V. Podgursky; A. Bogatov; **M. Yashin**; M. Viljus; A. P. Bolshakov; V. Sedov; O. Volobujeva; A. Mere; T. Raadik; V. Ralchenko, A comparative study of the growth dynamics and tribological properties of nanocrystalline diamond films deposited on the (110) single crystal diamond and Si (100) substrates. *Diamond and Related Materials*, 2019, 92, 159–167.
- Publication IV. **M. Yashin**; J. Baronins; P. Menezes; M. Viljus; T. Raadik; A. Bogatov; M. Antonov; V. Podgursky, Wear Rate of Nanocrystalline Diamond Coating under High Temperature Sliding Conditions. *Solid State Phenomena*, 2017, 267, 219–223.
- Publication V. Invention: Method to protect diamond films at high temperature to preserve tribological properties; Owners: Tallinn University of Technology, University of Tartu; Authors: V. Podgurski; A. Bogatov; **M. Yashin**; H. Vagiström; T. Jõgiaas, Priority number: P201900008; Priority date: 26.02.2019.

## **Author's Contribution to the Publications**

Contribution to the papers in this thesis is:

- Publication I. Co-author. Providing sliding tests, profilometer and SEM measuring, processing of data, calculations.
- Publication II. Main author. Providing sliding tests, profilometer and SEM measuring, processing of data, calculations, writing of text.
- Publication III. Co-author. Providing sliding tests, profilometer and SEM measuring, processing of data, calculations.
- Publication IV. Main author. Providing sliding tests, profilometer and SEM measuring, processing of data, calculations, writing of text.
- Publication V. Co-author. Providing sliding tests, profilometer and SEM measuring, processing of data, calculations.

## Other author's publications

List of author's publications, not included into the thesis:

- Publication I. A. Bogatov; M. Yashin; M. Viljus; P. Menezes; V. Podgursky, Comparative Analysis of Two Methods for Evaluating Wear Rate of Nanocrystalline Diamond Films. *Key Engineering Materials*, 2016, 721, 345–350.
- Publication II. A. Alamgir; A. Bogatov; M. Yashin; V. Podgursky, Mechanical and tribological properties of 100-nm thick alumina films prepared by atomic layer deposition on Si (100) substrates. *Proceedings of the Estonian Academy of Sciences*, 2019, 68 (2), 126–130.

## Introduction

Synthetic diamond was developed in the second half of the twentieth century. The developments in the deposition methods have contributed to applications of diamond coatings in the industry. Nowadays, thin diamond coatings have a wide range of applications. These coatings can be used in the manufacture of scratch-resistant optical lenses, highly loaded engine parts, microelectromechanical systems, etc. Due to high hardness and Young's modulus of diamond, one of the main tribological applications of diamond coatings is protection of cutting tools against wear [1].

Understanding of the mechanisms of wear of diamond coatings is necessary for improvements in the wear resistance of coatings. In previous studies, several characteristic types of the coefficient of friction (CoF) vs cycle curves were addressed during sliding [2, 3]. Formation of a carbonaceous layer, ripple and groove patterns were found within the wear scar [2, 4, 5], which indicates self-organization during friction. Self-organization is a process of formation of spatial, temporal, or functional structures due to the transformations of the nonequilibrium phase in an open system [6]. In previous studies, deflection of a diamond coating deposited on a silicon substrate was reported [3]. Coating deflection is a plastic deformation of the whole coating/substrate system during sliding.

Department of Mechanical and Industrial Engineering of Tallinn University of Technology has long-term experience in hard coating technologies, including preparation of different types of diamond coatings. The present PhD study is furthering previous research in the field of tribological properties of diamond coatings. The PhD thesis investigates the tribological behavior of different types of diamond films against a ceramic counterbody at room and high temperatures. Understanding of adaptive wear mechanisms of diamond coatings at room and elevated temperatures is the main goal of the thesis.

The results of the work are interpreted from the point of view of self-organization, and influence of the substrate properties, crystal structure of coatings and the temperature.

Scientific novelties of the PhD thesis:

- 1) Adhesive and abrasive wear of diamond coatings are explained as a consequence of self-organization.
- 2) Superlubricity on the NCD and MCD coatings tested at 300 °C was found for the first time.
- 3) Method of protection and preservation of the tribological properties of diamond coatings against oxidation at high temperature by deposition of an Al<sub>2</sub>O<sub>3</sub> layer on top of the diamond coating has been developed.

Results of the present doctoral study have been published in four scientific journals and one invention was submitted. The results were presented at two international conferences: 25th International Baltic Conference of Engineering Materials & Tribology 2016, 3 - 4th November, 2016, Riga, Latvia and 26th International Baltic Conference Materials Engineering 2017, 26 - 27 October, 2017, Kaunas, Lithuania.

## Abbreviations

AFM	Atomic Force Microscopy
CoF	Coefficient of Friction
CVD	Chemical Vapor Deposition
DLC	Diamond-Like Carbon
HFCVD	Hot Filament Chemical Vapor Deposition
HPHT	High Pressure High Temperature
HT	High Temperature
MCD	MicroCrystalline Diamond
MWPECVD	Microwave Plasma Enhanced Chemical Vapor Deposition
NCD	NanoCrystalline Diamond
N-V center	Nitrogen Vacancy center
PCD	PolyCrystalline Diamond
Recip.	Reciprocating
Ref.	Reference
Rotat.	Rotating
RT	Room Temperature
SCD	Single-Crystal Diamond
SEM	Scanning Electron Microscopy
UMT	Universal Material Tester
UNCD	Ultra-nanocrystalline diamond
XRD	X-ray diffraction

## Symbols

$R_a$	Average surface roughness [ $\mu\text{m}$ ]
$Y$	Probability of loss of thermodynamic stability
$n$	Number of interrelated process in tribosystem
$F_f$	Friction force [N]
$\mu$	Coefficient of friction
$F$	Normal load [N]
$p_{\text{max}}$	Contact pressure [GPa]
$R$	Radius of $\text{Si}_3\text{N}_4$ ball [mm]
$E$	Young's modulus [GPa]
$\nu$	Poisson's ratio
$J$	Thermodynamic flow [mol/L·s]
$A$	Real contact area [ $\mu\text{m}^2$ ]
$S$	Entropy [J/K]
$N$	Duration [Cycles]
$T$	Temperature [ $^{\circ}\text{C}$ ]
$\lambda$	Heat conductivity [W/m·K]
$X$	Thermodynamic force [J/mol·K]
$V$	Velocity of sliding test [RPM]
$r$	Radios of wear scar [mm]
$l$	Length of wear scar [ $\mu\text{m}$ ]
$S_s$	Cross-section area of wear scar [ $\mu\text{m}^2$ ]
$V_s$	Volume of wear scar [ $\text{mm}^3$ ]
$S_{\text{dr}}$	Surface area ratio [%]

# 1 Theoretical background

Diamond is an allotrope of carbon. The word 'diamond' is derived from the ancient Greek word  $\alpha\delta\acute{\alpha}\mu\alpha\varsigma$  (*adámās*), "unbreakable" [7]. Diamond is the hardest known natural mineral in the Mohs scale [8]. Diamond is the metastable form of carbon which transforms into graphite with time. Carbon  $C^{12}_6$  is the element of the fourth group of the Periodic System. It has the electronic configuration of external orbitals  $2s^2 2p^2$  (Fig. 1). Carbon atoms are in the state of  $sp^3$ -hybridization in diamond. Four new  $sp^3$ -hybrid orbitals are formed due to the hybridization of one 2s-orbital and three 2p-orbitals (See Excited state). The hybrid orbitals are angled at  $109.5^\circ$  to each other and directed to the vertexes of the tetrahedron formed by carbon atoms. Carbon atoms in diamond are bound with strong covalent bonds. These types of bonding of carbon atoms explain the high hardness of diamond [9].

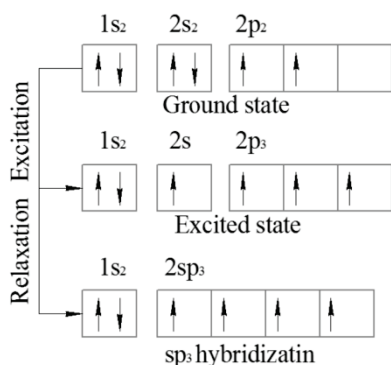


Figure 1. Scheme of hybridization of carbon [10].

## 1.1 Properties and application of diamond

Diamond possesses excellent properties due to specific crystal structure. Because of the material's exceptional properties, diamond has a wide range of applications. The properties of diamond are listed in Table 1.

The main distinguishing features of diamond are the highest hardness among materials [11]. High hardness causes exceptional wear resistance of diamond to abrasion. Diamond has a very low coefficient of friction to metal in the air. This is because of the formation of a thin carbonaceous tribolayer on the surface of diamond. The highest modulus of elasticity and the lowest compression ratio are characteristics of diamond.

Due to high hardness, diamond coatings are used to protect cutting tools: cutting inserts, twist drills, square end and ball nose end mills [12] used for machining of copper and aluminum alloys and composite materials. Besides that, diamond coatings are used for improving wear resistance of surgical instruments, for example, dental burs [13].

Pure diamond has very high thermal conductivity at room temperature [14]. This property makes it possible to use diamond as heat sink for high-power laser diodes and high-power transistors.

Diamond as a chemically inert material does not interact with the strongest acids and alkalis. Diamond oxidation does not occur in air at room conditions [15]. Biocompatibility allows the use of diamond in the manufacture of coatings on implants.

Diamond doped with boron or phosphorus is a wide-gap semiconductor [16]. High charge-carrier mobility and breakdown field strength are the characteristics of diamond [17]. The use of diamond as an active element of microelectronics, especially in high-current and high-voltage electronics, is a promising future trend [18].

A nitrogen-vacancy center (N-V center) is a type of the defect in diamond structure. A diamond-based quantum computer was developed using the N-V centers [19]. In addition, N-V centers can be used in scanning thermal microscopy [20].

Diamond has a wide optical transmission range [21]. This property enable use of diamond as window material for transmitting infrared and microwave radiation. Therefore, diamond coatings are used in the manufacture of windows for outputting radiation from high-power gyrotrons and lasers [22].

Table 1. Properties of diamond [11, 14, 16].

Properties	Unit	Value
Knoop Hardness	GPa	113
Young's Modulus	GPa	1053
Bulk modulus	GPa	442
Shear modulus	Gpa	574
Poisson's ratio		0.1
Anisotropic ratio		1.21
Density	g/cm <sup>3</sup>	3.52
Thermal Conductivity	W/m·K	900 – 2300
Thermal expansion coefficient	10 <sup>-6</sup> K <sup>-1</sup>	0.8
Debay temperature	K	1200
Resistivity	Ω·cm	10 <sup>13</sup> – 10 <sup>15</sup>
Dielectric constant		5.7

## 1.2 Classification of diamond coatings

Application of single-crystal diamond (SCD) in industry is complicated and expensive. An alternative is the production of synthetic diamond. Diamond coatings can be grown by chemical vapor deposition (CVD) methods on different substrates (WC-Co, steel, Si, etc.). These coatings have a wide range of tribological applications due to their low coefficient of friction (CoF), high hardness and Young's modulus, and chemical inertness [23].

Diamond coatings can be divided into two types, i.e., SCD and polycrystalline diamond (PCD). PCD, unlike SCD, consists of crystallite grains. Properties of the PCD coating strongly depend on diamond grain size, which is an important characteristic of diamond films. PCD coatings can be classified as microcrystalline diamond (MCD), nanocrystalline diamond (NCD) and ultra-nanocrystalline diamond (UNCD) coatings [24]. The size of the diamond grains determines the surface roughness of the diamond coating. MCD coatings possess high surface roughness. High wear of the counterbody against MCD films is observed during friction. MCD coatings consist of columnar grains and show significant anisotropy properties in different directions. Properties of PCD coatings are shown in Table 2. The size of diamond grains for specific coating can vary, for instance, in the case of MCD coating, the grain size is about 2 μm, see Ref. [25]. The surface roughness of NCD and UNCD coatings is significantly lower than that of MCD coatings, because these coatings have smaller grain size [26].

Unlike diamond coatings, DLC coatings have amorphous structure. DLC is a mixture of sp<sup>3</sup> and sp<sup>2</sup> carbon bonds, the surface of DLC coatings is smoother in contrast to diamond

coatings [27]. The present study focuses mainly on the investigation of the properties of the diamond coatings.

Table 2. Classification of diamond coatings [26].

Polycrystalline Diamond (PCD)	Grain size	Surface roughness	Electronic bonding
Microcrystalline diamond (MCD)	0.5 – 10 $\mu\text{m}$	0.4 – 1 $\mu\text{m}$	$\text{sp}^3$
Nanocrystalline diamond (NCD)	50 – 100 nm	50 – 100 nm	$\text{sp}^3$ + up to 50% $\text{sp}^2$
Ultra-nanocrystalline diamond (UNCD)	2 – 5 nm	20 – 40 nm	$\text{sp}^3$ + 2 – 5% $\text{sp}^2$

### 1.3 Tribological mechanisms of the wear of diamond coatings

Tribological application of diamond coatings related with friction and wear of these coatings under different conditions. Surface roughness, formation of tribological layer, environmental conditions, temperature, etc. have significant influence on the tribological behavior of diamond coatings. Investigation of these mechanisms is necessary to deeper understanding of friction and wear of diamond coatings.

#### 1.3.1 Surface roughness

Surface roughness is an important factor influencing the wear of diamond coatings. The fragmentation of diamond coatings occurs due to the contact between the irregularities of the counterbodies during sliding. The formed particles lead to micro-plowing of the surface [28]. In other words, self-polishing of the surface of the diamond coating occurs. Previous studies show that with decreasing roughness of the surface of the diamond coating, the CoF and the running-in period are reduced [29]. The size of the diamond grains and their orientation have influence on the surface roughness. For example, while the diamond coatings with [100] growth orientation have flat surface and show lower CoF during friction, diamond coatings with [111] texture have pyramidal shape of diamond grains [30]. Asperity interlocking and breaking and micro-ploughing occur at high roughness ( $R_a = 0.1 - 1 \mu\text{m}$ ) of coatings, i.e., for MCD and partially for NCD coatings. Diamond coatings with  $R_a = 0.01 - 0.1 \mu\text{m}$  show transformation  $\text{sp}^3 \rightarrow \text{sp}^2$  in sliding under high contact pressure and elevated temperatures [31].

#### 1.3.2 Tribological layer

A CoF value in the sliding test on diamond coatings against a number of materials is low [32, 33]. A thin tribolayer forms on the coating surface, which plays a role of a solid lubricant and decreases the wear. Gradual phase transformation of diamond in graphite causes formation of a tribolayer [33, 34, 35]. Thickness of the tribolayer formed on the surface of the coating is about 10 – 100 nm [36, 37]. The necessary conditions for the formation of a tribolayer assume energy transfer into the contact area between the counterbodies to generate  $\text{sp}^3 \rightarrow \text{sp}^2$  transformation. It is estimated that more than 90% of all the energy due to friction is located within the surface film [38]; this energy can be consumed to the formation of a tribolayer as well as to the wear.

## **Graphitization**

Graphitization of diamond coatings is the transformation of diamond into graphite  $sp^3 \rightarrow sp^2$ . This is a polymorphic transition, i.e., phase transition between different crystal structures of single chemical composition and involves extensive internal rearrangement and reconstruction of the crystal, which requires high quantity of energy [39]. Chemical analyses have shown that significant graphitization occurs after heating of single crystal diamond at 1600 °C in vacuum [40]. Diamond transforms completely to graphite when heated at about 2000 °C [40, 41]. Depending on the crystal size and crystallinity, oxidation of diamond coatings begins after heating to > 450-550 °C [42, 43, 44]. It is worth noting that graphite oxidation temperature is about 450 °C [45]. The graphitization temperature of carbon-related material coatings is about 200 °C for amorphous carbon coatings and 300 °C for DLC coatings [46].

Graphitization can occur during friction. Investigations by Raman spectra and TEM have revealed that a thin graphite layer is formed in the area of the wear scar [47]. It can be explained by the transformation of diamond to graphite under deformation [48] and HT during sliding [28]. Formation of a graphite layer can lead to a decrease of the CoF and the wear rate [28].

## **Graphitization and anisotropy of properties of diamond coatings**

Wear of single crystal diamond is anisotropic because wear depends on the crystallographic direction in diamond. There are «soft» and «hard» directions of polishing of monocrystalline diamond. High wear loss volume is observed in the «soft» direction under sliding wear [49]. Amorphous  $sp^2$  form of carbon was found in the wear scars formed along the «soft» directions. Noise, heat generation and low vibrations occur during sliding along «soft» directions [50]. Poisson's ratio is high in «soft» directions. Relatively high expansion corresponds to the bending of chemical bonds. Stretching and compressing of bonds require more energy than bending. Rehybridization from  $sp^3$  to  $sp^2$  occurs by bending of the bond during the sliding in «soft» directions. In other words, less energy is required to process rehybridization [51]. Diamond has greater wear resistance in «hard» directions [49]. Particles with  $sp^3$  bonding of carbon were observed in the wear scar after polishing in «hard» directions. It means that the fracture of the diamond occurs during friction. Large vibrations and little emitted heat were found when sliding in «hard» directions [50]. A large quantity of energy is required for stretching and compressing the bonds. The Poisson's ratio is smaller than for the «soft» directions [51].

## **Influence of high temperature on friction behavior**

Because there is shortage of data on the tribological behavior of diamond films at high temperature [52, 53, 54, 55, 56], it is constructive to consider the DLC behavior at HT as well. Namely, at 100 – 300 °C and at 600 °C, superlubricating behavior (super low CoF) was observed ( $\mu = 0.008 - 0.067$ ). In the case of the tests at 100 – 300 °C, it is explained by graphitization of the DLC coating surface due to influence of HT and high contact pressure [52]. On the other hand, at 600 °C the formation of self-generated composite oxide on the contact surface occurred, i.e. at this temperature, the low lubrication cannot be explained only by the properties of DLC [52]. Between 300 – 500 °C, the CoF was high ( $\mu = 0.3 - 0.54$ ) and at 700 °C,  $\mu = 0.45$  in the early period of sliding and after 20 min, the DLC was worn out rapidly [52]. It can be concluded that the DLC coating is stable and has good tribological properties at 100 – 300 °C or at special condition (e.g., as a result of composite oxide formation). However, with the temperature increasing, the DLC coating becomes unstable and can be worn out due to oxidation.

At the increase of the temperature, oxidation of the diamond coating surface increases, the CoF increases and tribological behavior becomes unstable. After 600 °C, surface oxidation occurs on the diamond coating [53, 54]. Results of the sliding test against SiC show an increase in  $sp^2$  bonds and degradation of tribological behavior of diamond coatings after heating to 400 °C [55].

However, diamond properties to resist oxidation at HT can be improved, for instance, by alloying with boron [56].

The fundamental drawback of carbon based coatings used in industry is the oxidation at HT under ambient conditions, which strongly reduces the applicability of these materials at elevated temperature.

### Environmental conditions

Tribological behavior of diamond coatings strongly depends on the environment, namely relative humidity plays a key role in sliding. The CoF and the loss volume wear of diamond coatings have low values in the sliding wear under room conditions. However, it increases several times with a decrease in the relative humidity or in vacuum [35, 57]. It is believed that this is due to the formation of a tribolayer on the surface of the diamond coatings. This layer is formed as a result of passivation of dangling bonds of carbon atoms with water particles and gases from the environment (hydrogen, oxygen etc.). Formation of the passivated layer leads to a decrease in the adhesion component of friction, and low CoF value can be observed during the sliding tests. The influence of passivation of dangling bonds can be confirmed by the sliding test in  $N_2$  medium [28, 58]. Results show that the loss wear volume on diamond coatings in open air is less than in dry  $N_2$ .

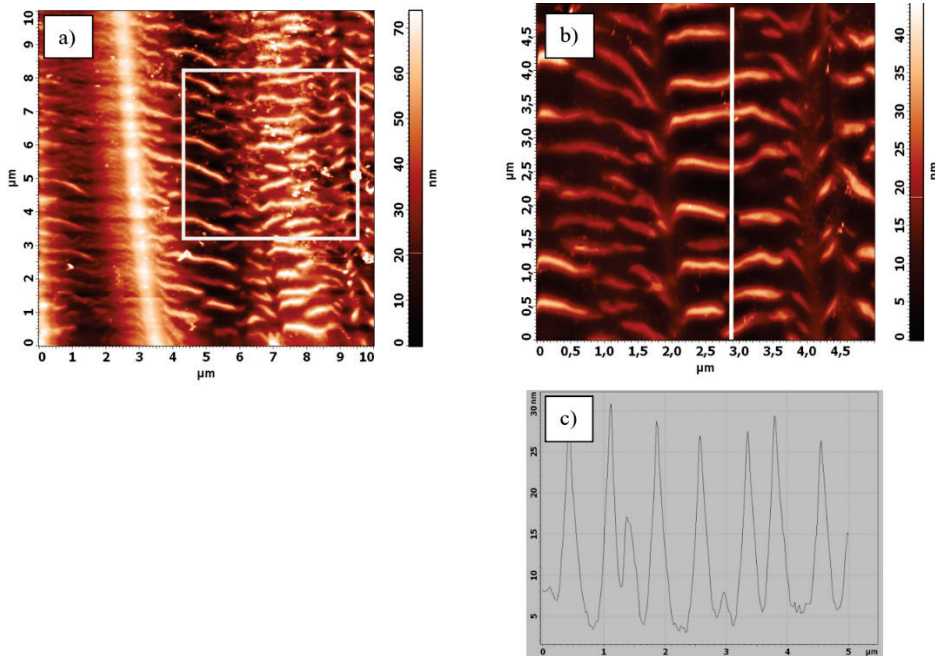


Figure 2. Examples of ripple patterns on the NCD coating after the wear tests at 2N, 5 Hz, 36000 cycles, AFM image of the bottom of the wear scar after sliding against  $\varnothing 3$  ZrO<sub>2</sub> ball (a and b), line scan of ripples (c) [4].

In conclusion, graphitization, passivation of dangling bonds, material of sliding counterbodies accumulating near the border of the wear scar and falling in the area of sliding [28, 58], and other factors can influence on the formation of the tribolayer. These processes occur during the entire sliding time. Because of complexity of the processes, the process of deterioration (wear) within the wear scar can differ at different stages of sliding.

### 1.3.3 Ripple patterns

Previous studies carried out in Tallinn University of Technology have found that ripple and groove patterns are formed within the wear scars after sliding tests on different types of diamond coatings [2, 5, 27, 4]. Examples of ripple patterns are shown in Fig. 2 a and b. Fig. 2 c shows the shape and size of ripples. Similar morphological structures were observed in other tribosystems on macro/micro/nano scales [59, 60, 61, 62].

It was suggested that ripple patterns are formed due to shear stresses between the counterbody and the diamond coating [4]. Frequency, load, sliding distance and duration can influence the morphology of ripple patterns [27, 2]. Formation of ripples and grooves is a dynamical process, for instance, density and size of ripples can vary during sliding [27].

Ripple and groove patterns are well-formed repeatable structures, indicating that self-organization takes place during sliding.

### 1.3.4 Plastic deformation within coating/substrate system

Wear, plastic and elastic deformations of coatings occur during sliding. Although studies of wear are widely discussed in the literature, the mechanisms of plastic and elastic deformation in the sliding wear have not been thoroughly investigated. The influence of substrate on the coating properties is an important aspect of coatings tribology. The load-carrying capacity of the film/substrate system is an ability to withstand pressure in the system without loss of the system functionality. Different types of coating/substrate systems are shown in Fig. 3.

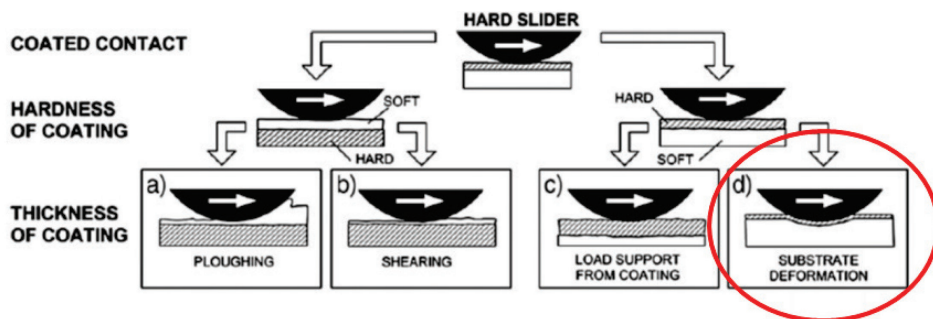


Figure 3. Schemes of coating/substrate systems [31].

Diamond is the hardest material, therefore in the case of diamond coating substrate, deformation can be expected during sliding (Fig. 3 d). One of the main goals of the present doctoral thesis is to estimate the influence of the plastic and elastic deformation on the wear and tribology behavior of diamond coatings under dry sliding for a hard/soft coating/substrate system.

### Coating deflection

Deflection of the coating was observed during the friction tests with different loads and durations on the NCD coating deposited on Si substrate in previous studies conducted in Tallinn University of Technology [3]. It was explained as a fatigue-induced evolution of the coating interface. Plastic and elastic deformation can be considered as an adaptation mechanism and therefore it is related to self-organization because it leads to a decrease in the contact pressure and thus the wear.

Elastic and plastic deformations within the substrate and coatings influence the friction and wear. The deflection is considered as a plastic and elastic deformation of the entire film under the contact zone between the diamond coating and the counterbody. It should be distinguished from the plastic and elastic deformation of the asperities of surface roughness [63]. This can occur when a load is applied to a thin hard coating deposited on a soft substrate. Diamond is harder in comparison to other substrate materials.

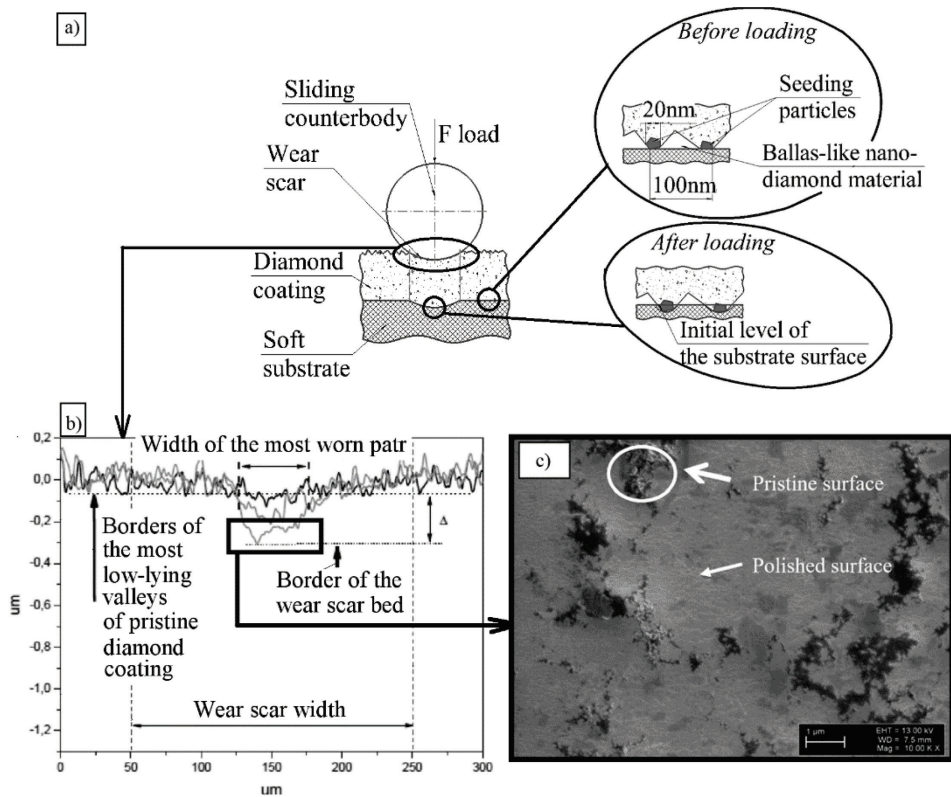


Figure 4. Scheme of diamond coating deflection (a, b), example of coating deflection on the NCD coating after 0.5 N load and 72000 cycles during the sliding test: line scans of the wear scar (c) and SEM image of the bottom of the wear scar (d) [3].

In addition, the conditions of the diamond coating deposition process cause plastic and elastic deformation. Namely, diamond particles are seeded on the surface of the substrate before deposition, at which the diamond coating growth begins. In tribological tests under the load, the hard seeding particles of diamond penetrate into the substrate,

as the small contact area between the seeding particles and the substrate can experience strong stress between the particles and the substrate. Figure 4 shows a scheme of diamond coating deflection. Diamond grains, hard seeding particles and ballas-like nano-diamond material were found in the interface of the diamond coating [64]. Change of the interface of the diamond coating after loading is shown in Fig. 4 (a). Depth of the top of irregularity in the bottom of the wear scar should be deeper than the border of the lower valley of surface roughness of the surface out of the wear scar (see Fig. 4 b). In addition, the morphology of the bottom of the wear scar should contain islands of pristine surface (Fig. 4 c) [3, 5].

The presence of coating deflection can also be proved by comparing the contact pressure of the seeding particle and the fracture strength of the substrate. If Hertz contact is suggested between the diamond coating and the counterbody, the maximum of contact pressure can be calculated. Figure 4 a shows the experimental set-up and the structure of the diamond coating. The load applied on the counterbody leads to loading of the seeding particles. The pressure between the seeding particles and the substrate can be calculated by the contact area. The distribution density of the seeding particles is about  $10^9 - 10^{10}$  particles/cm<sup>2</sup> or 1 particle per  $10^3 - 10^4$  nm<sup>2</sup> area [65]. According to other sources, nucleation densities are  $10^{11}$  particles/cm<sup>2</sup> [66]. The diameter of the single particle is about 20 nm [65]. This data allows the calculation of the contact area. For instance, contact pressure between the seeding particles and the Si substrate at 3 N normal load was calculated in a previous study [64]. Its value was 80 GPa at the distribution density of  $10^{10}$  particles/cm<sup>2</sup> and 8 GPa for the distribution density of  $10^{11}$  particles/cm<sup>2</sup> [64]. The obtained values of the contact pressure are higher than the fracture strength of Si (about 6.1 GPa [67]). Elastic deformations and local fracture of the Si substrate occur due to the high contact pressure on single seeding particles. It can result in coating deflection.

### **1.3.5 Summary on the wear mechanisms of diamond coatings**

Formation of ripple and groove patterns indicates that the self-organization takes place in diamond coating/ substrate tribosystem during sliding. Development of theoretical basis of self-organization for diamond coating/ substrate system is necessary to deeper understanding of adaptive wear mechanisms of diamond coatings. The phenomenon of diamond coating deflection was not thoroughly investigated in the past. Additional studies are crucial to investigate in more details deflection phenomenon, as well as to improve understanding the causes of deflection.

HT resistance is important factor for application of diamond coatings in industry. Thus, investigation of tribological behavior of diamond coatings at HT is of special interest. Diamond coatings become unstable due to oxidation, therefore the development of methods to protect diamond coatings against oxidation and preserve excellent tribological properties of diamond coatings at HT is necessary.

## **1.4 Goals of thesis**

The present thesis focuses on the tribological behavior of different types of diamond coatings in the sliding tests against ceramic counterbodies. Understanding of adaptive wear mechanisms of diamond coatings at room and elevated temperatures is the main goal of the thesis.

In the following section, the main goals are shown in more detail:

1. Achieve a comprehensive understanding of the mechanisms of friction and wear based on the self-organization theory and interpret the experimental results within the framework of the self-organization theory. Estimate the influence of surface morphology, surface roughness, real contact area between the counterbodies and the deflection of the diamond coating on the friction and wear mechanisms.
2. Achieve a deeper understanding of the influence of substrate properties on diamond coating deflection.
3. Achieve a deeper understanding of the influence of high temperature on the friction, wear and coating deflection of diamond coatings.
4. To develop a method for protection of diamond coatings against oxidation attack at high temperature and preserve excellent tribological properties of diamond coatings.

## 2 Materials and methods

### 2.1 Method of deposition of diamond coatings

Diamond coatings and DLC are usually produced by the chemical vapor deposition (CVD) method. The growth of a diamond coating is a complex multi-step process involving chemical reactions on the surface of the substrate [27]. There are two main conditions to grow diamond films by the CVD methods, namely using carbon and hydrogen containing gases ( $\text{CH}_4$ ,  $\text{C}_2\text{H}_2$ ,  $\text{H}_2$ , etc.). The activation of chemical reaction can involve thermal methods (e.g. HFCVD), electric discharge (e.g. DC, RF or MW), or a combustion flame (e.g. oxyacetylene torch). The substrate is heated above  $700 - 900\text{ }^\circ\text{C}$  to form diamond rather than amorphous carbon [68, 69].

Microwave plasma enhanced CVD (MWPECVD) is one of the most common methods of depositing diamond coatings (Fig. 5 a). This method is more expensive than the method of HFCVD. Microwave power is coupled into the chamber via dielectric quartz window in order to create a discharge. The dissociation of the gas mixture occurs under the influence of a gas-discharge plasma. Ions and active radicals are deposited on the surface of the substrate, which is immersed in the plasma [68, 70]. Commonly, microwave frequency of 2.45 GHz and power of up to 5 kW are used. Working pressure is 20 – 50 Torr, but for high power, MWPECVD pressure is 100-200 Torr [70]. The temperature of the substrate is  $900 - 1200\text{ }^\circ\text{C}$  [70]. Duration of deposition can reach for many hours. Plasma is formed immediately above the substrate. In such systems, the growth rate is well in excess of  $10\text{ }\mu\text{m}\cdot\text{h}^{-1}$  [68].

Another method of diamond coating deposition is the hot filament CVD (HFCVD) (Fig. 5 b). HF reactors use conditions approximately similar to the PECVD method. However, dissociation of the working gas occurs by HT of filament [68]. The pressure in the chamber is about 20 – 30 Torr. The substrate is heated by means of a heater to a temperature of  $700 - 900\text{ }^\circ\text{C}$ . The clearance between the filament and the substrate is a few millimetres. The filament is electrically heated to a temperature above  $2200\text{ }^\circ\text{C}$ . The filament is made of materials such as tungsten and tantalum that can stand high temperatures and not react with the working gas. The HFCVD method is relatively cheap and easy to operate. The deposition rate of a polycrystalline diamond film of acceptable quality is  $1 - 10\text{ }\mu\text{m}\cdot\text{h}^{-1}$  [68].

The samples for the present study were prepared on UPSA-100 (MWPECVD method). Maximum power of a microwave generator is 5 kW, frequency is 2.45 GHz. The working gas pressure in the chamber is 20 – 120 Torr and the substrate temperature  $700 - 1200\text{ }^\circ\text{C}$ .

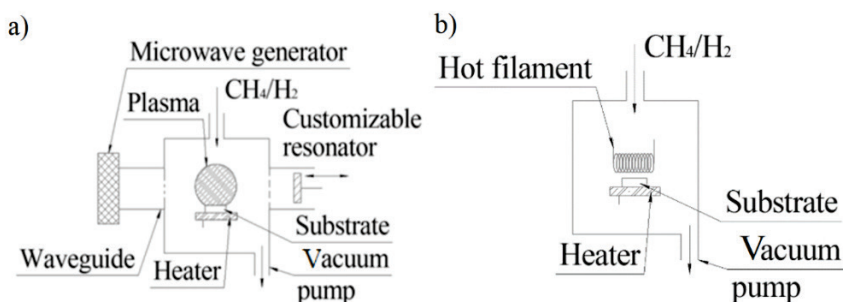


Figure 5. Scheme of the MWPECVD method (a) and the HFCVD method (b) [68].

Table 3. Types of the samples investigated in the present study [3, 64, 65].

Type of coating	NCD-1	NCD-2	NCD-3	NCD-4	MCD-1	MCD-2	DLC
Substrate	Si (100)	Si (100)	SCD (110)	WC-Co/CrN	WC-Co/CrN	Si (100)	WC-Co/CrN
Thickness [ $\mu\text{m}$ ]	2.7; 4.8; 9; 22	0.8	2.2; 8; 10.5; 14; 22.5	4	4	4	1.3
Roughness $R_a$ [ $\mu\text{m}$ ]	Sq = 55; 62; 63; 99 nm	0.019	0.014; 0.037; 0.02; 0.023, 0.058	0.22	0.2	0.33	0.3
Type of sliding test	Recip.	Recip.	Recip.	Rotat.	Recip.	Rotat.	Recip.
Length of wear scar l [mm]	1	1	1	-	1	-	1
Radius of the wear scar r [mm]	-	-	-	1.5	-	1.5	-
Counter body	Si <sub>3</sub> N <sub>4</sub> ball Ø 3 mm	Si <sub>3</sub> N <sub>4</sub> ball Ø 3 mm	Si <sub>3</sub> N <sub>4</sub> ball Ø 3 mm	Si <sub>3</sub> N <sub>4</sub> ball Ø 10 mm	Si <sub>3</sub> N <sub>4</sub> ball Ø 3 mm	Si <sub>3</sub> N <sub>4</sub> ball Ø 10 mm	Si <sub>3</sub> N <sub>4</sub> ball Ø 3 mm
Temperature T [°C]	RT	RT	RT	RT, 300, 450, 600	RT	RT, 300, 450	RT
Normal load F [N]	0.5; 2; 3	2	0.5	10	0.5; 2	3	0.5; 2
Velocity V [RPM]	300	120, 300, 600	300	300	300	300	300
Duration N [Cycles]	9000; 36000; 72000	14400; 21600; 36000; 54000; 72000; 108000	72000	54000	18000; 36000; 72000	54000	18000; 36000; 72000

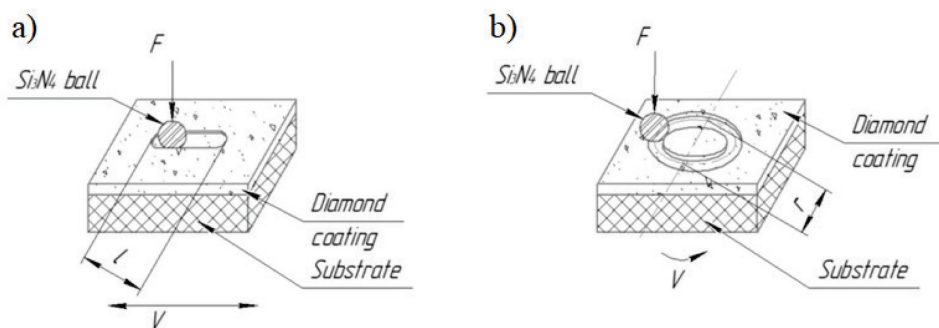


Figure 6. Scheme of reciprocating (a) and rotation (b) sliding tests.

## 2.2 Sliding tests

Sliding wear tests were carried out on a ball-on-plate servo-controlled tribometer (CETER /Bruker® UMT-2), using the reciprocating regime and then the unidirectional rotation regime. CoF was evaluated by dividing the friction force by the loading force, which was measured by a sensor. The system is based on a two-direction sensor and three drives. High temperature chamber with a rotation drive (S21ME-1000) was used for the sliding tests at HT. Si<sub>3</sub>N<sub>4</sub> ball (surface roughness  $R_a = 0.012 \mu\text{m}$ ) (REDHILL, Czech Republic) was selected as a counterbody, as it possesses high hardness (Hardness is 1400 – 1700 HV,  $E = 310 \text{ GPa}$  and  $\nu = 0.27$ ) [3, 71]. Figure 6 shows the scheme of the sliding tests, where  $F$  – normal load,  $V$  – velocity of sliding test,  $r$  – radius of the wear scar,  $l$  – length of the wear scar. These parameters as well as the duration of the test and the temperature varied in the tests. Table 3 shows the conditions of the sliding tests for each sample.

Ball-cratering tests (calotests) using a  $\varnothing 20 \text{ mm}$  steel ball were carry out for an additional investigation of tribological behavior of diamond coatings. The rotational speed and the duration of the test were 400 rpm and 20 min, respectively. The ball-cratering tests were conducted without diamond slurry.

## 2.3 Methods of structural study

Chemical compositions of diamond coatings were characterized by Raman spectroscopy (Horiba® LabRam HR 800) and X-ray diffraction (XRD). Each measurement was taken before and after the sliding test in the wear scar and on the pristine surface of the films. Scanning Electron Microscopy (SEM) (TM-1000 HITACHI®), Atomic Force Microscopy (AFM) and Optical microscopy were used for the investigation of the surface morphology of diamond coatings, and length, width and morphology of the wear scars on the diamond coatings after sliding tests and the surface morphology of the wear scars on the counterbodies. Shape and sizes in the cross section of the wear scars were estimated by Optical (Bruker® ContourGT-K0) and Mechanical profilometry (Mahr Perthometer® equipped with PGK 120 tracing arm). The five line scans were taken across each wear scar, they were averaged and final line scan was obtained. The volume of the wear scar ( $V_s$ ) was estimated using (Eq. 1), where  $S_s$  is the cross-section area and  $l$  is the wear scar length.

$$V_s = S_s \cdot l \quad (1)$$

The surface area ratio ( $S_{dr}$ ) parameter was used in the present study to characterize the contact area between the diamond coating and the  $Si_3N_4$  ball.  $S_{dr}$  is defined as the increment of the total (nominal) surface area relative to the sampling area in the XY (surface) plane.

The contact pressure can be calculated by (Eq. 2), where  $p_{max}$  – contact pressure,  $F$  – normal load,  $R$  – radius of  $Si_3N_4$  ball,  $a$  – contact area of radius.  $E$  can be estimated by (Eq. 3), where  $E_1$  and  $E_2$  – Young's modulus of counterbodies,  $\nu_1$  and  $\nu_2$  – Poisson's ratios of counterbodies [72].

$$p_{max} = \frac{3F}{2\pi a^2} = \frac{1}{\pi} \left( \frac{6FE^2}{R^2} \right)^{\frac{1}{3}} \quad (2)$$

$$\frac{1}{E} = \frac{1 - \nu_1^2}{E_1} + \frac{1 - \nu_2^2}{E_2} \quad (3)$$

### 3 Results and discussion

#### 3.1 Structure of the investigated diamond coatings and DLC

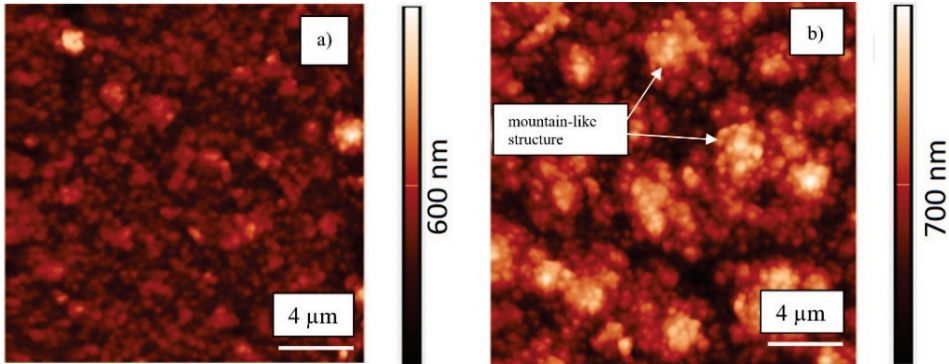


Figure 7. AFM images of surface morphology of NCD-1 coating with thickness of 2.7  $\mu\text{m}$  (a) and 22 (b)  $\mu\text{m}$  [65].

NCD coatings with the thickness of 2.7, 4.8, 9 and 22  $\mu\text{m}$  were prepared. AFM images of the surface of the NCD-1 coating with different thicknesses are shown in Fig. 7. Morphology of diamond coatings is homogeneous and cusp-like granular surface features can be observed. Surface morphology depends on the thickness of the coating. The 2.7  $\mu\text{m}$  thick NCD-1 (Fig. 7 a) has relatively flat surface with cusp-like morphology. In the case of NCD-1, a thick 22  $\mu\text{m}$  mountain-like structure can be observed. It should be noted that diamond particles for the seeding process were used before deposition in the case of NCD grown on the Si substrate [65, 73]. Thus, growth centres of the NCD-1 coating are located on the seeding particles. The morphological peculiarities occurred on the early stage of growth, which influence further growth dynamic. Conformal growth regime leads to the formation of the mountain-like patterns on the surface of NCD-1 coatings. The cusp-like patterns can be formed due to non-local effects and noise [74].

Raman spectra of the NCD-1 coating can be observed in Fig. 8 a. The diamond peak is at  $1332\text{ cm}^{-1}$ . The peaks at  $1136$ ,  $1190$  and  $1478\text{ cm}^{-1}$  relate to trans-polyacetylene (t-PA) at the grain boundaries. The peaks at  $1358$  and  $1557\text{ cm}^{-1}$  are the D and G bands corresponding to six-fold ring breathing vibrations of  $\text{sp}^2$  sites and the in-plane stretching of  $\text{sp}^2$  bonds, respectively. Figure 8 b shows the XRD pattern measured on a 22  $\mu\text{m}$  thick NCD-1 coating. The reflections from the diamond films Si and  $\beta\text{-SiC}$  were found. Five peaks correspond to diamond: (111) at  $43.94^\circ$ , (200) at  $56.34^\circ$ , (220) at  $75.54^\circ$ , (311) at  $91.7^\circ$  and (004) at  $119.9^\circ$ , which indicates the formation of diamond crystallites. However, a wide peak at  $2\theta \sim 10^\circ$  to  $60^\circ$  refers to an amorphous phase in the diamond coating. The SiC was formed between the diamond and the substrate during the deposition process. Evolution of the dependence of the intensity ratio and the strongest reflections (220) and (111) of the diamond versus the thickness of the coating is shown in Fig. 8 c. The orientation (220) becomes dominant for thicknesses  $> 5\text{ }\mu\text{m}$ .

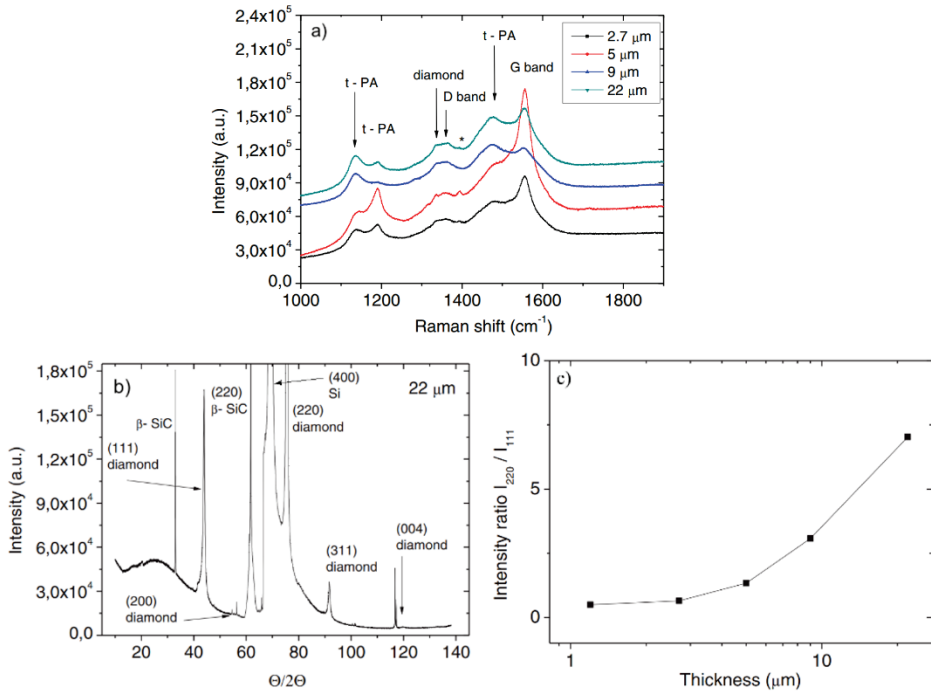


Figure 8. Raman spectra (a) XRD patterns measured on 22 μm thick NCD-1 coating (b), Intensity ratio between (220) and (111) XRD reflections (c) for coatings with different thicknesses [65].

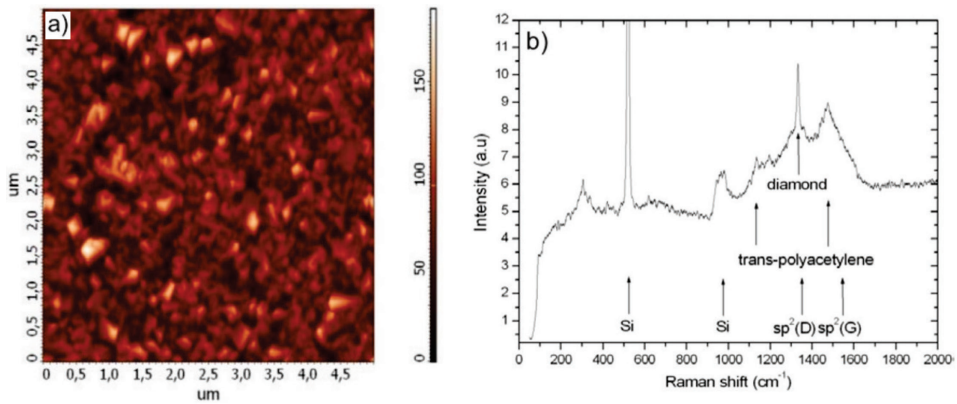


Figure 9. AFM image of surface morphology of NCD-2 coating (a) and Raman spectra (b) [5].

NCD-2 coating has a cauliflower-like surface morphology (Fig. 9 a). Thickness of the coating is 0.8 μm. Cusp-like granular surface can be observed. The grain size is about 0.5 μm. Raman spectra (Fig. 9 b) have a number of peaks which correspond to the characteristic peaks of the NCD coating.

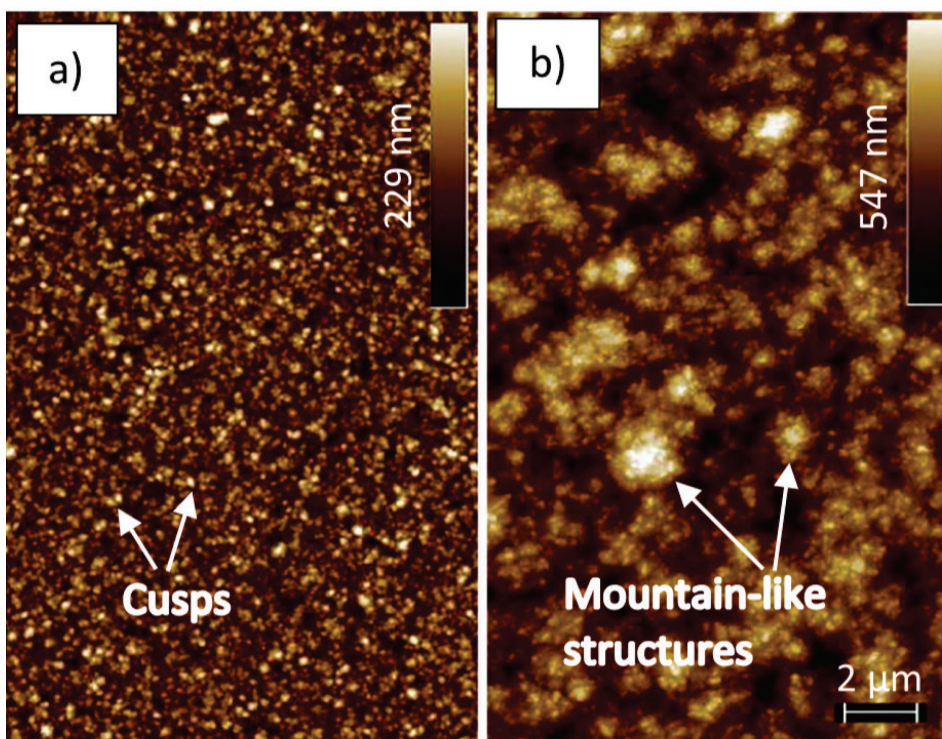


Figure 10. AFM images taken on the NCD-3 coating. The thickness of was as follows: 2.2  $\mu\text{m}$  (a) and 22.5  $\mu\text{m}$  (b) [Publication III].

The batch of samples NCD-3 were deposited on top of HPHT single crystal diamond (110) (Fig. 10). Thickness of the NCD-3 coatings varied between 2.2 – 22.5  $\mu\text{m}$ . Surface morphology changed with the increase of thickness. In the case of a thick coating (Fig. 10 b), a long chain of cusps was observed.

Scaling concept was used to estimate the growth kinetics of both types of the NCD coating [65, 75, 76]. The growth of the NCD coating is an unstable process because the growth rate and the value of roughness exponent change during deposition [77, 78]. Cauliflower-like morphology of the surface of the NCD-3 coatings was observed in both cases. Deposition of NCD-3 coatings was carried out on an SCD substrate, thus no seeding was used. It led to homogeneous growth of the NCD-3 coating along the entire surface of the SCD (110) substrate. At the early stage of growth, the single crystal thin layer forms on the SCD surface, which is fast transformed into the growth of the NCD coating. The shadowing, diffusional instabilities and other processes are the main processes during the NCD-3 coating growth [79, 80].

Raman spectra and XRD showed changes in the structure of NCD-3 coatings, which correlates with the thickness [Publication III]. Raman spectra are shown in Fig. 11 a. Several peaks can be observed, which correspond to diamond,  $\text{sp}^2$  structures (D and G bands) and trans polyacetylene. The intensity of the diamond peak decreases with the increase of coating thickness. It can be explained by high absorption of the NCD material. Figure 11 b shows the XRD patterns. The (111) and (311) peaks correspond to the diamond structure. Strong (220) peak relates to the SCD (110) substrate. It gives evidence

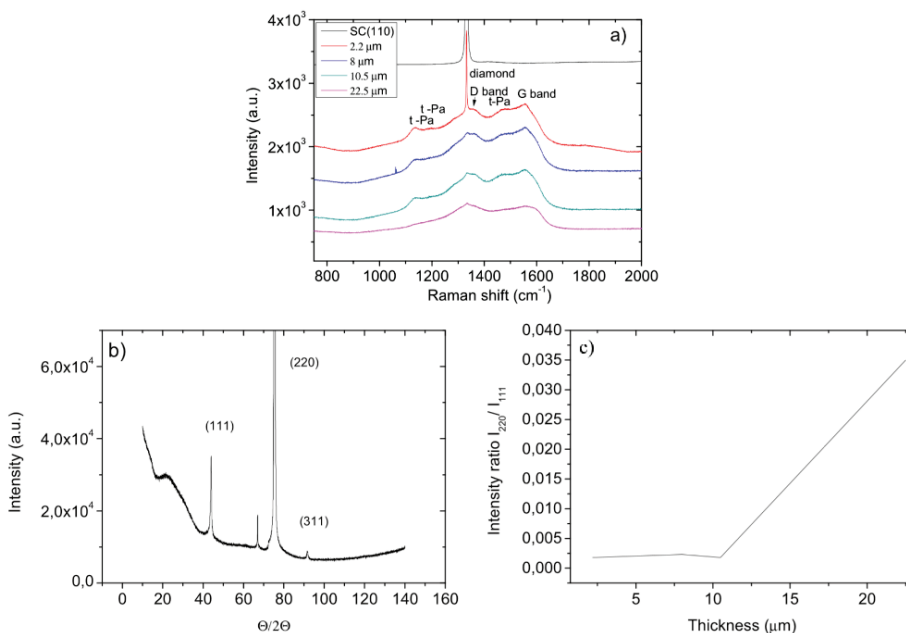


Figure 11. Raman spectra (a), XRD patterns measured on 22.5 μm thick NCD-3 coating (b) and intensity ratio between (220) and (111) XRD reflections for coatings with different thicknesses (c) [Publication III].

of the formation of well-ordered crystallites. The ratio of (220) and (111) peaks intensities can be observed in Fig. 11 c. Increase of the thickness of the coating leads to the increase of the fraction of the (111) oriented crystallites. These results show a correlation with the growth mechanisms of NCD-1 coating. In other words, there is no significant difference in growth for the later stages of the growth of NCD-3 with the growth of NCD-1. Similarity between Raman and AFM was observed as well.

A series of NCD-4 coatings was deposited on WC-Co substrates coated with a CrN layer. The coating has a cauliflower-like morphology (Fig. 12 a and b). The size of the diamond grains is about 0.1 – 0.15 μm, surface roughness R<sub>a</sub> is about 0.22 μm. Raman spectra (Fig. 12 c) have several peaks, which correspond to the peaks characteristic of NCD-4 coatings [Publication IV]. The peaks correspond to t-Pa (trans-polyacetylene at the grain boundaries), diamond, D band (disordered graphite) and G band (well-ordered graphite).

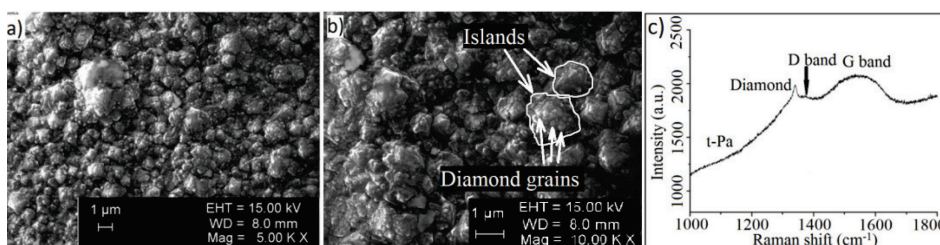


Figure 12. SEM image of surface morphology (a, b) and Raman spectrum (c) of the NCD-4 coating [Publication IV].

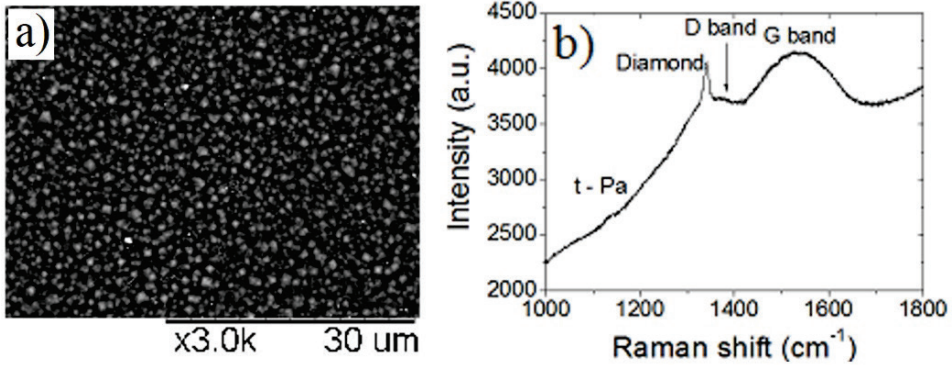


Figure 13. Surface morphology of MCD-1 coating (a) and Raman spectra (b) [Publication II].

An MCD-1 coating was deposited on a WC-Co substrate coated with a CrN layer as a buffer layer. Surface morphology is shown in Fig. 13 a. Thicknesses of the obtained MCD-1 coating and CrN were 4 and 2  $\mu\text{m}$ , respectively. The surface roughness  $R_a$  was 0.2  $\mu\text{m}$ . The diamond grain size is about 0.5 – 1.5  $\mu\text{m}$ . Raman spectra of MCD coatings are shown in Fig. 13 b [Publication II]. It has several peaks corresponding to trans-polyacetylene at the grain boundaries, diamond, D and G bands.

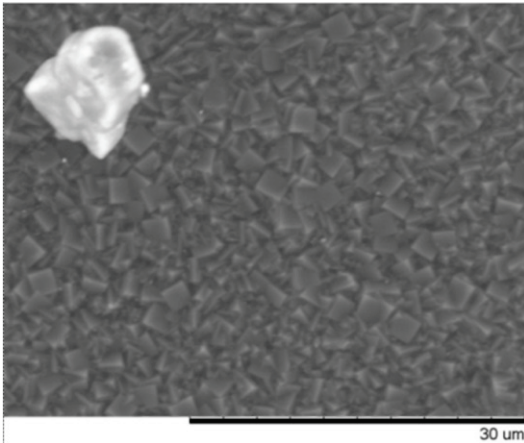


Figure 14. Surface morphology of the MCD-2 coating.

A series of MCD-2 coatings were deposited on Si plates with a thickness of 4  $\mu\text{m}$ . Surface morphology is shown in Fig. 14. Grain size is about 1 – 3  $\mu\text{m}$ . Sliding tests were carried out at room, 300 and 450  $^{\circ}\text{C}$ .

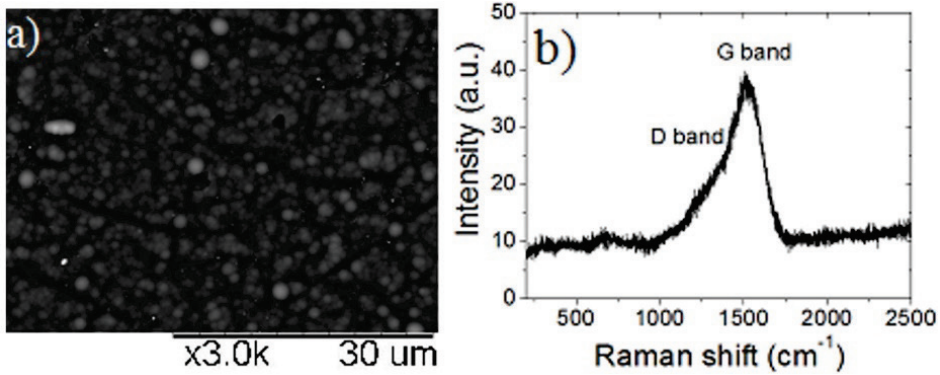


Figure 15. Surface morphology of the DLC coating (a) and Raman spectra (b) [Publication II].

Surface morphology of the DLC coating (Fig. 15 a) has a bubble shape of grains. DLC possesses amorphous structure, the size of cusps is about 1 – 2 μm, surface roughness is about 0.3 μm. Thickness of the DLC coating and the CrN layer is 1.3 and 3.3 μm respectively. A WC-Co plate was used as a substrate. Figure 15 b shows the Raman spectra of the DLC coating [Publication II]. Two characteristic peaks corresponding to G band at 1500 cm<sup>-1</sup> and D band at 1300 cm<sup>-1</sup>.

### 3.2 Wear behavior of diamond coatings

#### 3.2.1 Theory of self-organization for diamond coating/ substrate tribological system

Theoretical basis of self-organization for the diamond coating/ substrate system was developed during the course of the present PhD work. This theory is based on the concept of irreversible thermodynamics. The theory was initially developed by Nobel Prize winner I. Prigogine [81]. The present theoretical research is further development associated with the intensive experimental and theoretical studies of the friction and wear including approach based on irreversible thermodynamic developed by B. E. Klamecki [82], concept of tribo-film elaborated by B. I. Kostetsky [83], the concepts of tribological compatibility of N. A. Bushe [84] and “dissipative heterogeneity” of L. I. Bershadsky [85].

Self-organization is a process of spontaneous ordering, i.e., an emergence of spatial, temporal, spatial-temporal or functional structures formation in open non-linear systems [6]. Such dissipative structures cause a decrease of wear in the tribosystem including diamond coatings. Self-organization can occur at the loss of thermodynamic stability in the system. This phenomenon can be described by (Eq. 4), where  $Y$  is the probability of loss of thermodynamic stability and  $n$  is the number of the interrelated process in the tribosystem [86].

$$Y = 1 - \frac{1}{2n} \quad (4)$$

Equation (4) shows that the probability of losing thermodynamic stability increases with an increase in the number of interrelated processes. According to the Curie principle [87], any flows could correlate with each other in nonlinear areas [88]. The flows or the processes considered in section 1.3 can interact in nonlinear areas. In other words, roughness alternation, coating deformation, passivation of dangling bonds, external load

and velocity of sliding variation, influence of temperature, structure variation including doping of coating by different elements are processes that can be interrelated under nonequilibrium thermodynamic conditions, leading to elastodynamic, thermoelastodynamic, etc. instabilities [89, 90]. As a result of interaction between processes different in nature, self-organization can occur.

According to three friction laws (Amonton's First Law: The force of friction is directly proportional to the applied load, Amonton's Second Law: The force of friction is independent of the apparent area of contact, Coulomb's Law of Friction: Kinetic friction is independent of the sliding velocity), CoF does not depend on the nominal area of contact, speed and normal load. The real contact area in friction is an important factor [91]. It is a small part of the nominal contact area, because real contact occurs between the highest asperities on the surfaces. The real contact area is nearly directly proportional to the applied normal load [92]. The consequence of this is the linearity of the Amonton law  $F_f = \mu F$  ( $F_f$  – friction force,  $\mu$  – CoF,  $F$  – normal load). However, experiments show that CoF can non-linearly depend on the load, speed and area of contact [93, 94, 95].

The real contact area influences the type of the wear. Stronger adhesion occurs between the sample and the counterbody with a larger area of real contact, which causes stronger adhesive wear. In the case of abrasive wear, hardness of materials plays a decisive role. The smaller the contact area, the higher will be the stress between the counterbodies, therefore the hardness of materials will determinate the wear.

Nonequilibrium thermodynamics can be used to describe the nonlinear nature of friction [37, 89]. Reduced wear may occur due to self-organization under certain conditions. The formation of dissipative structures causes stationary processes, which lead to the negative production of entropy [37, 89, 90]. The wear volume depends on the amount of energy induced by sliding. However, due to self-organization, part of the induced energy can be consumed by the formation of dissipative structures; therefore, the wear can be reduced [37, 96]. It is believed that the work of the friction force  $F_f = \mu F$  dissipates in a thin contact layer and it is  $\mu FV$  per unit time, where  $V$  is velocity [97].

Equation (5), where thermodynamic flow is  $J = \mu FV$ , thermodynamic force is  $X = \mu FV/(\lambda T^2 A)$ ,  $A$  – real contact area,  $S$  – entropy,  $t$  – time,  $T$  – temperature, and  $\lambda$  – heat conductivity, describes the rate of change of entropy under the influence of processes in the tribological system [37, 98].

$$\frac{\partial S}{\partial t} = JX, \quad (5)$$

Lapunov's function is the second variation of entropy  $\delta^2 S$ . This function can be used to study the stability conditions of a thermodynamic system, namely if inequality  $\partial^2 \delta / \partial t^2 (\delta^2 S) \geq 0$  is not held, self-organization can occur. This derivative can be written as follows (Eq. 6) [37, 99]:

$$\frac{\partial}{2\partial t} (\delta^2 S) = \frac{1}{2} \delta^2 \left( \frac{(\mu FV)^2}{\lambda T^2 A} \right) = \delta X \delta J = \delta(\mu FV) \delta \left( \frac{\mu FV}{\lambda T^2 A} \right) \geq 0. \quad (6)$$

This means that the estimation of the variations of entropy is possible by the investigation of the variations of the thermodynamic flow and force.

Variation in roughness in the contact zone, deformations of the contacting surface and other factors have influence on the real contact areas between the counterbodies.

The influence of each factor can be described by the parameters  $\psi_1, \psi_2$ , etc. [37]. For simplicity, in the present study, parameter  $\psi$  describes either the influence of the roughness alternation or surface deformation. Therefore, the dependence between the CoF and the real contact area on  $\psi$  can be described as  $\mu = \mu(\psi)$  and  $A = A(\psi)$ . Equation (7) shows the variation of Eq. (3) with the parameter  $\psi$ .

$$\frac{\partial}{2\partial t}(\delta^2 S) = \frac{(FV)^2}{\lambda(TA)^2} \left[ \left( \frac{\partial \mu}{\partial \psi} \right)^2 A - \frac{\partial \mu \partial A}{\partial \psi \partial \psi} \mu \right] (\delta \psi)^2 \geq 0. \quad (7)$$

Self-organization can occur if the second term in the square brackets is greater than zero and Eq. (7) is not satisfied. Four cases satisfying the conditions are possible:

1. If  $\frac{\partial A}{\partial \psi} > 0$  (A and  $\psi$  increase),  $\frac{\partial \mu}{\partial \psi} > 0$  (as  $\psi$  increases,  $\mu$  must increase).
2. If  $\frac{\partial A}{\partial \psi} > 0$  (A and  $\psi$  decrease),  $\frac{\partial \mu}{\partial \psi} > 0$  (as  $\psi$  decreases,  $\mu$  must decrease).
3. If  $\frac{\partial A}{\partial \psi} < 0$  (A increases,  $\psi$  decreases),  $\frac{\partial \mu}{\partial \psi} < 0$  (as  $\psi$  decreases,  $\mu$  must increase).
4. If  $\frac{\partial A}{\partial \psi} < 0$  (A decreases and  $\psi$  increases),  $\frac{\partial \mu}{\partial \psi} < 0$  (as  $\psi$  increases,  $\mu$  must decrease).

Non-constructive self-organization can be observed in cases 1 and 3. It means that the real contact area can increase indefinitely, which leads to a seizure, i.e., a decrease in wear [37, 97]. In practice, however, adhesive wear is often observed [31]. This type of wear is caused by stress, which breaks the cohesive bond between the atoms. This leads to a change in the morphology of the sliding counterbody surfaces, i.e., adhesive wear.

Constructive self-organization is observed in cases 2 and 4. CoF value decreases due to the infinite reduction in the contact area between the sliding counterbodies. Wear is due to a strong increase of pressure in certain points of contact. In this case, abrasive wear is the leading type of wear.

The principle by Le Chatelier - Braun is formulated as follows: "the external influence that deviates a body from equilibrium enhances the processes in this body, which, in turn, strive to weaken the results of this influence" [87]. Therefore, the mentioned cases 1-4 can be considered as a reaction of a tribological system to reduce the wear. The system strives to adapt wear either by stop moving (seizure) or to decrease the contact between counterbodies to infinity.

It should be noted that the parameters  $\psi$ ,  $\mu$  and  $A$  can vary in the course of sliding, which results in difficulty in data analysis use (Eq. 7).

Other factors also can influence friction, for instance, the velocity of sliding and the load affect the wear of the diamond coating (see above-mentioned three laws of friction). Neither was the influence of temperature included in the theoretical study. The main factor that should be taken into consideration is the oxidation of the surface at high temperature. Oxidation lead to change in chemical composition of diamond coating surface and therefore it influences to friction and wear. The presented model fails to describe in detail the influence of the carbonaceous lubricating layer and chemical passivation of dangling carbon bonds by particles from the environment. It is assumed that after the run-in period, the full carbonaceous layer is already formed. In fact, the model can be extended to explicitly assume that they both effect the determinate value of the friction coefficient  $\mu$  as well, i.e.,  $\mu$  can be written  $\mu = \mu(\psi_1, \psi_2, \psi_3, \psi_4)$ , where  $\psi_1$  – influence of roughness,  $\psi_2$  – surface deflection,  $\psi_3$  – influence of the carbonatious layer, and  $\psi_4$  – influence of passivation of dangling bonds. Also, the influence of temperature can be included in theory.

### 3.2.2 Self-organization and wear types of diamond coating

Figure 16 shows two typical CoFs vs the number of cycle curves observed on the MCD and NCD coatings at room and HT in the course of the present doctoral thesis (see sections 3.2.3 and 3.2.4) [Publication II, Publication III, Publication IV]. Similar curves have been reported in other studies as well [3, 5, 2, 4]. It should be stressed that the shape of the CoF curve can vary between the tests carried out on the same sample under similar conditions. The friction and wear involved many different interacting processes as predicted by the Curie principle. Local character of the friction mechanisms is also an important factor influencing tribological behavior.

Observation of type 1 or 2 curves depends on the friction and wear mechanisms occurring during sliding. The fracture and self-polishing of the surface asperities take place at the beginning of sliding, i.e., at stages 1 and I [29, 100, 101]. Increasing of the real contact areas (A) due to polishing of diamond grains is expected. The roughness and therefore parameter  $\psi$  decrease, along with CoF decreasing. However, not all the cases described in (Eq. 7) correspond to this situation. Similar analysis at the surface deflection leads to the same conclusion. It indicates that initial polishing of the diamond coating does not lead to self-organization, in agreement with Gershman et al. [97]. Initial smoothing of the surface and formation of a carbonaceous layer can lead to a decrease in the CoF at stages 1 and I.

A change of the wear rate can give evidence of self-organization [97]. Change in the friction behavior (CoF) can be related to the change of the wear rate. Stages 1 and I look similar; however, due to bifurcation at the following stage the friction behavior can vary. The CoF can be stable or continuously descending, which corresponds to stage II of type 1. On the other hand, increase in CoF corresponds to the stage 2 of type 2. The behavior of the CoF curve in stage 2 can be explained by (Eq. 7). The CoF value increases at the increase of coating deflection ( $\psi$ ) [3]. It means that  $\frac{\partial \mu}{\partial \psi} > 0$ . In addition, the real contact

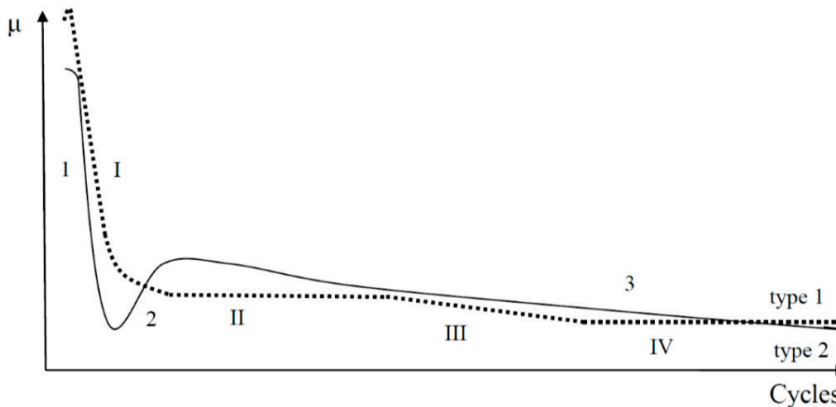


Figure 16. Schematics of two types of coefficient of friction (CoF) vs cycle curves observed during reciprocating sliding wear test on diamond coatings [Publication I].

area (A) increases due to the deflection of NCD or  $\frac{\partial A}{\partial \psi} > 0$ . These conditions correspond to the adhesive wear regime of sliding (Eq. 7. Case 1). The behavior of stages 2 and II can be understood also by taking into account the initial wear of diamond grains and increasing of polishing areas during stages 1 and I. Thus, an increase in the real contact

areas can be expected (Stage 1 and I). Therefore, in the case of type 2 stage 2, adhesive wear can be expected. In the case of stage II of type 1 curve, other wear and friction mechanisms can influence and the CoF value is approximately stable, i.e., there is no particular mechanism that would exclusively determine the wear, in contrast to the example of type 2 stage 2.

The surface morphology on the wear scar of the diamond coating and  $\text{Si}_3\text{N}_4$  ball is formed due to dynamic changes and coexistence of peaks, scratches, ripples and grooves. The shape of ripples and grooves can be changed and the peaks can be fractured. It can lead to permanent changes in the surface morphology of the wear scar of the counterbodies. The mentioned changes in morphology can occur locally. These aspects are important for understanding mechanisms occurring during stages III and 3. Various wear mechanisms can occur within different zones of contact. For instance, the real contact area can locally decrease, due to the formation of large grooves, etc. The CoF value decreases for stages III and 3. Decreasing of the CoF ( $\mu$ ) and the real contact area (A) corresponds to Eq. 7 in cases 2 and 4. Changes of the parameter  $\psi$  (surface roughness and coating deflection) occur in the course of sliding. However, for cases 2 and 4, variation of  $\psi$  has no influence on occurrence of constructive self-organization (Eq. 7). The abrasive wear can be the main wear mechanism in stages 3 and III.

The stabilization of the CoF value for stages II and IV can be related to passivation of carbon bonds, adhesive and abrasive wear, coating deflection and formation of a tribolayer. No significant changes were observed in the CoF in the steady stage regime IV (Fig. 16). It can be explained by the influence of different mechanisms.

Permanent changes in the landscape of the contact areas have been found to correlate with the adhesive and abrasive wear [102]. Mutual alignment of the surface of the diamond coating and the ball is a process of adaptive self-organization. In the present study, the running-in period of wear is explained as this process.

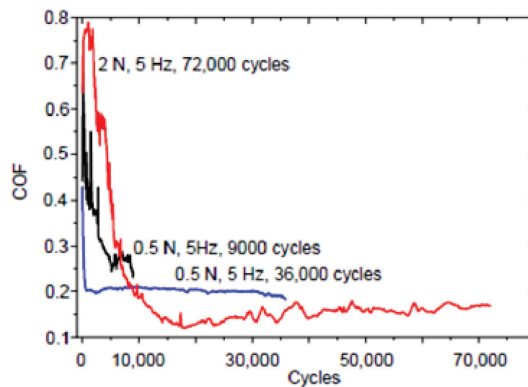


Figure 17. COF versus the number of cycles taken on the  $4.8 \mu\text{m}$  thick nanocrystalline diamond coating NCD-1 [Publication I].

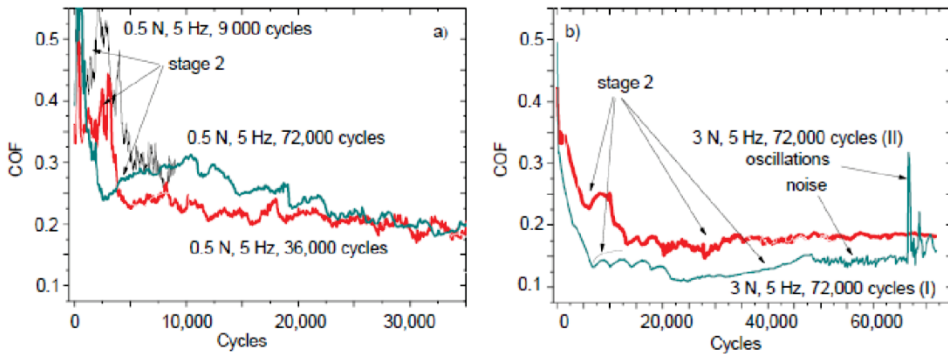


Figure 18. CoF versus the number of cycles taken on the 22  $\mu\text{m}$  thick NCD-1 coating at normal load at the 0.5 N (a) and 3 N (b). Two tests at the 3 N normal load were taken at different places on the sample [Publication I].

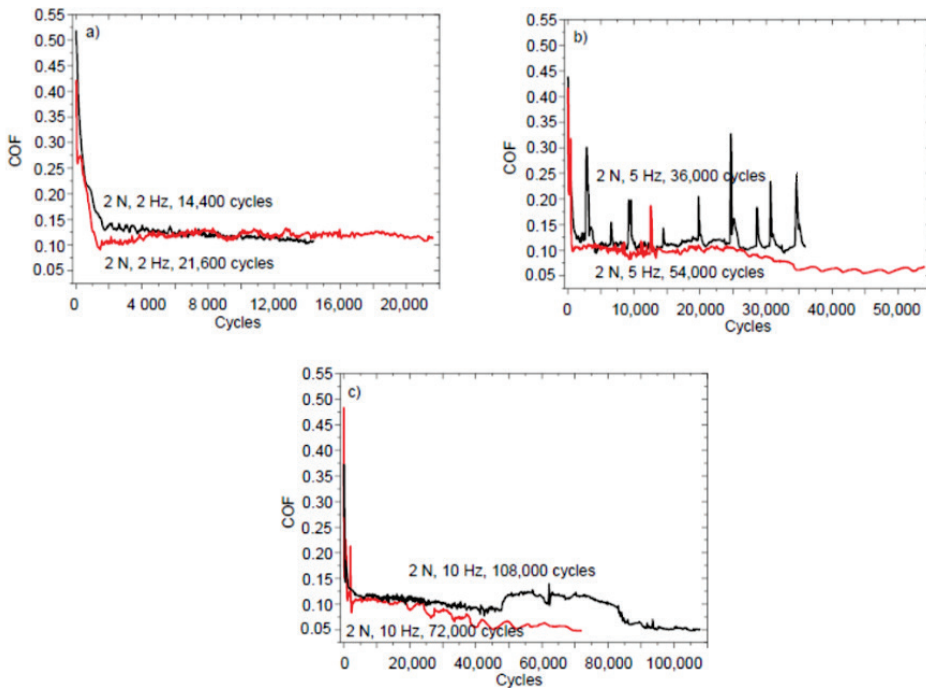


Figure 19. CoF versus cycle curves taken on the NCD-2 coating. The sliding wear test parameters were as follows: (a) 2 N and 2 Hz; (b) 2 N and 5 Hz; and, (c) 2 N and 10 Hz [Publication I].

### 3.2.3 Analysis of tribological behavior of NCD-1 and NCD-2 coatings

The evolution of the CoF recorded during sliding on NCD-1 (4.8  $\mu\text{m}$ ) is shown in Fig. 17. Under the same test conditions (0.5 N and 5 Hz), after 72000 cycles of the wear test, the shape of the obtained curve corresponds to type 2 (Fig. 16); however, for the test of 36000 cycles to type 1. In other words, the bifurcation takes place.

Figure 18 shows the CoF versus the number of cycle curves on NCD-1 (22  $\mu\text{m}$ ). The shape of the CoF curve corresponds to type 2 (Fig. 16) in the case of the sliding test performed at 0.5 N load. The shape of the CoF curves is different for the tests with different duration. It can be explained by the nonuniformity of surface roughness.

In addition, two tests at the 3 N normal load were carried out at different places of the NCD coating. The CoF curve recorded during the tests corresponds to type 2, but the CoF value differs significantly, indicating a different tribological behavior.

The CoF curve after the sliding tests at the NCD-2 coating ( $0.8\ \mu\text{m}$ ) is shown in Fig. 19. The CoF recorded after sliding at 2 N load and 2 Hz (Fig. 19 a) corresponds to types 1 and 2 (see Fig. 16). The results of the sliding tests at 5 Hz (Fig. 19 b) and 10 Hz (Fig. 19 c) indicate type 1 curve with variations. The stages II, III and IV can be recognized. The duration of stage II is varied for tests at 5 and 10 Hz, i.e., it decreases due to the increasing sliding frequency.

The  $\text{Si}_3\text{N}_4$  balls were investigated after the sliding tests on the NCD-1 coating with  $4.8\ \mu\text{m}$  thickness (Fig. 20). The surface of the wear scar on the ball after the test at 9000 cycles is smooth. Scratches and grooves were observed only after longer sliding tests at

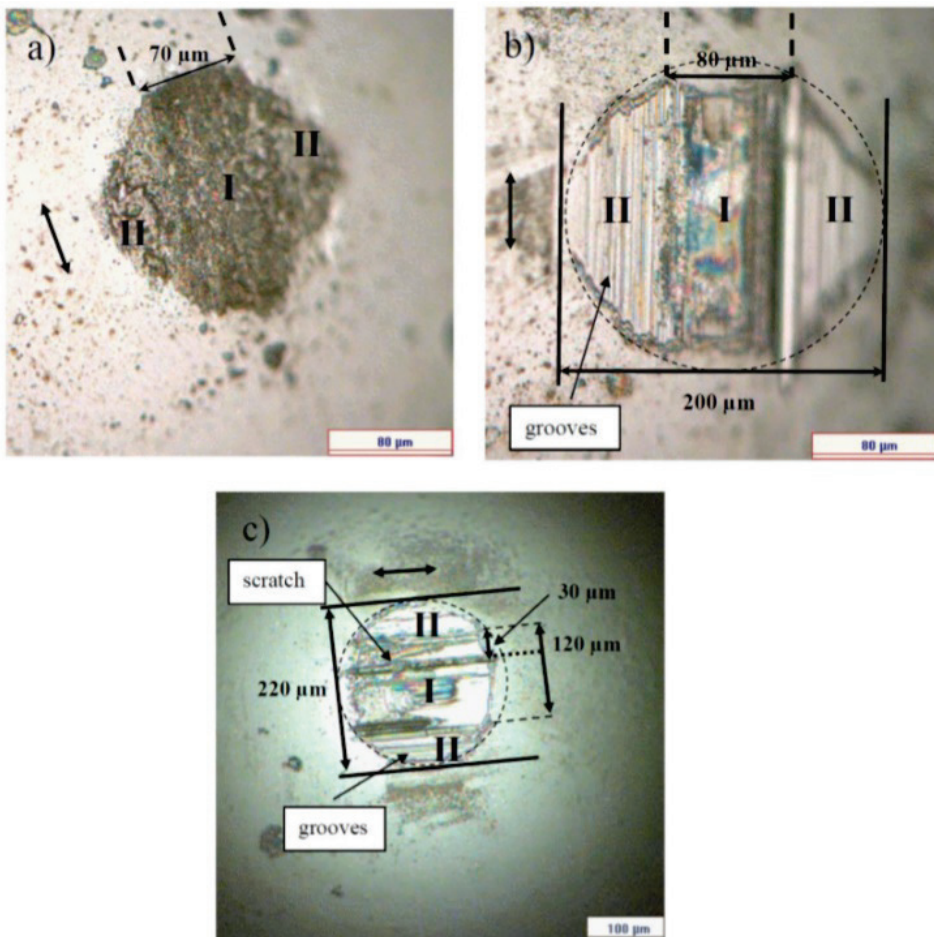


Figure 20. Surface morphology of the  $\text{Si}_3\text{N}_4$  balls after the sliding wear tests on the  $4.8\ \mu\text{m}$  thick NCD-1 coating. The test parameters were as follows: (a) 0.5 N, 5 Hz, 9000 cycles; (b) 0.5 N, 5 Hz, 36000 cycles; and, (c) 2N, 5 Hz, 72000 cycles [Publication I].

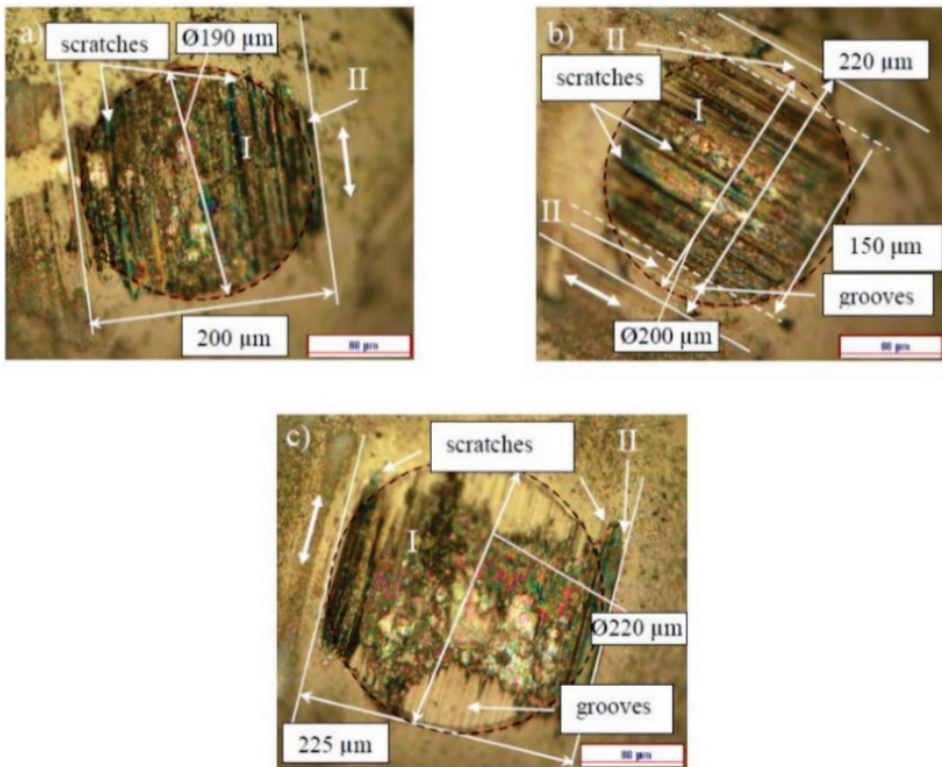


Figure 21. Surface morphology of the  $\text{Si}_3\text{N}_4$  balls after the sliding wear tests on the  $22\ \mu\text{m}$  thick NCD-1 coating. The sliding wear test parameters were as follows:  $0.5\ \text{N}$ ,  $5\ \text{Hz}$ ,  $9000$  cycles (a),  $0.5\ \text{N}$ ,  $5\ \text{Hz}$ ,  $36000$  cycles (b), and  $3\ \text{N}$ ,  $5\ \text{Hz}$ ,  $72000$  cycles (c) [Publication I].

$36000$  and  $72000$  cycles (Fig. 20 b and c). The wear scars after sliding at  $9000$  and  $36000$  cycles have oval shape; however, the wear scar after the test at  $72000$  cycles has a circular shape. Two different types of wear regimes after all sliding tests can be recognized on the surface of the ball: one stripe-like area (I) in the centre of the wear scar and two semicircle-like areas (II) on the sides. The surface morphology of both zones looks different. In addition, it indicates that different real contact areas exist between the zones of the ball and the NCD coating. The most significant difference between zones I and II can be observed after the sliding test at  $36000$  cycles (Fig. 20 b). The width of area I increases from  $70$  to  $120\ \mu\text{m}$  with the increase of the duration of sliding (Fig. 20). The two different zones observed on the ball, the presence of the grooves and scratches at different places of the wear scars indicate local character of the friction. One of the reasons can be the deflection of coatings.

The surface morphology of the wear scars on the  $\text{Si}_3\text{N}_4$  balls after the sliding test on the  $22\ \mu\text{m}$  thick NCD-1 coating is shown in Fig. 21. Areas I and II are not clearly seen in Fig. 21 a. However, these areas can be found on the wear scar after the tests at  $36000$  and  $72000$  cycles. The wear scar at  $9000$  cycles has a circular shape unlike those on the  $4.8\ \mu\text{m}$  thick NCD-1. It can be due to weaker deformation of a thick coating [3]. The width of area I increases with the increase of the duration of sliding, i.e., deformation of the diamond coating depends on the number of cycles. On analogy with the tests with

4.8  $\mu\text{m}$  thick film, the presence of the grooves and scratches indicates locality of the friction.

It should be noted that diameters of the wear scars after all tests on both types of coatings (4.8  $\mu\text{m}$  and 22  $\mu\text{m}$  thick) have approximately the same values about 200 – 220  $\mu\text{m}$ . This means that the influence of a normal load, duration of the test and thickness of a coating have insignificant influence on the size of the wear scar on the counterbody.

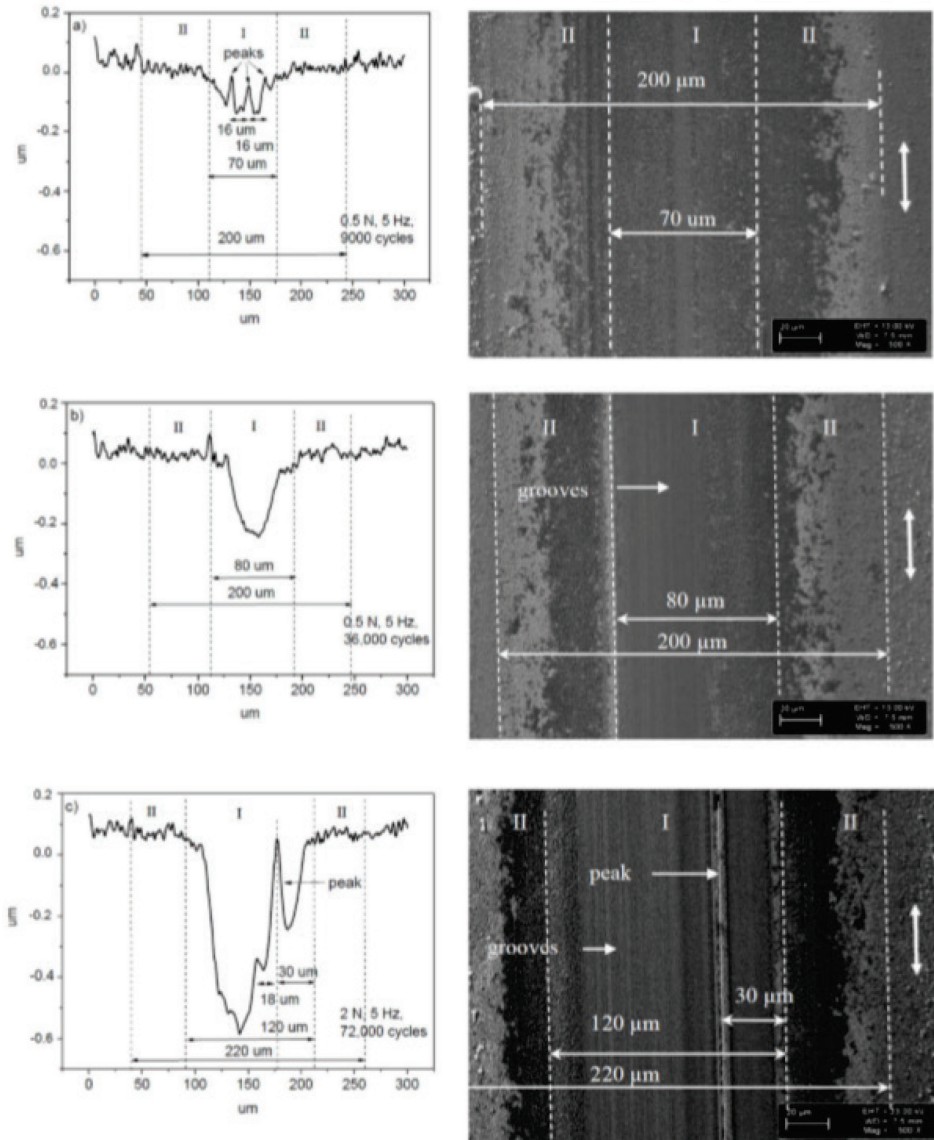


Figure 22. Line scans and SEM images taken on the wear scars of the 4.8  $\mu\text{m}$  thick NCD1 coating. The sliding wear test parameters were as follows: (a) 0.5 N, 5 Hz, 9000 cycles; (b) 0.5 N, 5 Hz, 36000 cycles; and, (c) 2 N, 5 Hz, 72000 cycles [Publication I].

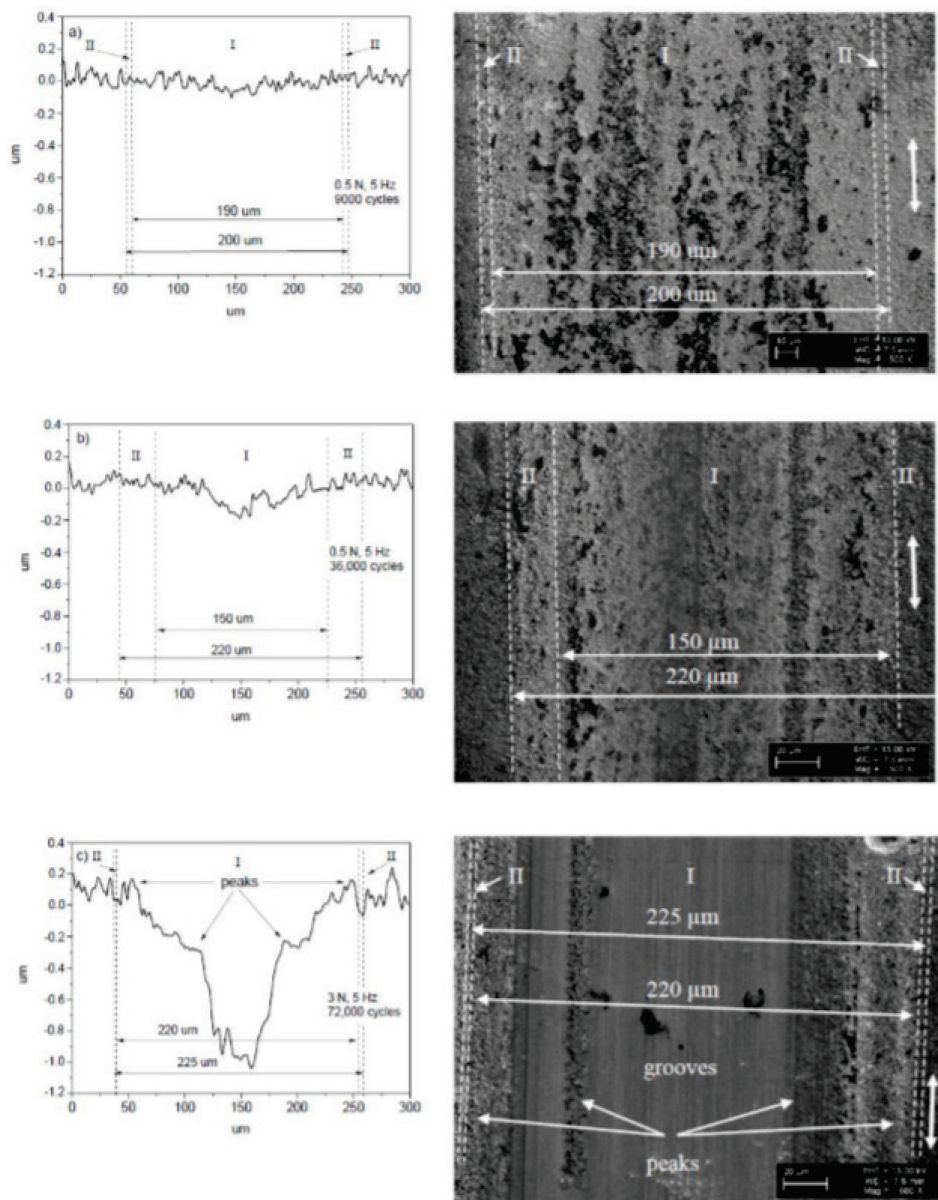


Figure 23. Line scans and SEM images taken on the wear scars of the 22  $\mu\text{m}$  thick NCD1 coating. The sliding wear test parameters were as follows: (a) 0.5 N, 5 Hz, 9000 cycles; (b) 0.5 N, 5 Hz, 36000 cycles; and, (c) 3 N, 5 Hz, 72000 cycles (I) [Publication I].

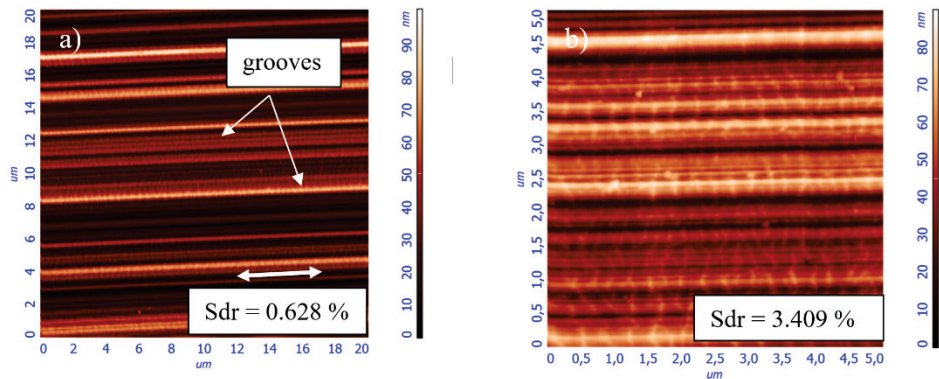
The local character of friction can be observed on the wear scars on the diamond films as well. Similar to the results observed on the balls, zones I and II with different types of wear can be found on the wear scars. The width of zone I after the sliding test on the NCD-1 coating (4.8  $\mu\text{m}$ ) steadily increases from 70 to 120  $\mu\text{m}$  (Fig. 22). The width of the wear scars does not change significantly, remaining at about 200  $\mu\text{m}$ . This value corresponds to the width of both areas I and II of the wear scars on the  $\text{Si}_3\text{N}_4$  ball. The single peak can be observed in the center of the wear scar after the sliding test at

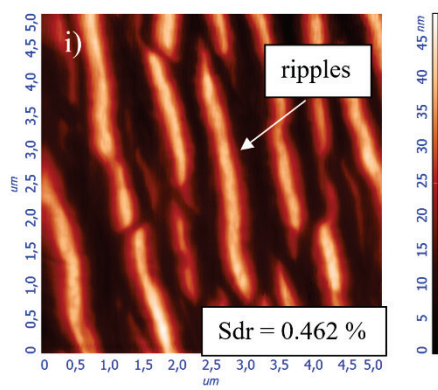
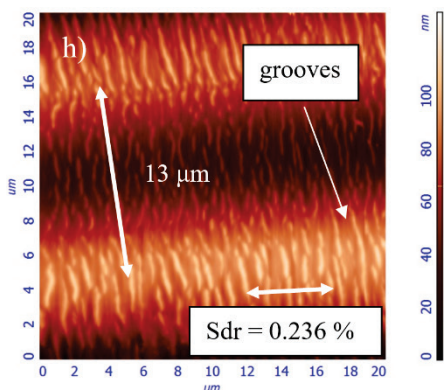
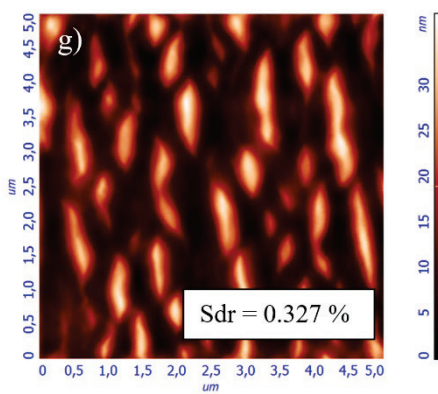
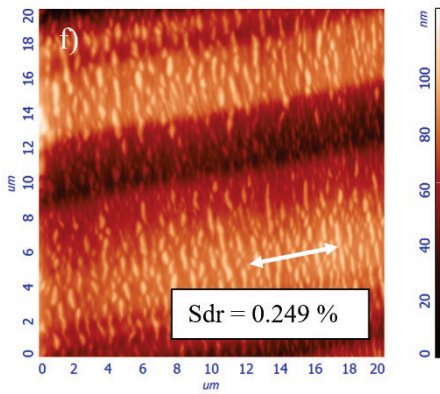
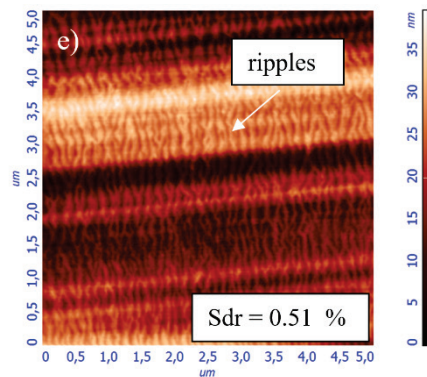
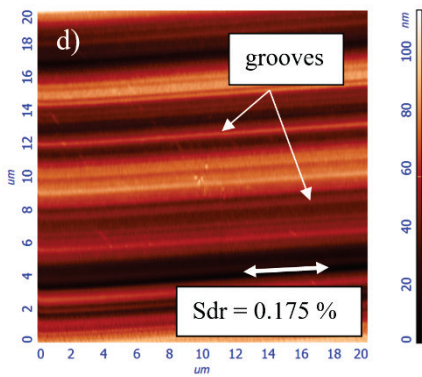
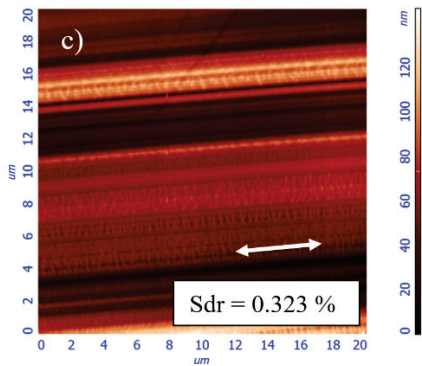
2 N load and 72000 cycles (Fig. 22 c). The height of this peak corresponds to the level of pristine surface. Position of scratch on the wear scar of the ball (Fig. 20 c) corresponds to the position of this peak within the wear scar of the NCD coating. It means that the lowest wear on the NCD coating is observed at the peak and the highest wear on the ball on the scratch, i.e., wear can be locally very non-uniform.

In the case of NCD-1 (22  $\mu\text{m}$ ), results in Fig. 23 show correspondence between the width of the wear scars on the diamond coating with the worn areas on the Si3N4 balls. The size of area II is very small unlike the wear scars after the sliding test on the NCD-1 coating (4.8  $\mu\text{m}$ ). The width of area I varies from 150  $\mu\text{m}$  to 220  $\mu\text{m}$ . The width of the wear scar is approximately 200 – 220  $\mu\text{m}$ . In addition, in Fig. 23 c four peaks are presented. Two peaks were found within the central part of the wear scar, and two more peaks at the border of the wear scar. As in the case of the NCD-1 coating, (4.8  $\mu\text{m}$ ) positions of peaks within the wear scar on the coating correspond to the position of scratches on the ball (Fig. 21 c). It is expected that the contact between the counterbodies occurs just between the corresponding peaks and scratches.

In conclusion, the asymmetric shapes of the wear scars were observed after the sliding tests on the NCD-1 samples of different thickness. Grooves, scratches and peaks were found on the wear scars of the coatings and balls. It indicates the locality of the friction and shows the variety of the types of contact between the counterbodies.

The AFM images taken on the bottom of the wear scars after the sliding tests on the NCD-2 coating (0.8  $\mu\text{m}$ ) are shown in Fig. 24. Grooves and ripples can be observed on the surface of the wear scar. Surface area ratio  $S_{dr}$  (see Section 2.3) can be used to characterize the real contact area between the NCD coating and the counterbody. The  $S_{dr}$  value is higher for shorter tests (Fig. 24 a and b). It indicates that different types of contact areas can be expected between the counterbodies for shorter and longer tests. Namely, because  $S_{dr}$  is higher for shorter tests, the contact area should be higher for shorter tests.





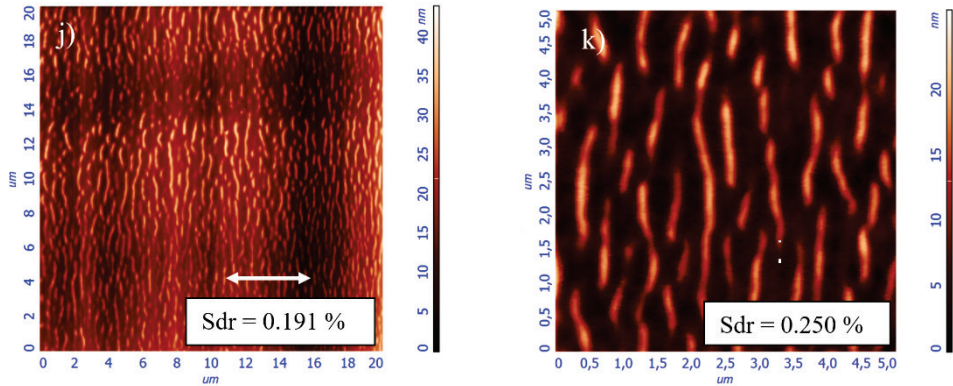


Figure 24. Atomic force microscopy (AFM) images taken on the wear scars of the NCD-2 coating after the sliding wear tests. The test parameters were as follows: (a, b) 2 N, 2 Hz, 14400 cycles; (c) 2 N, 2 Hz, 21600 cycles; (d, e) 2 N, 5 Hz, 36,000 cycles; (f, g) 2 N, 5 Hz, 54000 cycles; (h, i) 2 N, 10 Hz, 72000 cycles; and, (j, k) 2 N, 10 Hz, 108000 cycles [Publication I].

The shape of the CoF curves, surface morphology of the wear scars on the  $\text{Si}_3\text{N}_4$  ball and the NCD coating support the conclusion that the conditions for self-organization described in (Eq. 7) can be fulfilled for NCD 1 and NCD 2 coatings.

In the case of the sliding test at 72000 cycles on NCD-1 ( $22 \mu\text{m}$ ), type 2 of the CoF curve was observed (Fig. 18 b). Noises and oscillations were observed after increasing the CoF value, see curve I, which can be regarded as evidence of seizure like contact between the counterbodies. The position of scratches on the balls corresponds to the peaks on the diamond film, indicating the mechanism of seizure. It occurs locally, i.e., within the restricted zone of the contact. Formation of the local surface corrugations (peaks) in the area of the wear scar leads to an increase of surface roughness within this area of contact. The CoF and the contact area increase due to the increase in the size of the peaks on the film and scratches on the ball. It means that the adhesive wear regime is predominant during the sliding test on NCD-1 ( $22 \mu\text{m}$ ) and unconstructive self-organization occurs (Case 1 Eq. 7).

In the case of shorter tests on NCD-2, adhesive wear can be indicated by the formation of grooves and ripples (Fig. 24 a, b and c) in the early stage of sliding for the NCD-2 coating ( $0.8 \mu\text{m}$ ). The highest value of Sdr and the denser arrays of grooves of thinner width were found after a short duration sliding. It means that the contact area between the diamond coating and the sliding counterbody is high. The CoF value for the test at 21600 cycles increases after the running-in period and corresponds to type 2 (Fig. 19 a). However, CoF decreases at the end of the tests. In other words, CoF decreases for both tests (14 400 and 21 600 cycles), the contact surface (A) decreases also because  $S_{dr} = 0.628 \%$  (14 400 cycles) changes to  $0.323 \%$  (21 600 cycles), i.e., it corresponds to case 2 or 4 of Eq. (7). It can mean that the abrasive wear regime is predominant at the end of short tests. However, high absolute value of  $S_{dr}$  points out that adhesive wear plays a role at the early stage of sliding, as compared to the discussion (the text right below) regarding to longer tests.

In all longer tests (Fig. 19 b and c), a steady state regime can be observed as the CoF value is relatively stable. Because friction is a local process, the stabilized value of CoF can be explained by the relationship between the abrasive and the adhesive wear, passivation of dangling bonds, formation of a carbonaceous tribolayer and coating

deflection (see previous paragraph). A number of peaks observed on the CoF curve (Fig. 19 b) can be related to a local removal of the carbon-based tribolayer from the surface of the wear scar [58] and as well as with the seizure. It is assumed that all the processes mentioned above can be correlated. The  $S_{dr}$  value after sliding (Fig. 24 d, f, h and j) is lower than in the case of a short duration test (Fig. 24 a and c). It means that the real contact area is smaller for longer tests. The ripple size is the smallest and the density is the highest for shorter tests (Fig. 24 a, b, d and e). The groove size is the smallest and the density of the grooves is the highest for shorter tests (Fig. 24 a, b), the size of grooves increases for longer tests (Fig. 24 h, l, j and k). These results suggest that there is a difference in the contact area for longer and shorter tests. Although, different mechanisms of friction and wear lead to a constant CoF, probably the abrasive wear is predominant for longer tests, as the decreasing real contact area corresponds to cases 2 and 4 in (Eq. 7).

### 3.2.4 Investigation of deflection of diamond coatings

#### Comparative analysis of tribological behavior of MCD and DLC coatings

The behavior of CoF recorded during the sliding tests on MCD-1 and DLC coatings is shown in Fig. 25. The CoF value of the DLC coating stabilizes after a short run-in period for the test at 0.5 N. The CoF curve after sliding at 2 N on the DLC coating has approximately the same behavior during half number of cycles. But after that it starts to increase. In the case of MCD-1, CoF values recorded during sliding at 0.5 N and 2 N, an increase starts after the running-in period. However, after increasing to the highest value, the curves start decreasing. CoF value decreases more significantly after the sliding test at 2 N.

Figure 26 shows the average profile of the wear scar on the DLC coating after the sliding test at 2N load during 18000 cycles. Surface morphology of the bottom of the wear scar is shown in Fig. 26 b and c. The line scans were taken on the wear scars as shown in Fig. 26. Dark areas (II) in the area of the wear scar (Fig. 26 b) correspond to the pristine surface of the DLC coating (Fig. 26 a). Peak (II) has approximately the same height

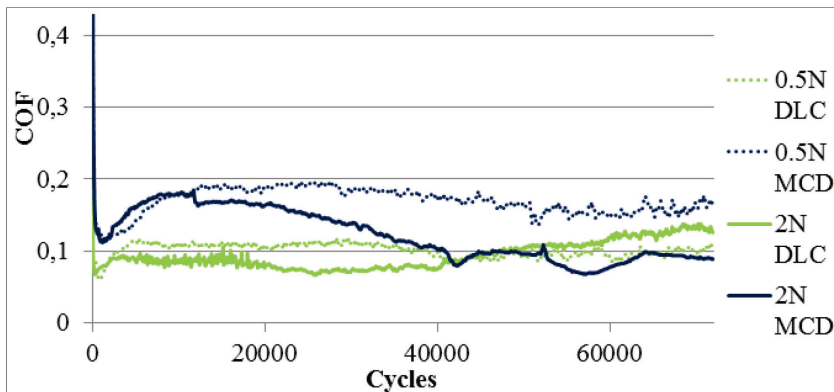


Figure 25. CoF versus the number of cycles recorded on the DLC and MCD-1 coatings [Publication II].

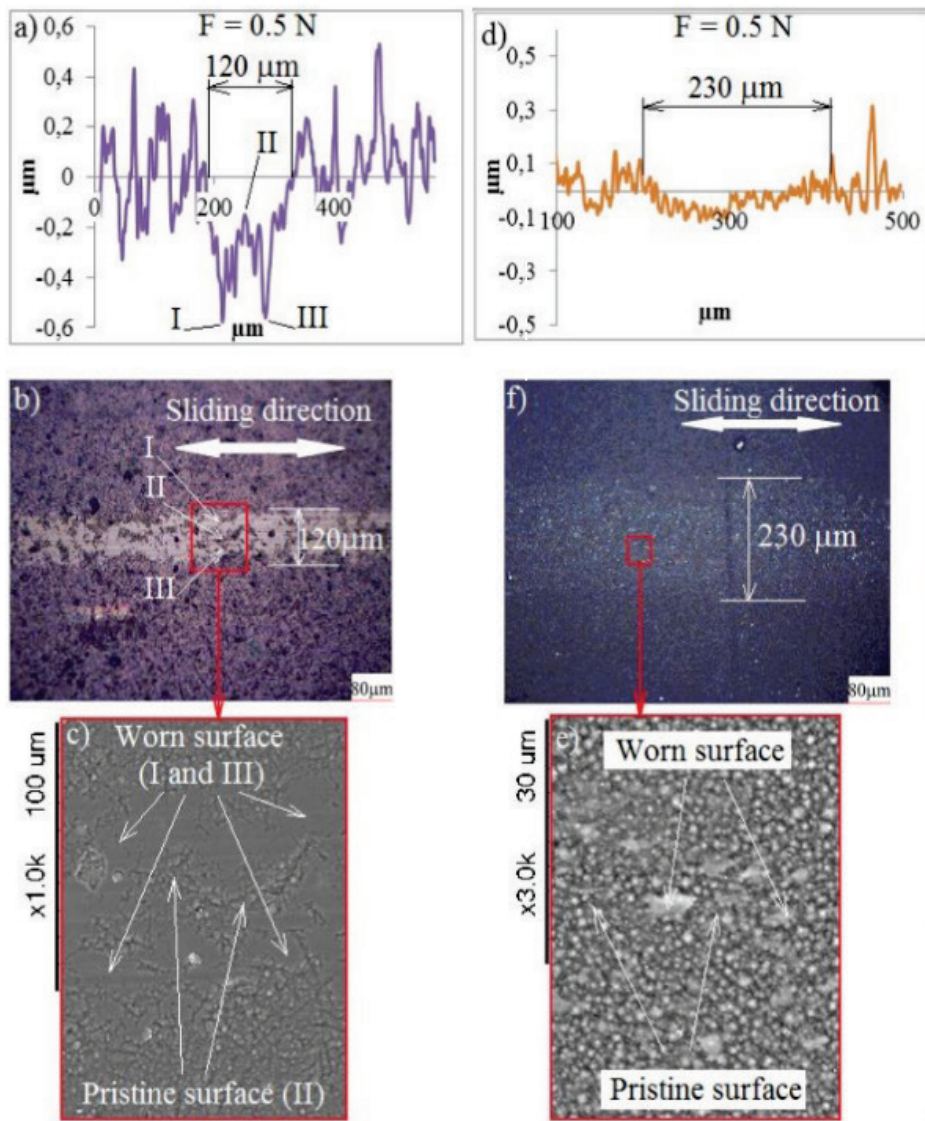


Figure 26. Line scans, optical microscope and SEM images taken after sliding tests with  $0.5\text{ N}$  (18000 cycles) on the DLC (a – c) and MCD-1 (d – e) [Publication II].

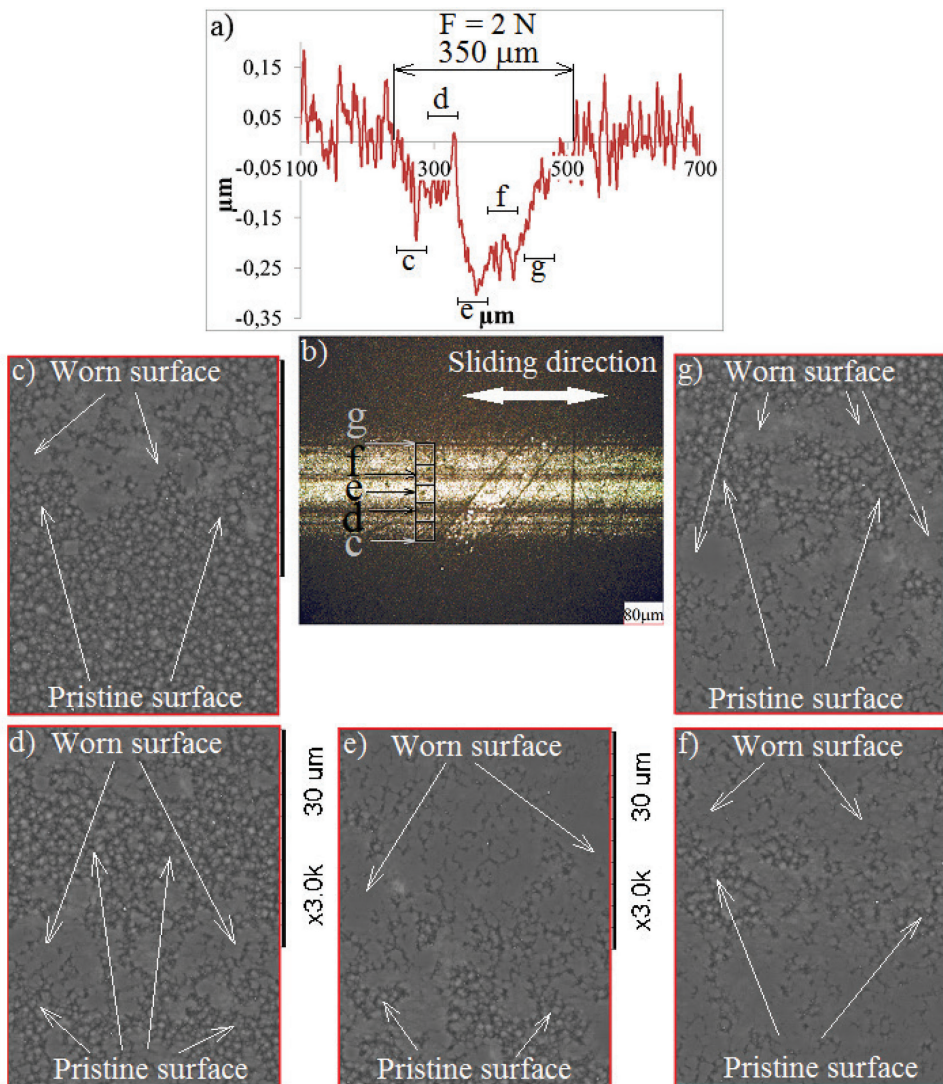


Figure 27. Line scan (a) taken on the wear scar after the test with 2 N (72000 cycles) on the MCD-1 coating. The optical microscope (b) and SEM (c – g) images taken on the same wear scar [Publication II].

level as the area out of the wear scar (Fig. 26 a). Bright areas (I and III) (Fig. 26 b) correspond to the valleys on the profile of the wear scar (Fig. 26 a), these values correspond to the polished structure of the DLC coating. The wear scar line scan after the sliding test at 0.5N load and 18000 cycles on MCD-1 coating is shown in Fig. 26 d, f and e. Clearly visible concave shape on the line scan (Fig. 26 d) could suggest that diamond coating is worn out significantly. However, only small islands of polished diamond grains can be observed in the centre of the wear scar (Fig. 26 e and f).

After the sliding test on the DLC coating at 2N load and 72000 cycles (not shown), it was found that the DLC coating is worn out during the sliding test.

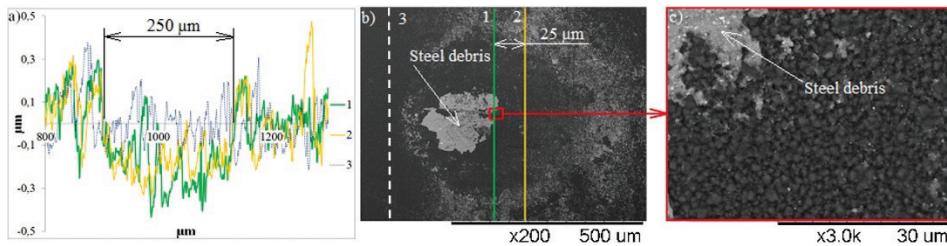


Figure 28. Lines scan (a) and SEM images (b, c) taken on the crater after ball test on the MCD-1 coating [Publication II].

Line scan of the wear scar after the sliding test at 2N load and 72000 cycles on the MCD-1 coating and surface morphology of the bottom of the wear scar are shown in Fig. 27. SEM images (c-g) were taken across the whole width of the wear scar, and its positions are shown in Fig. 27 b. Profile of the wear scar has no symmetrical shape. Apexes of peaks on the bottom of the wear scar (zones e and f in Fig. 27 a) are lower than the valleys on the pristine surface. The bright areas in Fig. 27 b correspond to the worn diamond surface, and dark areas correspond to the pristine surface or the surface with negligible wear. Slightly polished areas of the MCD-1 coating were found only on the bottom of the wear scar (Fig. 27 e and f). In conclusion, on analogy with the test with 0.5 N and 18000 cycles, the significant size of the wear scar profile along with insignificant worn parts of the diamond films provide a reason for a suggestion that coating deflection has taken place.

The result of the ball-cratering test is shown in Fig. 28. Three line scans were performed after the ball cratering test at 400 rpm during 20 min. Namely, the first was taken through the center (1), the second one on the side of crater (2) and the third one on the pristine surface of the MCD-1 coating (3) (Fig. 28 b). The SEM images (Fig. 28) show slightly polished diamond grains in the center of the crater with steel debris from the ball. The center of the crater is located below the level of the native surface of the coating is at about 0.2 µm. Therefore, it also indicates deflection of the diamond coating.

Table 4. Dependence of the wear loss volume on the number of cycles for the DLC and MCD-1 coatings.

Number of cycles	Wear loss volume [mm <sup>3</sup> ]			
	MCD-1		DLC	
	0.5 N	2 N	0.5 N	2 N
18000	0.004	0.031	0.0422	0.071
36000	0.015	0.038	0.0481	0.142
72000	0.016	0.043	-	-

The wear volume on the MCD-1 and DLC coatings after the sliding test was evaluated and the results are shown in Table 4. In the case of the DLC coating, only the wear volume for short duration tests (36000 and 18000 cycles) can be estimated, because it was worn out during the sliding test at 72000 cycles. Values of the wear volume of the MCD-1 coating are lower than those for the DLC coating in all cases. However, in the case of the

MCD-1 coating, plastic and elastic deformation influences wear, see discussion above. In other words, real wear volume of the MCD-1 coating can be even lower than the calculated values. It means that the MCD-1 coating has higher wear resistance than the DLC coating.

**Comparative analysis of tribological behavior of diamond coatings deposited on single crystal diamond (110) and Si (100) substrates**

NCD coatings were prepared on two types of substrates to investigate the influence of substrate properties on the tribological behavior of diamond coatings. Because substrates SCD and Si possess different mechanical properties, the normal load should be carefully applied to carry out sliding tests at the same contact pressure.

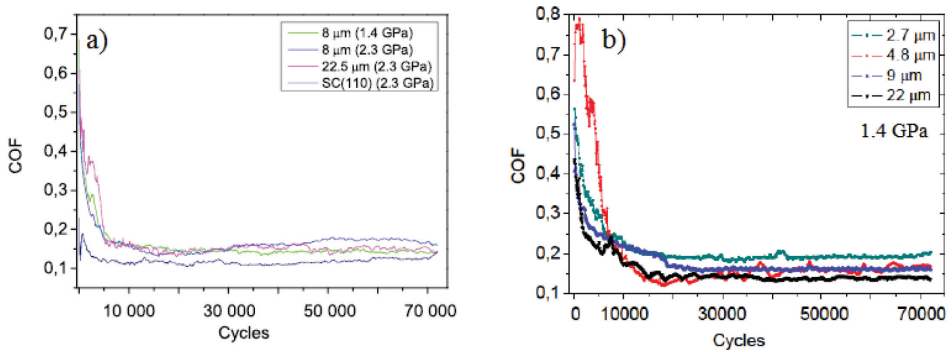


Figure 29. CoF versus the number of cycle curves taken on (a) the NCD-3/SCD (110) and (b) NCD-1/Si (100) samples [Publication III].

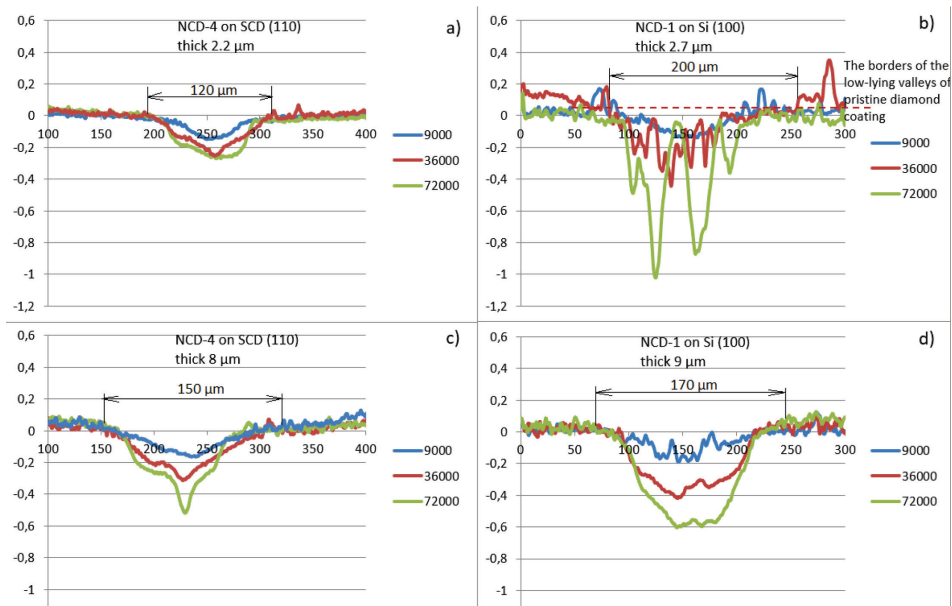


Figure 30. Line scans of wear scars of NCD-3 with 2.2 μm (a) and 8 μm (c) thickness and NCD-1 (100) with 2.7 μm (b) and 9 μm (d) thickness after sliding at contact pressure 1.4 GPa.

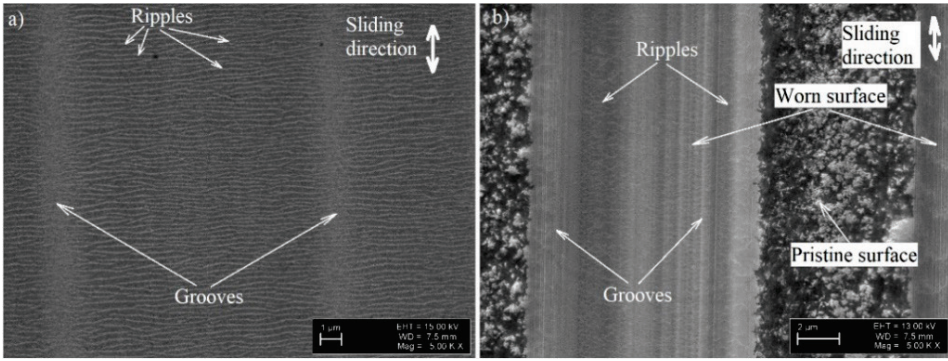


Figure 31. SEM images of the bottom of the wear scar after the test at the contact pressure of 1.4 GPa and distance of 36000 cycles on the 2.2  $\mu\text{m}$  thick NCD-3 (a) (see Fig. 31 a for 36000 cycles) and 2.7  $\mu\text{m}$  thick NCD-1 (b) coatings (see Fig. 31 b for 36000 cycles).

The NCD-3 coating deposited on SCD (110) has a contact pressure of 1.4 GPa at 0.5 N load. In case the sample is growing on the Si (100) substrate, the same contact pressure can be obtained at 2 N load.

The behavior of the CoF is very similar on both types of substrates (Fig. 29). The CoF on samples deposited on Si (100) substrate is stabilized at about 0.14. The same value was observed on the NCD-3 coating after stabilization. For the coatings deposited on SCD (110), the CoF value for the tests with higher contact pressure (2.3 GPa) was also about 0.14.

Profiles of wear scars after the sliding test at the 1.4 GPa contact pressure are shown in Fig. 30. The depth of the wear scar is significantly higher for the diamond films deposited on the Si (100) substrate. Thus, the wear loss volume is higher on the diamond films prepared on the Si (100).

Figure 31 shows the surface morphology of the wear scar after the sliding test at the same contact pressure on 2.2  $\mu\text{m}$  thick NCD-3 (a) and 2.7  $\mu\text{m}$  thick NCD-1 (b) coatings. Ripples and grooves can be observed in both cases. Presence of the pristine surface areas in the case of the NCD-1 coating can provide evidence of film deflection.

Evolution of the loss wear volume versus the number of cycles can be seen in Fig. 32. The wear volume increases with the increase of sliding test duration in both cases.

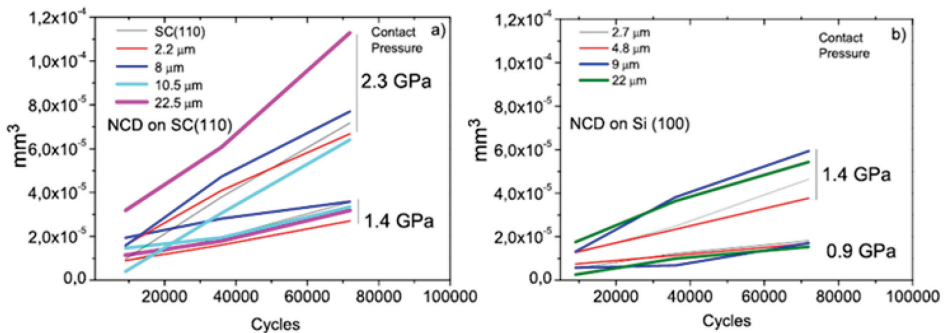


Figure 32. Wear loss volume versus cycles on NCD-1 (100) sample (a) and NCD-3 (110) sample (b) [Publication III].

The graph shows that the value of the loss wear volume on the NCD-3 coating is two times lower than that of NCD-1. Therefore, the substrate properties influence the wear, namely, due to the film deflection, the volume of the wear scar on the Si (100) is larger than on the SCD (110). The deflection was observed on the diamond films deposited on Si (100), see subsection 1.3.4.

### 3.2.5 Analysis of tribological behavior of diamond coatings at high temperature

In subsection 1.3.2, it is assumed that a carbonaceous layer is formed already after run-in. Evidence here is provided by the observation that the average CoF value for a steady state period usually does not strongly differ from the CoF value just after the run-in period. In addition, it was mentioned in the same subsection that the temperature can influence tribological properties due to the oxidation of the surface. The present part of the study focuses on the tribological behavior of diamond coatings at HT. The main goal of the study of wear at elevated temperatures is to obtain data to develop a method of protection of diamond coatings against oxidation attack.

#### NCD-4

The CoF curves recorded during the sliding tests are shown in Fig. 33; samples were tested at room and high temperature. At RT, the run-in period is relatively short, after that CoF value stabilizes at 0.12. Noises and small oscillations can be observed. However, duration of the running-in period increases with the increase of the temperature. CoF value stabilized at 0.35 during the sliding test at 300 °C and 0.4 at 450 °C.

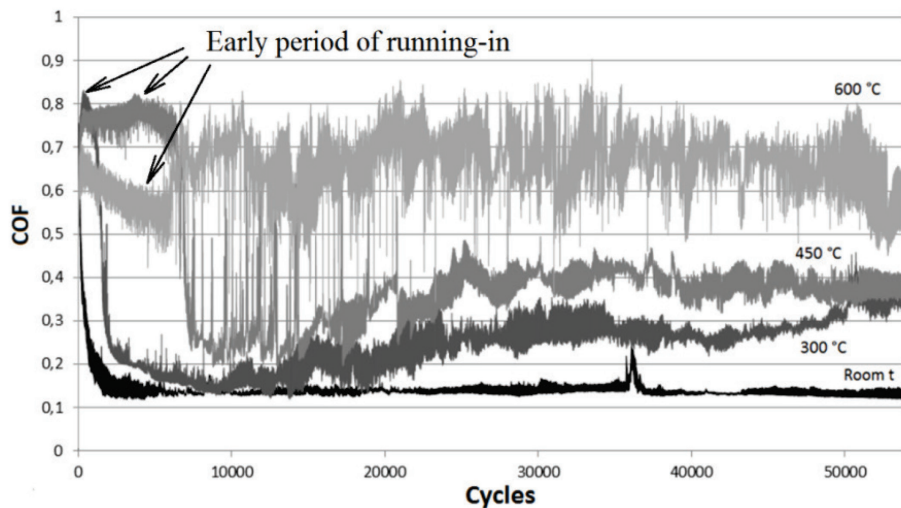


Figure 33. CoF vs the number of cycles curves recorded on the NCD-4 coating at room and elevated temperatures [Publication IV].

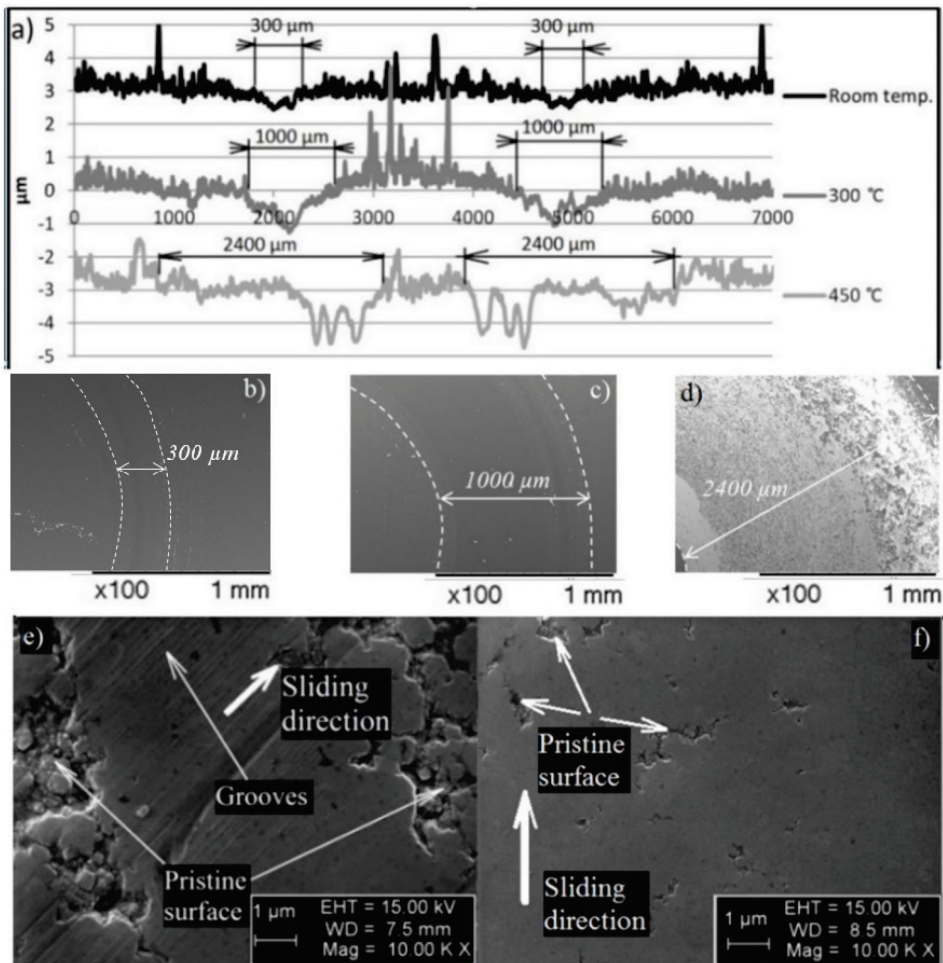


Figure 34. Line scans taken on wear scars (a), SEM images of wear scars after the test at room temperature (b), 300 °C and 450 °C, and bottom of wear scars after tests at room temperature (b) and 450 °C (c) [Publication IV].

Figure 34 a shows line scans and surface morphology of the wear scars. Depth and width of the wear scar increase with the increase of temperature. The shapes of wear scar after the test at RT and 300 °C are similar. However, the shape changed after the sliding test at 450 °C. The deepest part of the wear scar locates at the place closer to the axis of rotation, and the wear scar elongates in the opposite direction. The width of the wear scar increased significantly up to 2000 μm.

Images were taken in the deepest parts of the wear scars (Fig. 34 b – f). In all cases, grooves and islands of the pristine surface of the diamond coatings were observed. It should be noted that the level of the valleys at the bottom of the wear scars is lower than the level of the valleys located out of the wear scar in all cases. Presence of islands of the pristine surface in the bottom of the wear scar can indicate the deflection of NCD-4. Areas of the polished surface increase with the increase of the temperature of the tests. Changes in the behavior of CoF, shape and size of the wear scar can relate to changes in the wear mechanisms with the increase of the temperature. Increase of polished areas

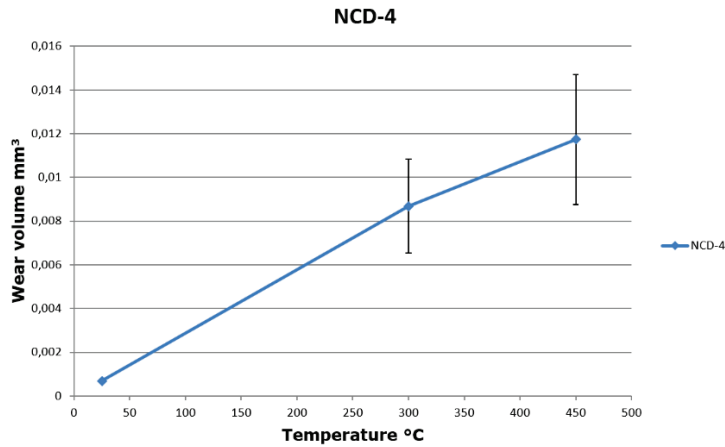


Figure 35. Wear loss volume of the NCD-4 coating versus temperature after the sliding tests at 10 N ( $p_{max} = 1.08$  GPa) and 54000 cycles.

in the bottom of the wear scar can provide evidence of the increase of real wear of the diamond coating. Deflection was observed after the sliding tests and its value increased with the temperature increasing.

Wear loss volume of the NCD-4 coating after the sliding tests at different temperatures was estimated and the results are shown in Fig. 35. Wear volume after the sliding test at RT is one order lower than that at 300 and 450 °C.

#### MCD-2

Figure 36 shows the CoF versus the number of cycle curves. The CoF value recorded after the sliding test at RT decreases after the run-in period and is stabilized at 0.1. With the increase of temperature to 300 °C, an effect of superlubricity is observed. CoF value stabilizes at about 0.006. The highest value of CoF observed during the sliding test is at 450 °C. After a short run-in period, CoF value drops to 0.15 and after 30000 cycles of sliding, CoF increases to 0.2.

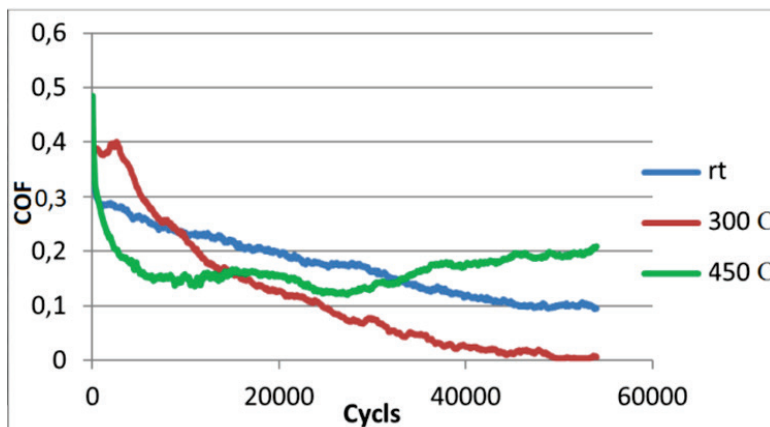


Figure 36. CoF versus the number of cycles recorded on the MCD-2 coating at room and elevated temperatures.

MCD-2 coatings have a relatively large size of diamond grains (see theoretical background), and possess high wear resistance.

Line scans of the wear scars and the surface morphology of MCD-2 coatings are shown in Fig. 37 a. The width of the wear scars did not significantly change with the increase of temperature. Depth of the wear scars after the sliding test at room and 300 °C is about 0.5 μm. However, the depth increases to 0.9 μm after the sliding test at 450 °C. Difference between high levels of peaks in the bottom of the wear scar and valleys of the area out of the wear scar is about 0.3 – 0.4 μm.

After the sliding test at RT, small islands of the polished surface are observed in the bottom of the wear scar (Fig. 37 e, f and g). With the increase of temperature, areas of polished surface increase. However, in the case of the sliding test at 450 °C, an island of the pristine surface can be observed in the bottom of the wear scar. Although the effect of coating deflection cannot be estimated in the sliding test at RT and 300 °C, it has visible influence on the wear scar depth at 450 °C.

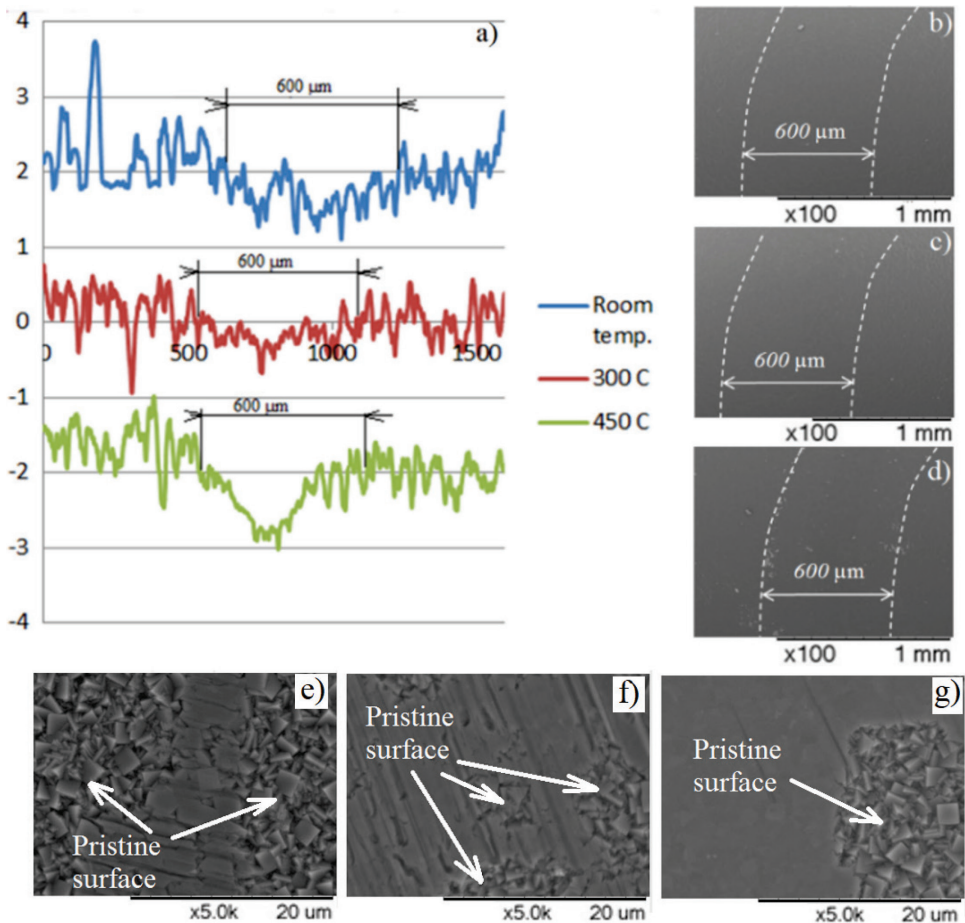


Figure 37. Line scans taken on the wear scars on the MCD-2 coating after room and HT sliding tests (a), SEM images of the wear scars after sliding tests on the MCD-2 coating at RT (b), 300 °C (c) and 450 °C (d) and SEM images of the bottom of the wear scar at RT (e), 300 °C (f) and 450 °C (g).

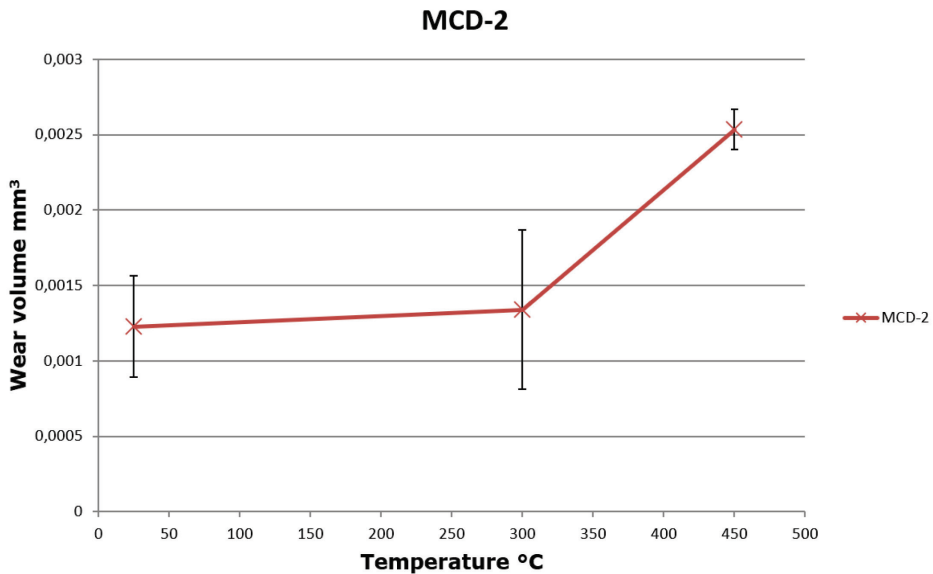


Figure 38. Wear loss volume of MCD-2 versus temperature after the sliding tests at 3 N ( $p_{max} = 1.06$  GPa) and 54000 cycles.

Evolution of the wear loss volume versus the temperature of the sliding test on the MCD-2 coating can be observed in Fig. 38. Its value has no significant difference for results at RT and 300 °C. However, the value of the wear loss volume after sliding at 450 °C is twice higher.

### 3.2.6 Protection of diamond coatings against oxidation attack at high temperature

It was found that the CoF and the wear loss volume increase after the sliding tests at 300 and 450 °C on the NCD-4 and after 450 °C on the MCD-2 coatings. Therefore, a solution is required to protect diamond coatings against oxidation attack and preserve excellent tribological properties of diamond coatings at HT.

$Al_2O_3$  layer was deposited on top of the NCD coating.  $Al_2O_3$  coating was chosen as a barrier layer due to its good mechanical and tribological properties. Rotation unidirectional sliding test at RT, 300 and 450 °C was carried out. A  $Si_3N_4$  ball was used as sliding counterbody. Superlubricity on the NCD and  $Al_2O_3$  /NCD coatings tested at 300 °C was found for the first time with the COF value within the range from 0.004 to 0.04. Width of the wear scars was sufficiently smaller for protected NCD coatings, in contrast to the unprotected NCD coating after the test at 450 °C. XPS analyses showed a difference in the chemical structure of the coating surfaces between the protected and the unprotected NCD coatings after the tests at different temperatures. The wear loss volume observed on the NCD coating coated with the  $Al_2O_3$  layer decreased as compared with unprotected NCD coatings tested at 450 °C. More details can be found in the invention [Publication V].

### 3.2.7 Summary of comparison of tribology behavior of MCD, NCD and DLC coatings

#### Comparison of tribological behavior of NCD-1 and NCD-2

Type of the wear of the NCD coating was estimated after reciprocating sliding tests at room temperature. Tribological behavior was interpreted from the point of view of

self-organization. Increase of the real contact area and the CoF value indicates an adhesive wear regime in the case of the NCD-1 coating. Decrease of the contact area and the CoF value with an increase of test duration was observed during the sliding test on the NCD-2 coating, which corresponds to the abrasive wear.

#### **Comparison of tribological behavior of NCD-1, NCD-3, NCD-4, MCD-1, MCD-2 and DLC at RT**

No evidence of coating deflection was found after sliding on the NCD-3 and the DLC coatings. However, it was observed in the case of NCD-1 and MCD-1 coatings. These variations of tribology behavior can be explained by the difference in the growth process of diamond coatings. Seeding was used only in cases of NCD-1 and MCD-1 coatings. According to previous research (subsection 1.3.3), hard seeding particles penetrate into the substrate, which leads to coating deflection.

Although the contact pressure was lower in the case of the sliding test of the NCD-1 coating than in the case of the MCD-1 coating (1.4 GPa and 1.62 GPa respectively), larger polished areas were observed within the wear scar after sliding on the NCD-1 coating (Fig. 31 b) than in the case of the MCD-1 coating (Fig. 27 c – g). It can be connected with larger diamond grains size of the MCD-1 coating.

#### **Comparison of tribological behavior of NCD-4 with MCD-2 at HT**

The MCD-2 and NCD-4 coatings were tested under HT sliding. The contact pressure was approximately the same in both cases (1.06 GPa for MCD-2 and 1.08 GPa for NCD-4).

Presence of coating deflection was found after sliding at RT, 300 and 450 °C on the NCD-4 coating. However, it was observed only after the wear test at 450 °C on the MCD coating. The reason can be that diamond coatings with large size of diamond grains possess higher stiffness than NCD coatings. Island of the pristine surface in the bottom of the wear scars decreased after the HT sliding tests in both cases. This indicates an increase of the real wear volume of diamond coatings.

Superlubricating behavior (super low CoF value) was found during the sliding test at 300 °C on the MCD-2 coating ( $\mu \approx 0.006$ ). It can be related with the changes within the thin carbonaceous layer on top of the MCD coating (according to subsection 1.3.2). In addition, at HT the passivation of film surface can be changed as well [42]. Although this effect was not found on NCD-4, we do not exclude appearance of this phenomenon under other tests conditions. In addition, changes in the wear mechanisms with increasing temperature occur.

Superlubricity was found on the NCD coating deposited on the Si substrate after sliding at 3 N load and 300 °C (nonpublished) [Publication V].

The influence of temperature was not taken into account in the theoretical part (subsection 3.2.1). It can be expected that at HT chemical reactions occur on the surface of the diamond coatings, which can influence the CoF value and the wear behavior. However, the deflection probably plays some role in the tribological behavior at high temperatures as well.

The method of protection and preservation excellent tribological properties of diamond coatings was developed based on the results of sliding tests at elevated temperatures.

## 4 Conclusions

Different types of diamond coatings were tested under various sliding conditions. The friction and wear are complex phenomena. Initial polishing of diamond grains, passivation of carbon bonds, formation of a tribolayer, coating deflection, etc. are processes occurring during friction and wear. Instabilities during sliding caused by changes in surface roughness, coating deflection, etc. lead to bifurcation behavior, resulting in different sliding regimes during the tests.

The main conclusions are as follows:

1. The abrasive and adhesive wear of diamond coatings were explained based on the self-organization theory. Two characteristic types of CoF curves were observed during sliding. Correlation between the wear mechanisms and changes in the surface morphology within the wear scars, real contact area between counterbodies, coating deflection and CoF behavior were found. Increase of the real contact area and the CoF value indicates an adhesive wear regime. In contrast, decrease of the contact area and the CoF value corresponds to the abrasive wear.
2. Mechanisms of deflection of diamond coatings under sliding were investigated in more detail. It was found that under similar test conditions, the apparent wear loss volume observed on the NCD coatings deposited on SCD (110) substrate is two times lower than in the case of the NCD coating deposited on Si (100). It is explained by the influence of coating deflection caused by the growth process. In the case of the NCD coating deposited on Si (100), the seeding of the Si surface with diamond particles prior to the deposition of NCD coating was used, which results in the penetration of the seeded diamond particles into the Si substrate under high contact pressure.
3. Diamond coating deflection was found after the test at elevated temperature. The magnitude of deflection increases with the temperature increasing. After high temperature sliding, the depth of the wear scar increases three times with the room temperature test in the case of the NCD-4 coating, and twice in the case of the MCD-2 coating. Increase of polished areas within the wear scars after high temperature wear tests indicate an increase in the real wear as compared to tests at room temperature.
4. The effect of superlubricity was observed on the MCD and NCD diamond coatings for the first time ( $\mu \approx 0.006$  in the case of the MCD and  $\mu \approx 0.004 - 0.04$  in the case of the NCD and  $\text{Al}_2\text{O}_3/\text{NCD}$  coatings tested at 300 °C).
5. Deposition of an  $\text{Al}_2\text{O}_3$  layer on top of the diamond coating leads to an improvement of tribological properties at high temperature. After high temperature sliding tests, the CoF value and the wear loss volume are lower than those of an unprotected diamond coating.

## **Future work**

Further development of the self-organization theory and the relation between self-organized criticality (SOC) and self-organization is necessary for better understanding of the wear mechanisms of diamond coatings and other materials.

Further investigation of diamond coating deflection is necessary. The plastic and elastic deformation of thin coatings including carbon based coatings is insufficiently studied. Plastic and elastic deformation within the UNCD coatings is the present research interest.

Future research can focus on the development of methods to preserve excellent tribological properties of diamond coatings against oxygen attack at high temperature.

## References

- [1] I. Reineck; M.E. Sjöstrand, "Diamond coated cutting tools," *International Journal of Refractory Metals and Hard Materials.*, vol. 14, pp. 187–193, 1996.
- [2] A. Bogatov; V. Podgursky; A.T. Raadik; A.R. Kamjula; T. Hantschel; M. Tsigkourakos; P. Kulu, "Investigation of morphology changes on nanocrystalline diamond film surfaces during reciprocating sliding against Si<sub>3</sub>N<sub>4</sub> balls," *Key Engineering Materials*, vol. 604, p. 126–129, 2014.
- [3] V. Podgursky; A. Bogatov; S. Sobolev; M. Viljus; V. Sedov; E. Ashkinazi; V. Ralchenko, "Effect of Nanocrystalline Diamond Films Deflection on Wear Observed in Reciprocating Sliding Tests," *Journal of Coating Science and Technology*, vol. 3, no. 3, p. 109–115, 2016.
- [4] V. Podgursky; T. Hantschel; A. Bogatov; E. Kimmari; M. Antonov; M. Viljus; V. Mikli; M. Tsigkourakos; W. Vandevorst; J.G. Buijnsters, "Rippling on wear scar surfaces of nanocrystalline diamond films after reciprocating sliding against ceramic balls," *Tribology Letters*, vol. 55, p. 493–503, 2014.
- [5] A. Bogatov; M. Viljus; T. Raadik; T. Hantschel; V. Podgursky, "Nanocrystalline Diamond Films Deformation Observed During Sliding Tests against Si<sub>3</sub>N<sub>4</sub> Balls as a Possible Cause for Ripple Formation on Wear Scars Surface," *MATERIALS SCIENCE (MEDŽIAGOTYRA)*, vol. 21, no. 3, pp. 349–352, 2015.
- [6] M. Prokopenko, "Guided self-organization," *Human Frontier Science Program journal*, vol. 3, no. 5, p. 287–289, 2009.
- [7] H.G. Liddell; R. Scott, "Adamas". A Greek-English Lexicon., Perseus Project.
- [8] W. S. Cordua, *The Hardness of Minerals and Rocks*, Lapidary Digest, 1990.
- [9] G. Peschel, *Carbon-Carbon bonds: Hybridization*, 2011.
- [10] R. B. Mathur; B. P. Singh; S. Pande, *Carbon Nanomaterials: Synthesis, Structure, Properties and Applications*, Taylor & Francis, 2017.
- [11] V. Blank; M. Popov; G. Pivovarov; N. Lvova; K. Gogolinsky; V. Reshetov, "Ultrahard and superhard phases of fullerite C<sub>60</sub>: comparison with diamond on hardness and wear," *Diamond and Related Materials*, vol. 7, pp. 427–431, 1998.
- [12] K. Kanda; S. Takehana; S. Yoshida; R. Watanabe; S. Takano; H. Ando; F. Shimakura., "Application of diamond-coated cutting tools," *Surface and Coatings Technology*, vol. 73, no. 1–2, pp. 115–120, 1995.
- [13] M. J. Jackson; L. J. Hyde; W. Ahmed; R. P. Flaxman, "Diamond-Coated Cutting Tools for Biomedical Applications," *Journal of Materials Engineering and Performance*, vol. 13, no. 4, pp. 421–430, 2004.
- [14] L. Wei; P. Kuo; R. Thomas; T. Anthony; W. Banholzer, "Thermal conductivity of isotopically modified single crystal diamond," *PHYSICAL REVIEW LETTERS*, vol. 70, no. 24, p. 3764–3767, 1993.
- [15] J.Y. Howe, *The Oxidation of Diamond*, New York: Alfred University, 2001.
- [16] A. Collins, "The Optical and Electronic Properties of Semiconducting Diamond," *Philosophical Transactions of the Royal Society*, vol. 342, no. 1664, p. 233–244, 1993.

- [17] C. J.H. Wort; R. S. Balmer, "Diamond as an electronic material," *Materials today*, vol. 11, no. 1–2, pp. 22–28, 2008.
- [18] M. Sakamoto; J. G. Endriz; D. R. Scifres, "120 W CW output power from monolithic AlGaAs (800 nm) laser diode array mounted on diamond heatsink," *Electronics Letters*, vol. 28, no. 2, p. 197–199, 1992.
- [19] A. P. Nizovtsev; S. Ya. Kilin; F. Jelezko; T. Gaebel; I. Popa; A. Gruber; J. Wrachtrup, "A quantum computer based on NV centers in diamond: Optically detected nutations of single electron and nuclear spins," *Optics and Spectroscopy*, vol. 99, pp. 233–244, 2005.
- [20] A. Laraoui; H. Aycock-Rizzo; Y. Gao; X. Lu; E. Riedo; C. A. Merilesb, "Imaging thermal conductivity with nanoscale resolution using a scanning spin probe," *Nature Communications*, vol. 20, p. doi: 10.1038/ncomms9954, 2015.
- [21] V. Ralchenko, "Diamond films prepared by Chemical Vapor Deposition," Tallinn University of Technology, Tallinn, 2013.
- [22] G. S. Nusinovich, Introduction to the physics of gyrotrons, JHU Press, 2004.
- [23] L. Pastewka; S. Moser; P. Gumbsch; M. Mosler, "Anisotropic mechanical amorphization drives wear in diamond," *Nature Materials*, vol. 10, pp. 34–38, 2011.
- [24] P. A. Nistor; P. W. May, "Diamond thin films: giving biomedical applications a new shine," *Journal of The Royal Society Interface*, vol. 14, no. 134, p. 20170382.
- [25] A. Bogatov; R. Traksmaa; V. Podgursky, "Changes in Surface Morphology, Deflection and Wear of Microcrystalline Diamond Film Observed During Sliding Tests Against Si3N4 Balls," *Key Engineering Materials*, vol. 674, pp. 145–151, 2016.
- [26] A. R. Krauss; O. Auciello; D. M. Gruen; A. Jayatissa; A. Sumant; J. Tucek; D. C. Mancini; N. Moldovan; A. Erdemir; D. Ersoy; M. N. Gardos; H. G. Busmann; E. M. Meyer; M. Q. Ding, "Ultrananocrystalline diamond thin films for MEMS and moving mechanical assembly devices," *Diamond & Related Materials*, vol. 10, p. 1952–1961, 2001.
- [27] A. Bogatov, Morphological Changes on Diamond and DLC Films During Sliding Wear, Tallinn: TALLINN UNIVERSITY OF TECHNOLOGY, 2015.
- [28] A. Erdemir; G.R. Fenske; A.R. Krauss; D.M. Gruen; T. McCauley; R.T. Csencsits, "Tribological properties of nanocrystalline diamond films," *Surface and Coatings Technology*, vol. 120–121, p. 565–572, 1999.
- [29] B. Bhushan; V.V. Subramaniam; A. Malshe; B.K. Gupta; J. Ruan, "Tribological properties of polished diamond films.," *Journal of Applied Physics*, vol. 74, p. 4174–4180, 1993.
- [30] A. Erdemir; C. Bindal; G. R. Fenske; P. Wilbur, "Tribological properties of hard carbon films on zirconia ceramics," *Tribology Transactions*, vol. 39, p. 735–741, 1996.
- [31] K. Holmberg; H. Ronkainen; A. Laukkanen; K. Wallin, "Friction and wear of coated surfaces — scales, modelling and simulation of tribomechanisms," *Surface & Coatings Technology*, vol. 202, p. 1034–1049, 2007.

- [32] D. W. Wheeler, "Applications of Diamond to Improve Tribological Performance in the Oil and Gas Industry," *Lubricants*, vol. 6, no. 84, 2018.
- [33] A. Erdemir; C. Donnet, "Tribology of Diamond and Diamond-Like Carbon Films: An Overview," in *Wear – Materials, Mechanics and Practice.*, G. W. John Wiley & Sons, 2005, pp. 191–222.
- [34] R. Dumpala; N.Kumar; S. K. Samji; S.Dash; B. Ramamoorthy; M.S. Ramachandra Rao, "Characterization of tribo-layer formed during sliding wear of SiC ball against nanocrystalline diamond coatings," *Materials Characterization*, vol. 95, pp. 252–258, 2014.
- [35] A. R. Konicek; D. S. Grierson; A. V. Sumant; T. A. Friedmann; J. P. Sullivan; P. U. P. A. Gilbert; W. G. Sawyer; R. W. Carpick, "Influence of Surface Passivation on the Friction and Wear Behavior of Ultrananocrystalline Diamond and Tetrahedral Amorphous Carbon Thin Films. 2012 Physical Review B, 85(15).," *Physical Review*, vol. 15, no. 85, p. 155448, 2012.
- [36] L.I. Bershadsky; D.S. Iosebidze; E.R. Kutelia, "Tribosynthesis of graphite-diamond films and its employment for obtaining structurally adaptive coatings," *Thin Solid Films*, vol. 204, no. 2, pp. 275–283, 1991.
- [37] G.S. Fox-Rabinovich; G.E. Totten, *Self-Organization during Friction*, USA: CRC Press: Boca Raton, 2006.
- [38] I. S. Gershman; N. A. Bushe, "Thin films and self-organization during friction under the current collection conditions," *Surface and Coatings Technology*, vol. 186, no. 3, p. 405–411, 2004.
- [39] K. L. Lerner; B. W. Lerner, *World of Earth Science*, Detroit : Thomson-Gale, 2003.
- [40] M. Seal, "Graphitization of Diamond," *Nature*, vol. 185, p. 522–523, 1960.
- [41] T. Evans; P. F. James, "A Study of the Transformation of Diamond to Graphite," *Proceedings of the Royal Society of London. Series A, Mathematical and Physical Sciences*, vol. 277, no. 1369, pp. 260–269, 1964.
- [42] T. Ando; K. Yamamoto; M. Ishii; M. Kamo; Y. Sato, "Vapour-phase oxidation of diamond surfaces in O<sub>2</sub> studied by diffuse reflectance fourier-transform Infrared and temperature-programmed desorption spectroscopy," *Journal of the Chemical Society Faraday Transactions*, vol. 89, no. 19, p. 3635–3640, 1993.
- [43] L. Jaworska; M. Szutkowska; P. Klimczyk; M. Sitarz; M. Bucko; P. Rutkowski; P. Figiel; J. Lojewska, "Oxidation, graphitization and thermal resistance of PCD materials with the various bonding phases of up to 800 °C," *International Journal of Refractory Metals and Hard Materials*, vol. 45, pp. 109–116, 2014.
- [44] A. Zolotukhin; P.G. Kopylov; R.R. Ismagilov; A.N. Obratsov, "Thermal oxidation of CVD diamond," *Diamond and Related Materials*, vol. 19, pp. 1007–1011, 2010.
- [45] L. Xiaowei; R. Jean-Charles; Y. Suyuan, "Effect of Temperature on Graphite Oxidation Behavior," *Nuclear Engineering and Design*, vol. 227, no. 3, pp. 273–280, 2003.
- [46] C. Jaoul; O. Jarry; P. Tristant; T. Merle-Mejean; M. Colas; C. Dublanche-Tixier; J.M. Jacquet, "Raman analysis of DLC coated engine components with complex shape: understanding wear mechanisms," *Thin Solid Films*, vol. 518, p. 1475–1479, 2009.

- [47] Y. Liua; A. Erdemir; E.I. Meletis, "A study of the wear mechanism of diamond-like carbon films," *Surface and Coatings Technology*, vol. 82, no. 1–2, pp. 48–56, 1996.
- [48] Y. Gogotsi; A. Kailer; K. G. Nickel , "Transformation of diamond to graphite," *Nature* , vol. 401, p. 663–664, 1999.
- [49] J. R. Hird; J. E. Field, "A wear mechanism map for the diamond polishing process," *Wear*, vol. 258, p. 18–25, 2005.
- [50] F. M. van Bowelen; J. E. Field; L. M. Brown, "Electron microscopy analysis of debris produced during diamond polishing," *Philosophical Magazine*, vol. 83, no. 7, p. 839–855, 2003.
- [51] F. M. van Bowelen; W. J. P. van Enckevort, "A simple model to describe the anisotropy of diamond polishing," *Diamond & Related Material*, vol. 8, p. 840–844, 1999.
- [52] Q. Zeng; O. Eryilmaz; A. Erdemir, "Superlubricity of the DLC films-related friction system at elevated temperature," *RSC Advances*, vol. 5, p. 93147, 2015.
- [53] A. P. Semenov; M. M. Khrushchov, "Influence of environment and temperature on tribological behavior of diamond and diamond-like coatings," *Journal of Friction and Wear*, vol. 31, pp. 195–218, 2010.
- [54] S. Shimada; H. Tanaka; M. Higuchi; T. Yamaguchi; S. Honda; K. Obata, "Thermochemical wear mechanism of diamond tool in machining of ferrous metals," *CIRP Annals - Manufacturing Technology*, vol. 53, p. 2004, 57–60.
- [55] A. Erdemir; G. R. Fenske, "Tribological Performance of Diamond and Diamondlike Carbon Films at Elevated Temperatures," *Tribology Transactions*, vol. 39, pp. 787–794, 1996.
- [56] M. Herrmann; B. Matthey; T. Gestrich, "Boron-doped diamond with improved oxidation resistance," *Diamond and Related Materials*, vol. 92, pp. 47–52, 2019.
- [57] R. Rani; K. Panda; N. Kumar; A. Kozakov; V. Kolesnikov; A. Sidashov; I-Nan Lin, "Tribological Properties of Ultrananocrystalline Diamond Films: Mechanochemical Transformation of Sliding Interfaces," *Scientific Reports*, vol. 8, pp. 283-299, 2018.
- [58] A. Erdemir; M. Halter; G. R. Fenske; C. Zuiker; R. Csencsits; A. R. Krauss; D. M. Gruen, "Friction and Wear Mechanisms of Smooth Diamond Films During Sliding in Air and Dry Nitrogen," *Tribology Transactions*, vol. 40, pp. 667–675, 1997.
- [59] S. L. Grassie, "Rail corrugation: characteristics, causes and treatments," *Journal of Rail and Rapid Transit*, vol. 223, no. 6, pp. 581–596 , 2009.
- [60] W. Shi; H. Dong; T. Bell, "Tribological behaviour and microscopic wear mechanisms of UHMWPE sliding against thermal oxidation-treated Ti6Al4V," *Materials Science and Engineering A*, vol. 291, pp. 27–36 , 2000.
- [61] A. Socoliuc; E. Gnecco; R. Bennewitz; E. Meyer, "Ripple formation induced in localized abrasion," *Physical review B*, vol. 68, no. 11, pp. 115416-1–4, 2003.
- [62] B. Such; F. Krok; M. Szymonski, "AFM tip-induced ripple pattern on AlIBV semiconductor surfaces," *Applied Surface Science*, vol. 254, pp. 5431–5434, 2008.
- [63] B. Bhusha, *Introduction to Tribology*, New York: John Wiley & Sons, 2002.

- [64] A. Bogatov; M. Yashin; M. Viljus; P. Menezes; V. Podgursky, "Comparative Analysis of Two Methods for Evaluating Wear Rate of Nanocrystalline Diamond Films," *Key Engineering Materials*, vol. 721, pp. 345–350, 2017.
- [65] V. Podgursky; A. Bogatov; V. Sedov; I. Sildos; A. Mere; M. Viljus; J. G. Buijnsters; V. Ralchenko, "Growth dynamics of nanocrystalline diamond films produced by microwave plasma enhanced chemical vapor deposition in methane/hydrogen/air mixture: scaling analysis of surface morphology," *Diamond and Related materials*, vol. 58, pp. 172–179, 2015.
- [66] O. A. Williams; O. Douheret; M. Daenen; K. Haenen; E. Osawa; M. Takahashi, "Enhanced diamond nucleation on monodispersed nanocrystalline diamond," *Chemical Physics Letters*, vol. 445, pp. 255–258, 2007.
- [67] F. Ericson; J.A. Schweitz., "Micromechanical fracture strength of silicon," *Journal of Applied Physics*, vol. 68, p. 5840–5844, 1990.
- [68] P.W. May, "Diamond thin films: a 21st-century material," *Philosophical Transactions of The Royal Society A Mathematical Physical and Engineering Sciences*, vol. 358, no. 1766, pp. 473–495, 2000.
- [69] B. Dischler; C. Wild, *Low-Pressure Synthetic Diamond Manufacturing and Applications*, Berlin: Springer-Verlag, 1998.
- [70] S. Koizumi; C. Nebel; M. Nesladek, *Physics and Applications of CVD Diamond*, Wiley-VCH Verlag GmbH & Co. KGaA, 2008.
- [71] R. Andrievskii, "Silicon nitride: synthesis and properties," *Russian Chemical Reviews*, vol. 64, pp. 291–308, 1995.
- [72] K. L. Johnson, "Normal contact of elastic solids: Hertz theory," in *Contact mechanics*, 1985, Cambridge University Press, 1985, pp. 84–106.
- [73] J. G. Buijnsters; L. Vázquez, "Growth Dynamics of Nanocrystalline Diamond Thin Films Deposited by Hot Filament Chemical Vapor Deposition: Influence of Low Sticking and Renucleation Processes," *The Journal of Chemical Physics*, vol. 115, p. 9681–9691, 2011.
- [74] M. Castro; R. Cuerno, M. Nicoli; L. Vazquez; J.G. Buijnsters, "Universality of cauliflower-like fronts: from nanoscale thin films to macroscopic plants," *New Journal of Physics*, vol. 14, pp. 103039-1–103039-15, 2012.
- [75] J.G. Buijnsters; L. Vazquez, "Growth dynamics of nanocrystalline diamond films deposited by hot filament chemical vapor deposition: influence of low sticking and renucleation processes," *The Journal of Chemical Physics*, vol. 115, p. 9681–9691, 2011.
- [76] A. L. Barabasi; H.E. Stanley, *Fractal Concepts in Surface Growth*, Cambridge: Cambridge University Press,, 1995.
- [77] M. Nicoli; M. Castro; R. Cuerno, "Unified moving-boundary model with fluctuations for unstable diffusive growth," *Physical Review*, vol. 78, pp. 021601-1–021601-17, 2008.
- [78] P. A. Orrillo; S. N. Santalla; R. Cuerno; L. Vázquez; S. B. Ribotta; L. M. Gassa; F. J. Mompean; R. C. Salvarezza; M. E. Vela, "Morphological stabilization and KPZ scaling by electrochemically induced co-deposition of nanostructured NiW alloy films," *Scientific Reports*, vol. 7, p. 17997, 2017.

- [79] B.C. Mohanty; H.R. Choi; Y.S. Cho, "Fluctuations in global surface scaling behavior in sputter-deposited ZnO thin films," *Europhysics Letters*, vol. 93, pp. 26003-p1–26003-p6, 2011.
- [80] J.M. Lopez; M. Castro; R. Gallego, "Scaling of local slopes, conservation laws, and anomalous roughening in surface growth," *Physical Review Journals*, vol. 94, pp. 166103-1–166103-4., 2005.
- [81] H. Haken , *Synergetics: an approach to self-organization*. In *Self-Organizing Systems*, New York: Ed., Yates, F.E. Plenum Press, 1987 .
- [82] B.E. Klamecki, "An entropy-based model of plastic deformation energy dissipation in sliding," *Wear*, vol. 96, p. 319–329, 1984.
- [83] B.I. Kostetsky, "An evolution of the materials' structure and phase composition and the mechanisms of the self-organizing phenomenon at external friction," *Friction and Wear*, vol. 14, no. 4, p. 773–783, 1993.
- [84] N.A. Bushe; V.V. Kopitko, *Compatibility of Rubbing Surfaces*, Moscow: Science, 1981.
- [85] L.I. Bershadsky, "On self-organizing and concept of tribosystem self-organizing," *Friction and Wear*, vol. 8, no. 6, p. 1077–1094, 1992.
- [86] G. S. Fox-Rabinovich; I. S. Gershman; K. Yamamoto; A. Biksa; S. C. Veldhuis; B. D. Beake; A. I. Kovalev, "Self-Organization during Friction in Complex Surface Engineered Tribosystems," *Entropy*, vol. 12, pp. 275–288, 2010.
- [87] G. Fox-Rabinovich; G. E. Totten, *Self-Organization During Friction: Advanced Surface-Engineered Materials and Systems Design*, CRC Press, 2007.
- [88] Y. Demirel, *Nonequilibrium Thermodynamics Transport and Rate Processes in Physical, Chemical and Biological Systems*, Lincoln, USA: Copyright © 2014 Elsevier B.V. All rights reserved, 2014.
- [89] M. Nosonovsky; V. Mortazavi, *Friction-Induced Vibrations and Self-Organization*, FL, USA: CRC Press: Boca Raton, 2014.
- [90] I. Prigogine; D. Kondepudi, *Modern Thermodynamics*, NY, USA: John Wiley & Sons: New York, 1999.
- [91] M. Nosonovsky; B. Bhushan, "Dissipative Mechanisms and Hierarchical Surfaces Friction," in *Superhydrophobicity and Biomimetic*, Germany, Springer: Berlin/Heidelberg, 2008, p. 13–47.
- [92] J.A. Greenwood; J.B.P. Williamson, "Contact of normally flat surfaces," *Proceedings of the Royal Society A*, vol. 295, p. 300–319, 1966.
- [93] R. Stark; G. Schitter; A. Stemmer, "Velocity dependent friction laws in contact mode atomic force microscopy," *Ultramicroscopy*, vol. 100, p. 309–317, 2004.
- [94] J.R. Hird; J.E. Field, "Diamond polishing," *Proceedings of the Royal Society A*, vol. 460, p. 3547–3568, 2004.
- [95] S.E. Grillo; J.E. Field; F.M. Van Bouwelen, "Diamond polishing: The dependency of friction and wear on load and crystal orientation," *Journal of Physics D*, vol. 33, pp. 1–6, 2000.
- [96] M. Nosonovsky, B. Bhushan, "Multiscale friction mechanisms and hierarchical surfaces in nano- and bio-tribology," *Materials Science & Engineering R*, vol. 58, p. 162–193, 2007.

- [97] E.I. Gershman; A.E. Mironov; G.S. Fox-Rabinovich; S.C. Veldhuis, "Application of the SelfOrganization Phenomenon in the Development of Wear Resistant Materials — A Review," *Entropy*, vol. 18, p. 385, 2016.
- [98] G. Fox-Rabinovich; S.C. Veldhuis; A.I. Kovalev; D.L. Wainstein; I.S. Gershman; S. Korshunov; L.S. Shuster; J.L. Endrino, "Features of self-organization in ion modified nanocrystalline plasma vapor deposited AlTiN coatings under severe tribological conditions," *Journal of Applied Physics*, vol. 102, p. 074305, 2007.
- [99] M. Nosonovsky; B. Bhushan, "Thermodynamics of surface degradation, self-organization and self-healing for biomimetic surfaces," *Philosophical Transactions of the Royal Society A*, vol. 367, p. 1607–1627, 2009.
- [100] C.S. Abreu; M. Amaral; A.J.S. Fernandes; F.J. Oliveira; R.F. Silva; J.R. Gomes, "Friction and wear performance of HFCVD nanocrystalline diamond coated silicon nitride ceramics," *Diamond and Related Materials*, vol. 15, p. 739–744, 2006.
- [101] A. Erdemir; C. Donnet, "Tribology of Diamond, Diamond-Like Carbon, and Related Films," in *Modern Tribology Handbook*, CRC Press LLC: Boca Raton, 2001, p. 871–909.
- [102] V. Mortazavi; M. Nosonovsky, "Wear-Induced Microtopography Evolution and Wetting Properties of SelfCleaning, Lubricating and Healing Surfaces," *Journal of Adhesion Science and Technology*, vol. 25, no. 12, p. 1337–1359, 2011.

## Acknowledgements

First, I wish to express my special gratitude to my supervisor Senior Research Scientist Vitaly Podgursky for his continuous support, guidance and encouragement in my PhD work in Tallinn University of Technology.

I would like to express my very great thanks to Senior Research Scientist Maksim Antonov, Engineer Andrey Bogatov and PhD Janis Baronins for their research cooperation in tribology of diamond coatings and organization of wear tests.

My special acknowledgement goes to PhD Mart Viljus for the help with SEM measurements and Technician Heinar Vagiström for help with sample preparation.

In addition, I am grateful to Professor Ľubomír Čaplovič and PhD Martin Sahul for providing me an opportunity to carry out of part of my research at Slovak University of Technology in Bratislava (STU).

I also want to thank every single person of my teachers at Tallinn University of Technology, especially to Professor Priit Kulu and Professor Fjodor Sergejev for the help with the preparation of my PhD thesis.

Finally, I would like to thank my family and friends for their everyday support and encouragement, especially my friend Galina Kiseleva.

This study was supported by the Estonian Ministry of Education and Research under financing projects PUT 1369 "Adaptation mechanisms of diamond films in dry sliding wear", IUT19-29 "Multi-scale structured ceramic-based composites for extreme applications (1.01.2014–31.12.2019)" and Estonian Research Council project IUT19-4.

## **Abstract**

# **Adaptive Wear Mechanisms of Diamond Coatings at Room and High Temperatures**

High hardness and wear resistance, low coefficient of friction and chemical inertness are the key properties of diamond coatings that enable a wide range of tribology applications. One of the main applications is protection of cutting tools in the engineering industry.

Previous studies in Tallinn University of Technology have revealed the formation of a carbonaceous layer, ripples and grooves patterns on the wear scars surface and deflection of diamond coatings. These results indicate self-organization during the friction. Theoretical basis of self-organization and wear mechanisms of diamond coatings is necessary for deeper understanding of excellent tribological properties of the diamond coatings. In addition, effective protection of cutting tools is required for high temperature applications of the coatings. Therefore, the present PhD work deals with tribological investigation of MCD and NCD coatings at room and high temperature sliding, development of the self-organization theory within the nonequilibrium thermodynamical approach and investigation of diamond coating deflection.

The main goals of the present study were: a) understanding of friction and wear processes of diamond coatings based on the self-organization theory, b) investigation of the effect of the substrate and temperature on coating deflection and c) development of a method for protection of diamond coating against oxidation at high temperatures.

Diamond coatings were grown by the MWPECVD method on Si and hard metal substrates. Raman spectra, XRD, SEM, AFM, optical microscopy and mechanical profilometry were used for the analysis of the results of sliding tests.

As a result of the present research, the wear behavior of diamond coatings was interpreted from the point of view of self-organization. Interconnection between the change of the real contact area, surface roughness, coating deflection, behavior of CoF and adhesive and abrasive wear was found. Conditions of occurrence of adhesive and abrasive wear were identified.

The mechanisms of coating deflection were investigated. It was found that part of apparent wear volume of the diamond coating is due to deflection. Correlation between growth mechanisms of diamond coatings and coating deflection was confirmed.

The wear loss volume measured after sliding at elevated temperature on MCD and NCD coatings increases in contrast to the results at room temperature. A super low CoF value (superlubricating behavior) was found after high temperature wear tests on MCD and NCD coatings. The deflection was found on both coatings after the tests at high temperature as well.

The effective method for protection and preservation of the tribology properties of diamond coatings under high temperature sliding was developed. Deposition of  $\text{Al}_2\text{O}_3$  layer on top of a diamond coating leads to a decrease in the wear loss volume and CoF value in comparison with unprotected coating.

## Lühikokkuvõte

### Teemantpinnete adaptiivkulumise mehhanismid toa- ja kõrgendatud temperatuuridel

Teemantpinnete suur kõvadus, hea kulumiskindlus ja madal hõõrdekoefitsient on nende võtmeomadused, võimaldades neid kasutada laialdaselt triboloogilistes rakendustes. Üheks teemantpinnete põhiliseks kasutusalaaks masinaehituses on lõikeriistad.

Varasemad uuringud TTÜ-s puudutavad süsinikku sisaldavate kihtide moodustumist, kulumisel lainete ja vagude teket pinnal ja teemantpinnete läbipainet. Saadud tulemused osutasid pinde iseseadustumisele hõõrdumisel. Teemantpinnete pinna iseseadustumise teoreetilised alused ja kulumise mehhanismid on vajalikud pinnete triboloogiliste omaduste sügavamaks mõistmiseks. Lisaks sellele on lõikeriistade efektiivse kaitse vajalik tööks pinnete korral kõrgtemperatuursetes kasutustes. Käesolev doktoritöö käsitleb mikro-(MCD) ja nanokristalsete (NCD) teemantpinnete tribouuringuid toa- ja kõrgendatud temperatuuridel, nende iseseadustumist lähtudes mittetasakaalulisest termodünaamilisest käsitlusest ja teemantpinnete läbipaindest.

Töö eesmärkideks oli a) hõõrdumisel ja kulumisel aset leidvate protsesside mõistmine lähtudes iseseadustumise teooriast, b) selgitada välja alusmaterjali ja temperatuuri mõju kulumisel pinde läbipainele ja c) arendada meetodit teemantpinde kaitseks oksüdatsiooni vastu kõrgetel temperatuuridel.

Teemantpinned saadi mikrolaine-plasmakeemilise sadestuspindmise (MWPECVD) teel ränialusele. Liugekulumise katsete tulemuste uuringutes kasutati Raman spetroskoopiat, XRD, SEM, AFM meetodeid, optilist mikroskoopiat ja mehaanilist profilomeetriat. Teemantpinnete käitumist kulumisel interpreteeriti iseseadustumise seisukohalt. Leiti seosed reaalse kontaktpinna, pinnakareduse, pinde läbipainde ja hõõrde teguri vahel adhesiiv- ja abrasiivkulumisel. Määratleti tingimused adhesiiv- ja abrasiivkulumise ilmnemiseks.

Uuriti teemantpinnete läbipainde mehhanisme. Leiti, et nähtav kulumine on tingitud teemantpinde läbipaindest. Leidis kinnitust korrelatsioon pinde kasvumehhanismi ja läbipainde vahel. Kõrgtemperatuurisel liugekulumisel mõõdetud pinnete (MCD ja NCD pinded) mahuline kulum suurenes võrreldes tulemustega toatemperatuuril. MCD ja NCD pinnete korral täheldati kõrgtemperatuursetel kulumiskatsetel eriti madalat hõõrdekoefitsienti. Pinnete läbipaine kõrgendatud temperatuuril kulumiskatsetel leidis aset mõlema pinde korral.

Töö tulemusena selgitati välja kulumise mehhanismid, võimalik läbipaine nii toa- kui kõrgtemperatuursetel kulumisel ja supermäärimise ilming, arendati välja efektiivne moodus triboomaduste tagamiseks kõrgtemperatuursete liugekulumise tingimustes. Alumiiniumoksiidpinde ( $Al_2O_3$ ) sadestamine pealmise kihina tõi kaasa mahulise kulumi ja hõõrde teguri väärtuste vähenemise võrreldes mittekäetud pinnaga.

## Appendix

### Publication I

V. Podgursky; A. Bogatov; **M. Yashin**; S. Sobolev; J. S. Gershman, Relation between Self-Organization and Wear Mechanisms of Diamond Films. *Entropy*, 20 (4) (2018) 279–295.

Article

# Relation between Self-Organization and Wear Mechanisms of Diamond Films

Vitali Podgursky <sup>1,\*</sup> , Andrei Bogatov <sup>1</sup>, Maxim Yashin <sup>1</sup>, Sergey Sobolev <sup>2</sup> and Iosif S. Gershman <sup>3</sup> 

<sup>1</sup> Department of Mechanical and Industrial Engineering, Tallinn University of Technology, Ehitajate tee 5, 19086 Tallinn, Estonia; andrei.bogatov@mail.ru (A.B.); mayash@ttu.ee (M.Y.)

<sup>2</sup> Department of Mechanical Engineering, Gubkin Russian State University of Oil and Gas, Leninsky Prospect 65, 119991 Moscow, Russia; sobolev.ceo@gmail.com

<sup>3</sup> Joint Stock Company Railway Research Institute, Moscow State Technological University “Stankin” (MSTU “STANKIN”), 3rd Mytischinskaya Street 10, 129851 Moscow, Russia; isgershman@gmail.com

\* Correspondence: vitali.podgurski@ttu.ee; Tel.: +372-620-3358

Received: 1 February 2018; Accepted: 10 April 2018; Published: 13 April 2018



**Abstract:** The study deals with tribological properties of diamond films that were tested under reciprocal sliding conditions against Si<sub>3</sub>N<sub>4</sub> balls. Adhesive and abrasive wear are explained in terms of nonequilibrium thermodynamic model of friction and wear. Surface roughness alteration and film deformation induce instabilities in the tribological system, therefore self-organization can occur. Instabilities can lead to an increase of the real contact area between the ball and film, resulting in the seizure between the sliding counterparts (degenerative case of self-organization). However, the material cannot withstand the stress and collapses due to high friction forces, thus this regime of sliding corresponds to the adhesive wear. In contrast, a decrease of the real contact area leads to the decrease of the coefficient of friction (constructive self-organization). However, it results in a contact pressure increase on the top of asperities within the contact zone, followed by material collapse, i.e., abrasive wear. Mentioned wear mechanisms should be distinguished from the self-lubricating properties of diamond due to the formation of a carbonaceous layer.

**Keywords:** self-organization; tribology; diamond films

## 1. Introduction

Friction and wear mechanisms were intensively investigated in the past. Three laws of friction state that a friction force ( $F$ ) depends linearly on the normal load ( $W$ ) and does not depend on the nominal area of contact and velocity ( $V$ ). These laws can be also formulated as dynamical coefficient of friction (COF) independence of applied normal load, nominal area of contact, and velocity [1].

The real contact area ( $A$ ) is a key parameter for tribological characterization. The real contact area is only a fraction of the nominal contact area, since contacts occur only on top of asperities. The linearity of Amontons friction law  $F = \mu W$  ( $\mu$ —coefficient of friction) is a consequence of the fact that the real contact area is almost directly proportional to the applied normal load. The linear dependence of the real contact area on the small normal load was shown theoretically by Greenwood and Williamson [2] for Gaussian and by Bush et al. [3,4] for randomly rough surfaces, respectively. It was suggested by Bowden and Tabor [5] that  $F = \tau A$ , where  $\tau$  is shear strength due to adhesion on the interface. In practice, friction is nonlinear in nature. For instance, it was shown that the COF can depend on the sliding velocity, load, and contact area [1,6–10].

By definition, the adhesive and abrasive wear are related to the concept of the real contact area. The larger real contact area between the sample and counterbody (other things being equal) leads

to stronger adhesion between bodies, thus to the stronger adhesive wear. Hardness is the important material property for the understanding of the abrasive wear, it is characteristic of material to withstand the stress without plastic deformation. Material with the higher hardness experiences lower abrasive wear. However, the amount of stress in the material body depends on the real contact area and the applied load.

The nonlinear character of friction can be described by nonequilibrium thermodynamics [11,12]. Theory predicts conditions that can lead to self-organization, which can reduce wear. The definition and physical meaning of self-organization relate to the formation of dissipative structures [11–13]. These are stationary processes leading to the negative excessive entropy production [11,14,15]. Elastodynamic, thermoelastodynamic, etc. instabilities can trigger the formation of dissipative structures [12,13]. Wear is one of the many processes occurring during sliding. The energy that is induced by friction can be consumed by other processes, thus reducing the wear rate [14]. The entropy production ( $\partial S/\partial t$ ), i.e., a rate of change in entropy due to processes that are occurring within the tribological system, can be written as follows:

$$\partial S/\partial t = JX, \quad (1)$$

where thermodynamic flow  $J = \mu WV$ , thermodynamic force  $X = \mu WV/(\lambda T^2 A)$ , entropy ( $S$ ), time ( $t$ ), temperature ( $T$ ), and heat conductivity ( $\lambda$ ) [11,15]. It is assumed that the work by friction force  $F = \mu W$  is  $\mu WV$  per unit time, which dissipates within the thin contact layer. The derivation of thermodynamic flow and force for frictional sliding can be found elsewhere [15,16].

The stability conditions for the thermodynamic system can be analyzed using the Lapunov's function  $\delta^2 S$  (where  $\delta^2 S$  is the second variation of entropy). Self-organization can occur in the system if inequality  $\partial/\partial t (\delta^2 S) \geq 0$  is not fulfilled. The next equation shows how the calculation of this derivative can be simplified [11,16]:

$$\frac{\partial}{\partial t} (\delta^2 S) = \frac{1}{2} \delta^2 \left( \frac{(\mu WV)^2}{\lambda T^2 A} \right) = \delta X \delta J = \delta(\mu WV) \delta \left( \frac{\mu WV}{\lambda T^2 A} \right) \geq 0. \quad (2)$$

In other words, only variations of thermodynamic flow and force must be evaluated in order to estimate the variation of entropy.

Wear of diamond is a velocity- and load-dependent process [9,10]. In the case of sliding in the air, the chemical passivation of dangling carbon bonds by species from ambient environment decreases COF [17–20]. Tribological behavior of diamond films during running-in is affected by the initial roughness of contacting bodies. Higher surface roughness results in higher initial friction with a following decrease of COF value due to surface smoothing [21–23]. In addition, stress-induced mechano-chemical formation of the carbonaceous lubricating layer takes places already at the beginning of running-in, leading to a decrease of COF value as well [21–27]. In spite of the counterbodies smoothing and formation of carbonaceous layer, the different types of COF curves were observed after the tests on diamond films. An increase of the COF value at the beginning of sliding was found in the tests with a larger normal load on the thicker films [28,29] and on the thinner films with the same normal load [30], which indicates the importance of stress and deformation to explain the tribological behavior of diamond films.

The present review is based on the analysis of deflection phenomenon on diamond films investigated in our recent studies [31–35]. The deflection is considered as a plastic deformation of the whole film within contact zone and it should be distinguished from the plastic deformation of the asperities [36]. Diamond is a brittle material, thus the fracture of asperities can occur [1]. The origin of deflection phenomenon can be the film/substrate structure and film bending (elastic and plastic deformation) during sliding [31,32]. The film deflection increases with an increasing of the test duration and normal load and can be explained in terms of fatigue [31].

The study aims to estimate the variation of the real contact area with the film bending and surface roughness alteration and interpret tribological behavior of diamond films by means of self-organization.

## 2. Materials and Methods

The tribological system that is under investigation can be viewed as a thin hard film (diamond film) on a softer substrate (Si, WC-Co). Two types of diamond films (nanocrystalline diamond (NCD), microcrystalline diamond (MCD)) were investigated, see for details our publications [26,31–35,37,38]. The NCD films were grown under different conditions, therefore they are abbreviated by NCD-1 [31,32,37], NCD-2 [26,38] and NCD-3 [33]. The thickness of the NCD films was as follows: 4.8, 9 and 22  $\mu\text{m}$  (NCD-1) and 0.8  $\mu\text{m}$  (NCD-2, NCD-3). The thickness of MCD films was 5  $\mu\text{m}$ . The films were characterized by Raman spectroscopy, optical microscopy, atomic force microscopy (AFM), scanning electron microscopy (SEM), and mechanical profilometry. The reciprocal sliding tests [26,39] were carried out at room temperature in ambient air using  $\text{Si}_3\text{N}_4$  balls. The frequency varied between 2–10 Hz and normal load between 0.5–3 N. ISO 3D parameter Surface Area Ratio (Sdr) was used in the current research to characterize the contact area between the ball and the film. Sdr is defined as the increment of the total (nominal) surface area relative to the sampling area in the XY (surface) plane.

## 3. Theoretical Background

The real contact area between the counterparts changes during sliding due to the variation of the local roughness (wear of material), deformation of the contacting surfaces, etc. In general, the influence of each of the mentioned factors on the real contact area can be described by introducing parameters  $\psi_1$ ,  $\psi_2$ , etc. [11]. In the present study, for the sake of simplicity, parameter  $\psi$  corresponds to either the diamond film deformation or surface roughness. It is assumed that  $\mu$  and  $A$  depend on the parameter  $\psi$ , as follows:  $\mu = \mu(\psi)$  and  $A = A(\psi)$ . By varying parameter  $\psi$  in inequality (2), we end up with:

$$\frac{\partial}{\partial t} (\delta^2 S) = \frac{(WV)^2}{\lambda(TA)^2} \left[ \left( \frac{\partial \mu}{\partial \psi} \right)^2 A - \frac{\partial \mu}{\partial \psi} \frac{\partial A}{\partial \psi} \mu \right] (\delta \psi)^2 \geq 0. \quad (3)$$

Self-organization can occur if inequality (3) is not fulfilled, i.e., the second term in the square brackets is positive. There are only four cases with the positive second term:

1. Case 1: If derivative  $\partial A/\partial \psi$  is positive ( $\psi$  increases,  $A$  increases),  $\partial \mu/\partial \psi$  must be positive (as  $\psi$  increases  $\mu$  must increase).
2. Case 2: If derivative  $\partial A/\partial \psi$  is positive ( $\psi$  decreases,  $A$  decreases),  $\partial \mu/\partial \psi$  must be positive (as  $\psi$  decreases  $\mu$  must decrease).
3. Case 3: If derivative  $\partial A/\partial \psi$  is negative ( $\psi$  decreases,  $A$  increases),  $\partial \mu/\partial \psi$  must be negative (as  $\psi$  decreases  $\mu$  must increase).
4. Case 4: If derivative  $\partial A/\partial \psi$  is negative ( $\psi$  increases,  $A$  decreases),  $\partial \mu/\partial \psi$  must be negative (as  $\psi$  increases  $\mu$  must decrease).

Cases 1 and 3 correspond to a situation when the real contact area can infinitely increase up to the instant when counterbodies stick together. Thus, a seizure can be considered as an effect that reduces wear (unconstructive self-organization) [11,14]. In practice, it is not always observed that counterbodies tend to stop moving. The cohesive bonding between the atoms can be broken by induced stress, therefore adhesive wear occurs and a morphology of contact surfaces changes instantly. In other words, an indication of adhesive wear regime in the test might be the COF increase. On the other hand, Cases 2 and 4 correspond to the situation when the real contact area can decrease up to a fictional loss of contact between sliding counterbodies, resulting in COF and wear decrease (constructive self-organization). At a certain instant, the pressure on certain contact points strongly

increases, causing material collapse. The harder material can withstand higher stress than softer one, therefore Cases 2 and 4 can correspond to the abrasive wear. In analogy with the adhesive wear, the COF decrease can be associated with the abrasive wear.

The application of obtained inequality (3) to the analysis of the experimental data can be hampered due to the estimation of the behavior of  $\psi$ ,  $\mu$  and  $A$  parameters, as they can vary during the different stages of sliding.

#### 4. Results and Discussions

Two typical COF versus cycles curves (with some variations) were observed in sliding tests with NCD [26,31,33,38] and MCD [34,35] films (Figure 1). The shape and length of stages 1–3 and I–IV can vary for the tests that are performed on the same sample under the same test conditions. Stage IV was observed in the COF curve of type 1, which corresponds to the steady state regime of sliding. The COF curve of type 2 corresponds to the running-in regime of sliding.

Figure 2 shows the COF versus cycles curves taken on the 4.8  $\mu\text{m}$  thick NCD-1 film. The shape of the curve after the test with 72,000 cycles is similar to the shape of type 2 curve (Figure 1). The surface morphology of the  $\text{Si}_3\text{N}_4$  balls after the tests with 9000 and 36,000 cycles (0.5 N, 5 Hz) and 72,000 cycles (2 N, 5 Hz) is shown in Figure 3. Circles (dashed lines) are shown as a guide for eyes.

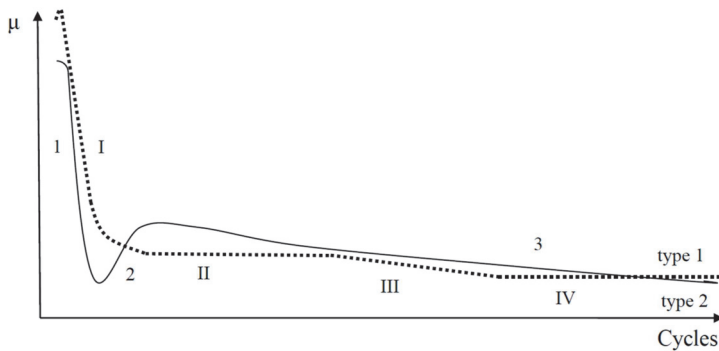


**Figure 1.** Schematics of two types of coefficient of friction (COF) versus cycles curves observed during reciprocation sliding wear test on diamond films.

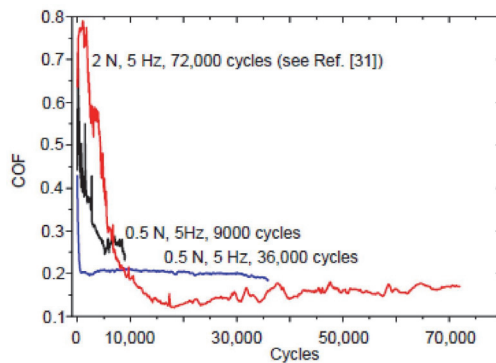


**Figure 2.** COF versus cycles curves taken on the 4.8  $\mu\text{m}$  thick nanocrystalline diamond (NCD)-1 film.

The surface of the ball after 9000 cycles is considerably smoother than that after 36,000 cycles, namely no grooves and scratches were observed. A stripe-like area and two semicircle-like areas are marked by I and II on the ball surface, respectively. The morphological patterns on the ball surface for both of the areas look the same (Figure 3a). However, the patterns within the areas I and II look differently after the test with 36,000 cycles (Figure 3b), indicating the dissimilarity of wear regimes at the different parts of the ball. This can mean that real contact areas between the ball and film within the areas I and II are different, due to the difference in surface morphology. In other words, single type of wear regime dominates for the test with 9000 cycles of sliding, and for the longer tests (36,000 cycles), a differentiation of wear mechanisms occurs, namely at least two types of wear regimes can be distinguished. The width of the area I increases steadily from 70 to 120  $\mu\text{m}$  (Figures 3 and 4).

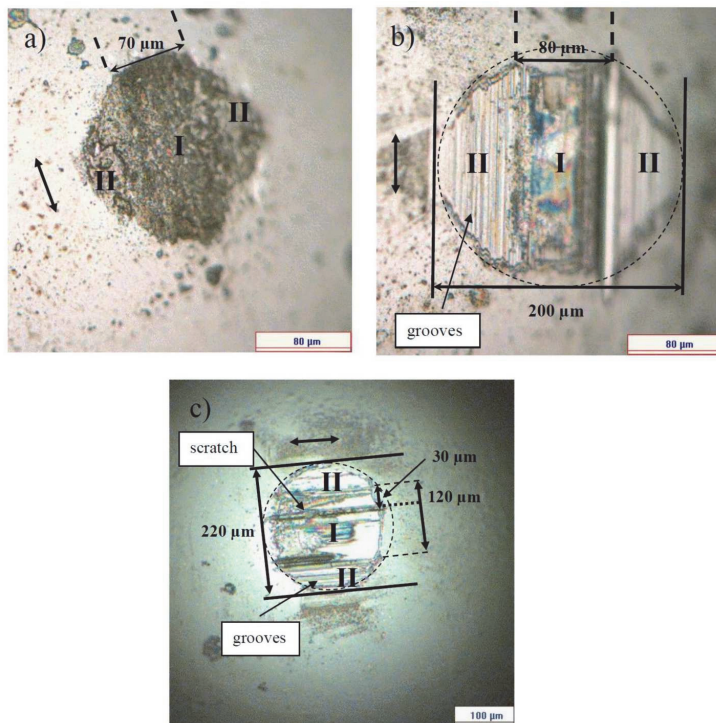
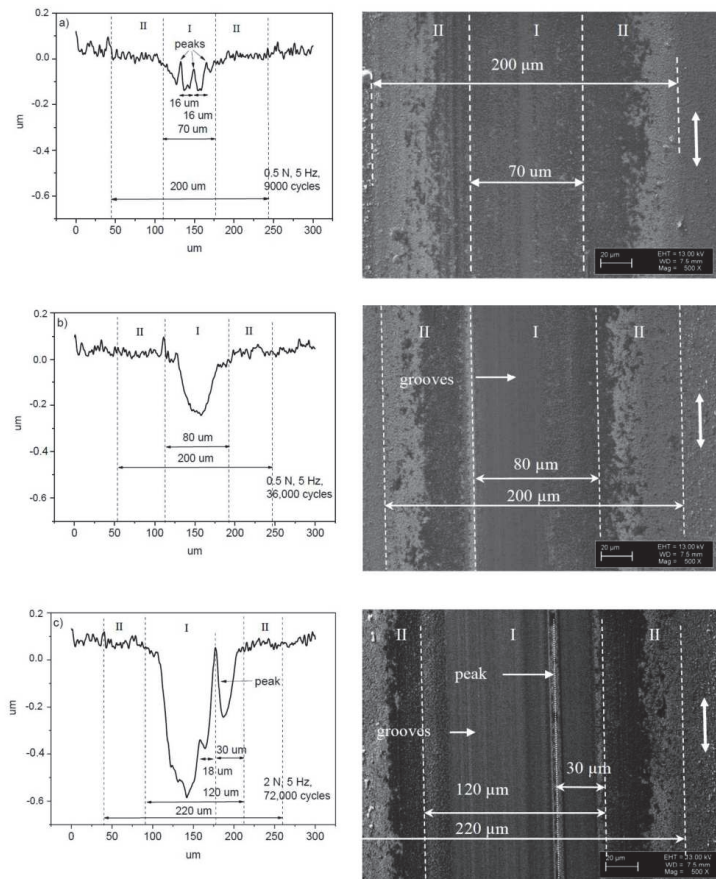


**Figure 3.** Surface morphology of the Si<sub>3</sub>N<sub>4</sub> balls after the sliding wear tests on the 4.8  $\mu\text{m}$  thick NCD-1 film. The test parameters were as follows: (a) 0.5 N, 5 Hz, 9000 cycles; (b) 0.5 N, 5 Hz, 36,000 cycles; and, (c) 2 N, 5 Hz, 72,000 cycles.

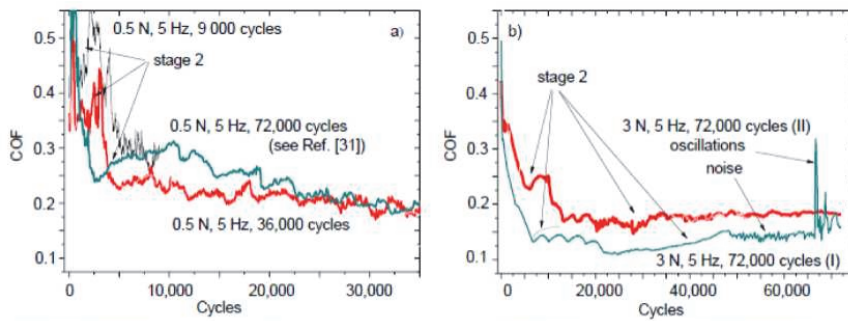
Figure 5 shows the COF versus cycles curves that were taken on the 22  $\mu\text{m}$  thick NCD-1 film. The film roughness  $S_q$  (root mean square) was 99 nm in comparison with 62 nm for 4.8  $\mu\text{m}$  thick film [31]. The COF curves that are similar to the type 2 curve (Figure 1) can be seen for the tests that were taken at the 0.5 N load (Figure 5a). The position and shape of the stage 2 for the tests with 9000 and 36,000 cycles differ from the one with 72,000 cycles. It indicates that the running-in regime of sliding can vary for similar tests, due to probably fluctuation of the surface roughness. Variation of tribological behavior in sliding tests with the higher load (3 N, 5 Hz, 72,000 cycles) was found as well (Figure 5b).

Figure 6 shows the surface morphology of the balls after the sliding tests on the 22  $\mu\text{m}$  thick NCD-1 film. There is some difficulty in distinguishing between areas I and II on the wear scar after the

test with 9000 cycles, however, these areas can be clearly discriminated after 36,000 cycles (Figure 6b). The shape of the wear scars after 9000 cycles is circle-like in contrast to ones that were observed on thinner film (Figure 3a), likely due to a weaker deformation of the thicker film [31]. In addition, the increase of area II suggests that the film deformation (deflection) increases gradually for the tests from 9000 to 36,000 cycles (Figure 6a,b). This finding indicates fatigue [31]. Interesting that the width of the wear scars on the balls (Figures 3 and 6) after the shorter (9000 cycles) (not shown in Figure 3a) and longer (36,000 and 72,000 cycles) tests is nearly the same, i.e., about 200–225  $\mu\text{m}$ , and is nearly independent of film thickness, load (0.5, 2 and 3 N), and duration. It worth comparing the size of areas I and II for both of the films (4.8 and 22  $\mu\text{m}$ ) that were tested in similar tests, i.e., at 0.5 N and 5 Hz (36,000 cycles) (Figures 3b, 4b, 6b and 7b). The size of area I is 80 and 150  $\mu\text{m}$ , and area II is 120 and 70  $\mu\text{m}$  for 4.8 and 22  $\mu\text{m}$  thick films, respectively. The difference in size of areas as well as in the shape and depth of line scans (Figures 4b and 7b) clearly indicate the difference in wear regimes. In addition, morphological patterns after the tests on 22  $\mu\text{m}$  thick film differ from those on the 4.8  $\mu\text{m}$  thick film. Scratches can be observed already after 9000 cycles of sliding, which is probably due to the higher roughness of the 22  $\mu\text{m}$  thick film.



**Figure 4.** Line scans (see Ref. [31]) and SEM images taken on the wear scars of the 4.8  $\mu\text{m}$  thick NCD-1 film. The sliding wear test parameters were as follows: (a) 0.5 N, 5 Hz, 9000 cycles; (b) 0.5 N, 5 Hz, 36,000 cycles; and, (c) 2 N, 5 Hz, 72,000 cycles.



**Figure 5.** COF versus cycles curves taken on the 22  $\mu\text{m}$  thick NCD-1 film: (a) at the 0.5 N; (b) 3 N normal load condition. Two tests at the 3 N normal load were taken at the different places on the sample.

The position of the scratch on the ball surface corresponds to the position of the peak on the wear scar (Figures 3c and 4c). The strongest wear of the ball occurs within the scratch, and, correspondingly, the lowest wear of the diamond film is on the peak. For the longer tests, a highly asymmetric profile of the wear scars was often observed on the different types of diamond films [31,34,35]. In other words, wear can be locally highly non-uniform. Thus, a variation of the real contact area can be expected within the contact zone. For instance, a contact between two bodies could take place mainly between the peak and area II on the film, and between the scratch and area II on the ball, thus a reduction in real contact area can be expected within the area I (Figures 3c and 4c). Another type of the contact between the ball and film can be distinguished after the observation of the surface morphology of the ball and film in Figures 6c and 7c. There is a correspondence between the positions of the scratches on the ball and the peaks on the film, which indicates the primary regions of contact between the ball and film. Thus, the reduction in the real contact area can be expected within the central part of the wear scar (area I). In conclusion, grooves, scratches, and peaks of the different shapes and sizes were observed on the surface of balls and films (Figures 3, 4, 6 and 7), thus a diverse range of contact types between the film and ball can be expected, leading to the different tribological behavior.

Figure 8 shows the COF versus cycles curves taken on the 0.8  $\mu\text{m}$  thick NCD-2 film. Generally, the shape of the curves in Figure 8 is similar to the shape of the curve type 1 (Figure 1). Type 2 curve was observed, for instance, for the test with 21,600 cycles (2 N, 2 Hz) (Figure 8a). Stage II of the curve type 1 corresponds to the sliding regime with a nearly constant or slightly descending COF value. The duration of this stage varies, i.e., it decreases with an increasing of sliding velocity. The COF value decreases for the longer tests and stabilizes to value 0.05 at stage IV.

Figure 9 shows the surface patterns that were observed on the NCD-2 film after sliding tests. AFM images were taken at the central part of corresponding wear scars. The real contact area between the sliding counterparts can be characterized by the surface area ratio parameter  $S_{\text{dr}}$ , see Experimental. The  $S_{\text{dr}}$  value is greater for shorter tests (Figure 9), i.e., for the tests with 2 Hz, and it is smaller for the longer tests with 5 and 10 Hz, which can be clearly seen in the higher resolution images. Higher contact surface area for shorter tests means more adhesive contact between the counterbodies. For the longer tests, the  $S_{\text{dr}}$  value decreases together with a COF value decrease and stabilization. In other words, the decrease of contact area within the central part of wear scars for the longer tests is similar to the that were results obtained on NCD-1 film, see discussion above.

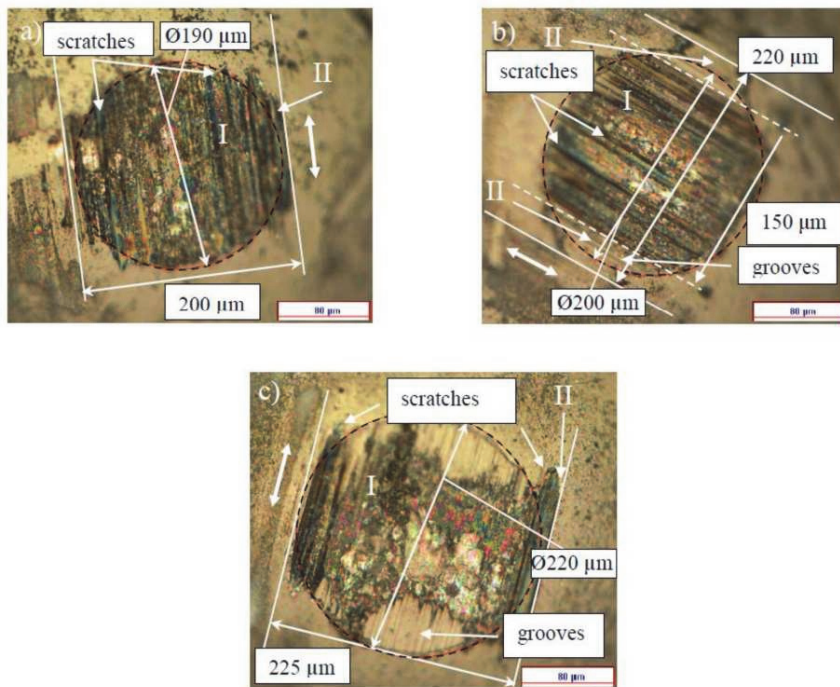


**Figure 6.** Surface morphology of the Si<sub>3</sub>N<sub>4</sub> balls after the sliding wear tests on the 22 μm thick NCD-1 film. The sliding wear test parameters were as follows: 0.5 N, 5 Hz, 9000 cycles (a), 0.5 N, 5 Hz, 36,000 cycles (b), and 3 N, 5 Hz, 72,000 cycles (I) (c).

More similarity between the surface morphology of NCD-1, NCD-2, and NCD-3 films can be found in Figures 3, 4, 6 and 9. The distance between small peaks within the wear scar (Figure 4a) is about 16 μm for the NCD-1 film, which is in good agreement with the distance between the peaks that were found on the NCD-2 film, i.e., 13 μm (Figure 9h). The height of peaks for both of the patterns is similar, namely about 100 nm, see height bar in Figure 9h. In addition, the distance between two peaks is 18 μm (Figure 4c), which could indicate that the large peak (Figure 4c) is formed from a smaller peak, which is similar to ones in Figure 4a. On the other hand, the emergence of shallow grooves and deeper scratches on the surface of balls (Figures 3 and 6) also suggests the dynamic formation and annihilation of these peculiarities during sliding. The groove and ripple patterns on the surface of wear scars were observed on all NCD (NCD-1, NCD-2, and NCD-3) films, indicating the formation of the well-ordered spatial structures during sliding [11,40].

The tribological behavior of MCD films was investigated in our studies [34,35]. The shape of the COF versus cycles curves (not shown) corresponds to the type 2 curve (Figure 1). The grooves, ripples and film deflection were observed [34,35]. The wear scar profile (not shown) on the film similar to one shown in Figure 4c (i.e., with the large peak within the wear scar) was found after the sliding test on the MCD film [34].

There is a correlation between Cases (1–4) describing conditions for self-organization to occur, the shape of the COF curves (Figures 1, 2, 5 and 8) and the morphological patterns on the balls (Figures 3 and 6) and films (Figures 4, 7 and 9) surfaces. An interpretation of results needs an estimation of influence of all types of friction and wear mechanisms to tribological behavior. The principal mechanism (or mechanisms) is mostly predetermined the type of COF curve, for instance, the emergence of either stage 2 or II. The shape of the COF versus cycles curves can depend on many

processes [41,42]. Both kinds of stages (2 and II) were found in the COF curves after the tests on the same film tested under the same test conditions (Figure 8a). A more complete description of the friction needs to take into account the possible synergetic effects or the mutual relationships between the all involved processed as well.

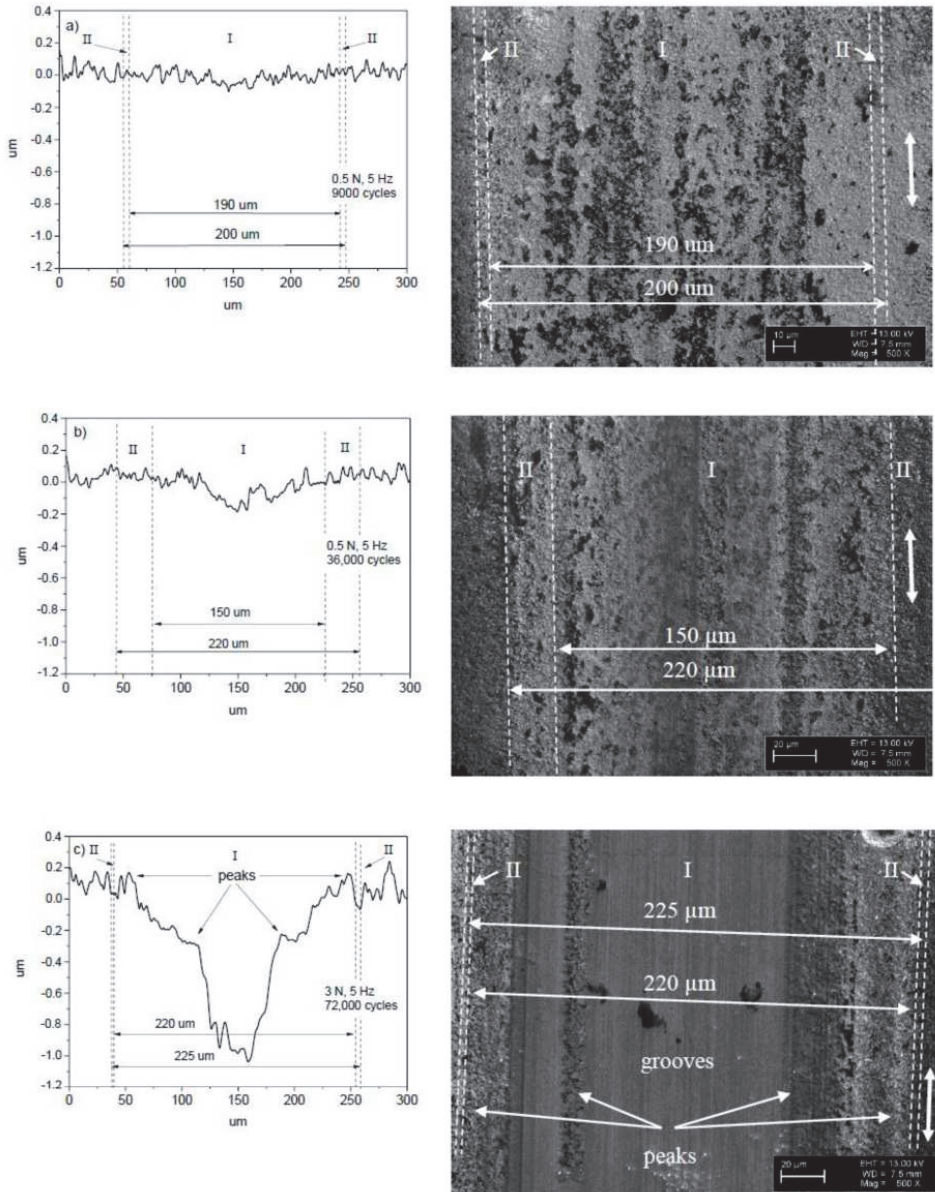


**Figure 7.** Line scans (see Ref. [31]) and SEM images taken on the wear scars of the 22  $\mu\text{m}$  thick NCD-1 film. The sliding wear test parameters were as follows: (a) 0.5 N, 5 Hz, 9000 cycles; (b) 0.5 N, 5 Hz, 36,000 cycles; and, (c) 3 N, 5 Hz, 72,000 cycles (I).

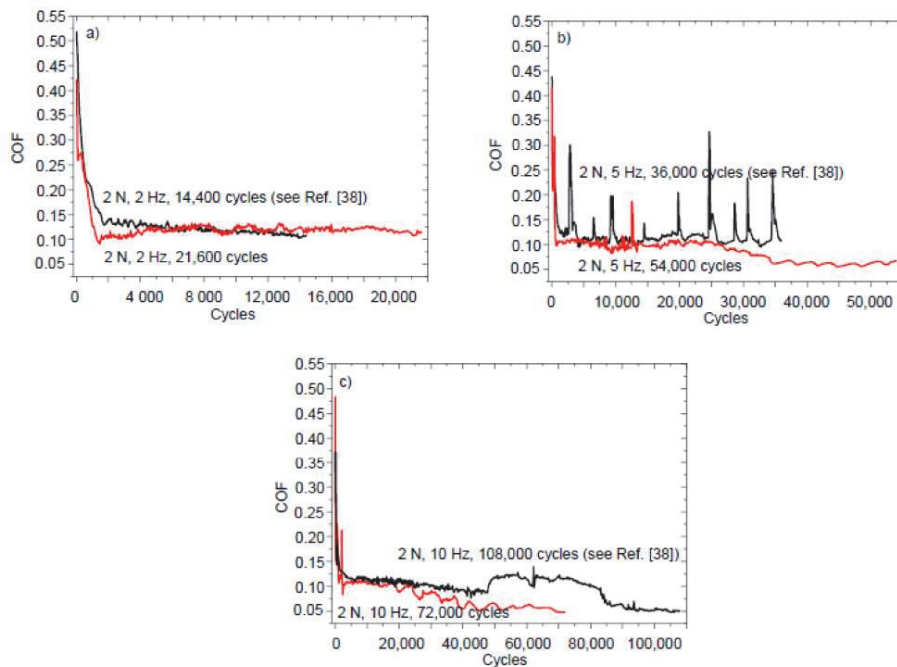


**Figure 8.** COF versus cycles curves taken on the NCD-2 film. The sliding wear test parameters were as follows: (a) 2 N and 2 Hz; (b) 2 N and 5 Hz; and, (c) 2 N and 10 Hz.

At the beginning of sliding test, the surface asperities interlocking results in material fracture and self-polishing [21–23]. These wear mechanisms, as well as passivation of dangling bonds and bonds breaking, formation of carbonaceous layer, and surface deformation influence on the diamond film tribological behavior at the early stages of the sliding, see stages 1 and I (Figure 1). The real contact area increases due to the initial polishing of surface asperities. In the case of surface roughness alteration, parameter  $\psi$  decreases (as the roughness decreases) along with the decrease of  $\mu$  and increase of  $A$ . This situation cannot correspond to any of the mentioned above cases, see Theoretical background. Therefore, the fracture and initial polishing mechanisms cannot be related with self-organization, which is in good agreement with conclusions by Gershman et al. [14]. In the case of surface deformation,  $\psi$  increases as the film deflection increases [31], together with a decreasing in  $\mu$  and an increasing in  $A$ , thus no self-organization occurs as well. The decrease of COF value at stages 1 and I can be related with the formation of carbonaceous layer as well, however during some initial period of sliding, the fracture and the initial polishing mechanisms should dominate, as formation of the carbonaceous layer needs a certain period of time [26].

An indication of self-organization can be a change of the wear rate [14]. The evaluation of the wear rate of the tribological system with deflection is a challenge as the surface deformation influences on the estimation of the wear volume [31,32]. The change of the wear rate can be related to a change of the wear regime. For instance, after relatively similar stages 1 and I, a bifurcation takes place, and the COF value follows the dynamics corresponding to either stage 2 or II (Figure 1). Different processes (dangling carbon bonds passivation and bonds breaking, adhesive and abrasive wear, film deformation, and formation of carbonaceous layer, etc.) can be distinguished for the later stages of sliding, which can cause to formation of the dissipative structures. A fraction of the friction energy can be dissipated into the breaking or passivation of the dangling bonds, formation of carbonaceous layer, and well-ordered morphological patterns, etc. [14]. A thermodynamical analysis

of mentioned processes should show if they proceed with negative or positive entropy production, thus decreasing or increasing wear, respectively.

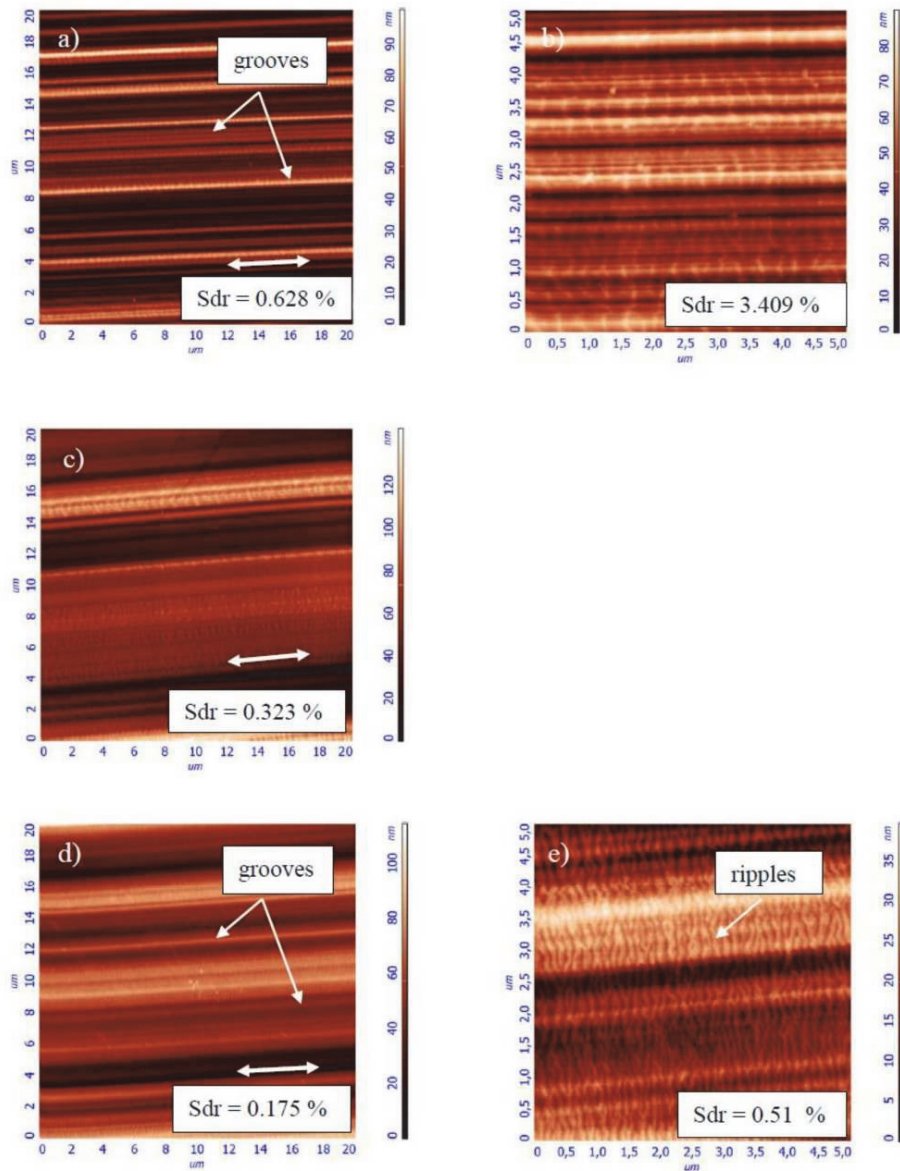
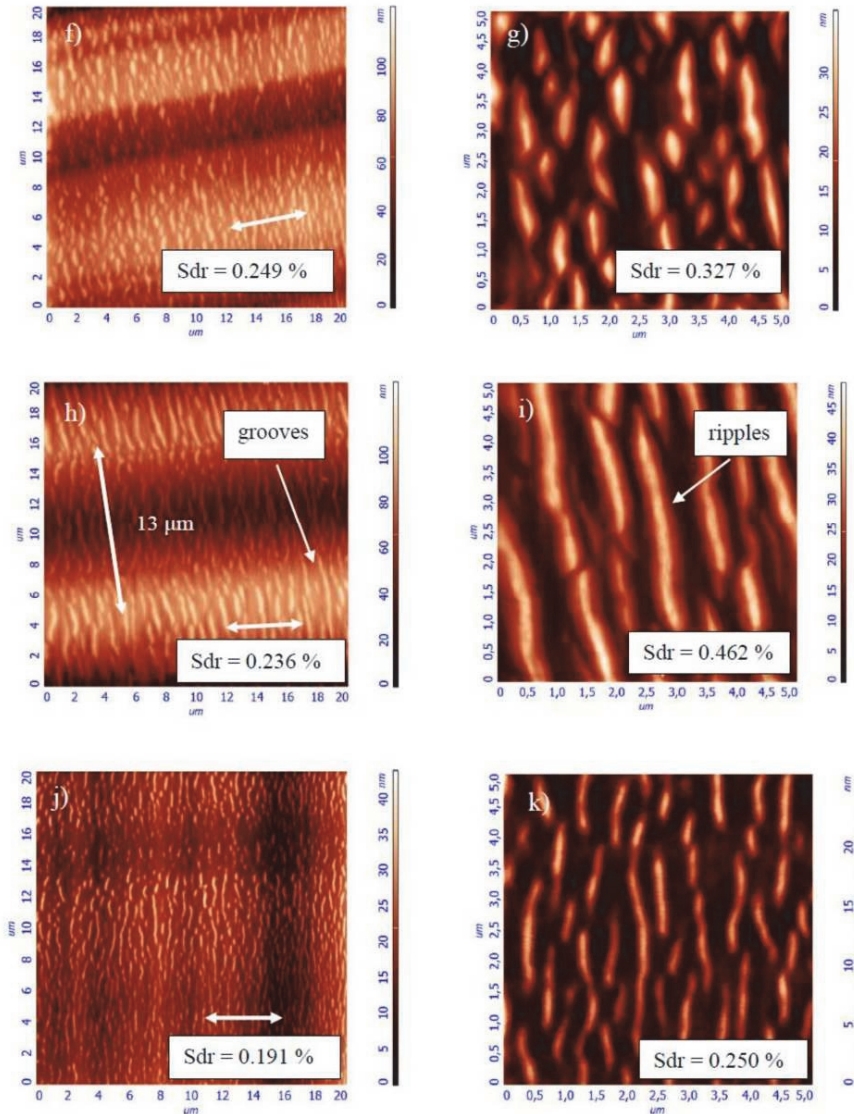


Figure 9. Cont.



**Figure 9.** Atomic force microscopy (AFM) images (see Ref. [38]) taken on the wear scars of the NCD-2 film after the sliding wear tests. The test parameters were as follows: (a,b) 2 N, 2 Hz, 14,400 cycles; (c) 2 N, 2 Hz, 21,600 cycles; (d,e) 2 N, 5 Hz, 36,000 cycles; (f,g) 2 N, 5 Hz, 54,000 cycles; (h,i) 2 N, 10 Hz, 72,000 cycles; and, (j,k) 2 N, 10 Hz, 108,000 cycles.

Tribological behavior during stage 2 (Figure 1) can be explained by using inequality (3), as follows. With regard to the role of film deformation, the film deflection increases at the early stages of sliding [31], i.e., parameter  $\psi$  increases. The COF value increases, i.e.,  $d\mu/d\psi > 0$ . The deformation of film causes the real contact area increase, thus  $\partial A/\partial\psi > 0$  as well. Therefore, the behavior corresponds to the Case 1 and adhesive wear regime of sliding. A correlation between the surface corrugation and COF behavior of NCD-1 film can be found in Figures 5b, 6c and 7c. Noise, oscillations, and an increase of COF

value can be observed in Figure 5b, likely indicating a seizure-like contact between the ball and film. Increasing contact surface area between the peaks and corresponding scratches (Figures 6c and 7c) due to the shape of these peculiarities could cause to adhesive wear and seizure. In other words, the surface corrugation increases at stage 2, i.e.,  $\psi$  increases along with  $\mu$  and  $A$ . Therefore, it corresponds to the Case 1 as well. The formation of the groove patterns on the early stages of sliding (Figure 9) can be additional evidence of an adhesive wear regime. For the NCD-2 film, the denser arrays of grooves and the highest Sdr value were observed after shorter tests (Figure 9a,b). The predominance, or at least the manifestation, of the adhesive wear regime can be expected for these tests due to a higher contact area between counterbodies. The existence of the adhesive wear regime at the early stages of sliding (parts 2 and II in Figure 1) can be easily understood as a consequence of the wear mechanisms occurring within parts 1 and I (Figure 1), namely due to the initial polishing of the asperities the contact area increases, see discussion above. However, further increase of contact area can result in COF value increase (part 2). In the case of type 1 curve (Figures 1 and 8), the nearly constant COF value for part II indicates an interplay between adhesive and other friction and wear mechanisms. It was assumed that the real surface area can infinite increase in the case of adhesive wear, see Cases 1 and 3 in Theoretical background. A fractal surface is an object with the infinite surface area, see, for example, Koch fractal [1].

The justification of the type of wear regime occurring during stages II, 3, III, and IV of the COF curves is as follows. First, the analysis of tribological behavior of diamond films for stages 3 and III is presented. The COF value decreases at stages 3 and III. The wear mechanisms can differ within the separate regions of contact zone. The real contact area can locally decrease, for instance, within the central part of the wear scar, as it was shown for NCD-1 and NCD-2 films, see discussion above. In the case of NCD-2 film, the surface morphology alteration leads to the formation of larger grooves, and finally to relatively flat contact surface within the central part of the wear scar (Figure 9f–k). It can be a leading factor, which influences tribological behavior. The decrease of both  $A$  and COF corresponds to the Cases 2 and 4. It is interesting that variations of  $\psi$  is not important, i.e., independent of changes in surface roughness and film deformation constructive self-organization can occur. In conclusion, the dominant type of wear mechanism corresponding to stages 3 and III can be the abrasive wear. The relationship between the bonds passivation and bonds breaking, adhesive and abrasive wear, film bending and formation of carbonaceous lubricating layer can lead to the COF value equalization observed for the stages II and IV. The COF value slightly varies during the steady stage regime IV (Figure 8), which can be attributed to the interplay between different mechanisms. However, the intensity of COF value fluctuations is lower in comparison to the processes occurring at the earlier stages of sliding (I–III and 1–3).

The surface patterns on the balls and films appear as a consequence of a dynamic coexistence of ripples, grooves, scratches, and peaks. The grooves can undergo a structural transformation into the scratches and the peaks can be destroyed, which changes the landscape of the contact zone on the ball and film. A close relationship between adhesive and abrasive wear explained in terms of permanently changed surface morphology is in good agreement with the results of a study by Mortazavi and Nosonovsky [43]. In this study, the running-in period of sliding was explained as the adaptive self-organization process or the mutual adjustment of counterbodies.

## 5. Conclusions

The friction and wear of diamond films originate from the complex processes. There is a relationship between the fracture and the initial polishing of the surface asperities, dangling bonds passivation and bonds breaking, formation of carbonaceous layer, adhesive and abrasive wear, and film deformation during the different stages of sliding. The adhesive and abrasive wear of diamond films can be explained as a consequence of self-organization in the tribological system. After an initial period, the bifurcation behavior is caused by instabilities that were induced by surface roughness alteration, film bending, etc. The bifurcation denotes a sudden change of the real contact area. The increase of the

real contact area between the sliding counterparts indicates the adhesive wear regime. On the other hand, the decrease of the real contact area corresponds to the abrasive wear.

**Acknowledgments:** We would like to acknowledge our colleagues from Belgium (T. Hantchel) and Russia (V. Ralchenko, V. Sedov) for providing the samples and fruitful discussions. This study was financially supported by the Estonian Ministry of Education and Research under financing project PUT 1369, the Russian Scientific Foundation No. 15-19-00217, (Thermodynamic analysis) and No. 14-19-01033 (Results). The Ministry of Education of the Russian Federation supported this work by contract No. 14.577.21.0199, a unique identifier of contract RFMEFI57715X0199.

**Author Contributions:** Vitali Podgursky designed the study and wrote the paper. Andrei Bogatov, Maxim Yashin, Sergey Sobolev contributed to the experiment and Vitali Podgursky and Iosif S. Gershman to the development of friction model based on nonequilibrium thermodynamics and analysis of results.

**Conflicts of Interest:** The authors declare no conflict of interest.

## References

- Nosonovsky, M.; Bhushan, B. *Multiscale Dissipative Mechanisms and Hierarchical Surfaces Friction, Superhydrophobicity and Biomimetics*; Springer: Berlin/Heidelberg, Germany, 2008; pp. 13–47.
- Greenwood, J.A.; Williamson, J.B.P. Contact of normally flat surfaces. *Proc. R. Soc. A* **1966**, *295*, 300–319. [[CrossRef](#)]
- Bush, A.W.; Gibson, R.D.; Thomas, T.R. The elastic contact of a rough surface. *Wear* **1975**, *35*, 87–111. [[CrossRef](#)]
- Bush, A.W.; Gibson, R.D.; Keogh, G.P. The limit of elastic deformation in the contact of rough surfaces. *Mech. Res. Commun.* **1976**, *3*, 169–174. [[CrossRef](#)]
- Bowden, F.P.; Tabor, D. *The Friction and Lubrication of Solids*; Clarendon Press: Oxford, UK, 1986.
- Stark, R.; Schitter, G.; Stemmer, A. Velocity dependent friction laws in contact mode atomic force microscopy. *Ultramicroscopy* **2004**, *100*, 309–317. [[CrossRef](#)] [[PubMed](#)]
- Muser, M.; Urbakh, M.; Robbins, M.O. Statistical mechanics of static and low-velocity kinetic friction. *Adv. Chem. Phys.* **2003**, *126*, 187–272.
- Carpick, R.W.; Agrait, N.; Ogletree, D.F.; Salmeron, M. Measurement of interfacial shear (friction) with an ultrahigh vacuum atomic force microscope. *J. Vac. Sci. Technol. B* **1996**, *14*, 1289–1295. [[CrossRef](#)]
- Hird, J.R.; Field, J.E. Diamond polishing. *Proc. R. Soc. Lond. A* **2004**, *460*, 3547–3568. [[CrossRef](#)]
- Grillo, S.E.; Field, J.E.; Van Bouwelen, F.M. Diamond polishing: The dependency of friction and wear on load and crystal orientation. *J. Phys. D* **2000**, *33*, 1–6. [[CrossRef](#)]
- Fox-Rabinovich, G.S.; Totten, G.E. (Eds.) *Self-Organization During Friction*; CRC Press: Boca Raton, FL, USA, 2006.
- Nosonovsky, M.; Mortazavi, V. *Friction-Induced Vibrations and Self-Organization*; CRC Press: Boca Raton, FL, USA, 2014.
- Prigogine, I.; Kondepudi, D. *Modern Thermodynamics*; John Wiley & Sons: New York, NY, USA, 1999.
- Gershman, I.; Gershman, E.I.; Mironov, A.E.; Fox-Rabinovich, G.S.; Veldhuis, S.C. Application of the Self-Organization Phenomenon in the Development of Wear Resistant Materials—A Review. *Entropy* **2016**, *18*, 385. [[CrossRef](#)]
- Fox-Rabinovich, G.; Veldhuis, S.C.; Kovalev, A.I.; Wainstein, D.L.; Gershman, I.S.; Korshunov, S.; Shuster, L.S.; Endrino, J.L. Features of self-organization in ion modified nanocrystalline plasma vapor deposited AlTiN coatings under severe tribological conditions. *J. Appl. Phys.* **2007**, *102*, 074305. [[CrossRef](#)]
- Nosonovsky, M.; Bhushan, B. Thermodynamics of surface degradation, self-organization and self-healing for biomimetic surfaces. *Philos. Trans. R. Soc. A* **2009**, *367*, 1607–1627. [[CrossRef](#)] [[PubMed](#)]
- Gardos, M.N.; Soriano, B.L. The effect of environment on the tribological properties of polycrystalline diamond films. *J. Mater. Res.* **1990**, *5*, 2599–2609. [[CrossRef](#)]
- Konicek, A.R.; Grierson, D.S.; Sumant, A.V.; Friedmann, T.A.; Sullivan, J.P.; Gilbert, P.U.P.A.; Sawyer, W.G.; Carpick, R.W. Influence of surface passivation on the friction and wear behavior of ultrananocrystalline diamond and tetrahedral amorphous carbon thin films. *Phys. Rev. B* **2012**, *85*, 155448. [[CrossRef](#)]
- Konicek, A.R.; Grierson, D.S.; Gilbert, P.U.P.A.; Sawyer, W.G.; Sumant, A.V.; Carpick, R.W. Origin of Ultralow Friction and Wear in Ultrananocrystalline Diamond. *Phys. Rev. Lett.* **2008**, *100*, 235502. [[CrossRef](#)] [[PubMed](#)]
- Miyoshi, K.; Wu, R.L.C.; Garscadden, A. Friction and wear of diamond and diamond like carbon coatings. *Surf. Coat. Technol.* **1992**, *54–55*, 428–434. [[CrossRef](#)]

21. Abreu, C.S.; Amaral, M.; Fernandes, A.J.S.; Oliveira, F.J.; Silva, R.F.; Gomes, J.R. Friction and wear performance of HFCVD nanocrystalline diamond coated silicon nitride ceramics. *Diam. Relat. Mater.* **2006**, *15*, 739–744. [[CrossRef](#)]
22. Erdemir, A.; Donnet, C. Tribology of Diamond, Diamond-Like Carbon, and Related Films. In *Modern Tribology Handbook*; Bhushan, B., Ed.; CRC Press LLC: Boca Raton, FL, USA, 2001; Volume 2, pp. 871–909.
23. Bhushan, B.; Subramaniam, V.V.; Malshe, A.; Gupta, B.K.; Ruan, J. Tribological properties of polished diamond films. *J. Appl. Phys.* **1993**, *74*, 4174–4180. [[CrossRef](#)]
24. Chromik, R.R.; Winfrey, A.L.; Lüning, J.; Nemanich, R.J.; Wahl, K.J. Run-in behavior of nanocrystalline diamond coatings studied by in situ tribometry. *Wear* **2008**, *265*, 477–489. [[CrossRef](#)]
25. Pastewka, L.; Moser, S.; Gumbsch, P.; Moseler, M. Anisotropic mechanical amorphization drives wear in diamond. *Nat. Mater.* **2011**, *10*, 34–38. [[CrossRef](#)] [[PubMed](#)]
26. Podgursky, V.; Hantschel, T.; Bogatov, A.; Kimmari, E.; Antonov, M.; Viljus, M.; Mikli, V.; Tsigkourakos, M.; Vandevorst, W.; Buijnsters, J.G.; et al. Rippling on wear scar surfaces of nanocrystalline diamond films after reciprocating sliding against ceramic balls. *Tribol. Lett.* **2014**, *55*, 493–503. [[CrossRef](#)]
27. Erdemir, A.; Fenske, G.R.; Krauss, A.R.; Gruen, D.M.; McCauley, T.; Csencsits, R.T. Tribological properties of nanocrystalline diamond films. *Surf. Coat. Technol.* **1999**, *120*, 565–572. [[CrossRef](#)]
28. Kumar, N.; Panda, K.; Dash, S.; Popov, C.; Reithmaier, J.P.; Panigrahi, B.K.; Tyagi, A.K.; Baldev, R. Tribological properties of nanocrystalline diamond films deposited by hot filament chemical vapor deposition. *AIP Adv.* **2012**, *2*, 032164. [[CrossRef](#)]
29. Zhao, Y.; Yue, W.; Lin, F.; Wang, C.; Wu, Z. Friction and wear behaviors of polycrystalline diamond under vacuum conditions. *Int. J. Refract. Met. Hard Mater.* **2015**, *50*, 43–52. [[CrossRef](#)]
30. Pimenov, S.M.; Smolin, A.A.; Obraztsova, E.D.; Konov, V.I.; Bögli, U.; Blatter, A.; Maillat, M.; Leijala, A.; Burger, J.; Hintermann, H.E.; et al. Tribological behaviour of smooth diamond films. *Surf. Coat. Technol.* **1995**, *76–77*, 572–578. [[CrossRef](#)]
31. Podgursky, V.; Bogatov, A.; Sobolev, S.; Viljus, M.; Sedov, V.; Ashkinazi, E.; Ralchenko, V. Effect of Nanocrystalline Diamond Films Deflection on Wear Observed in Reciprocating Sliding Tests. *J. Coat. Sci. Technol.* **2016**, *3*, 109–115. [[CrossRef](#)]
32. Bogatov, A.; Yashin, M.; Viljus, M.; Menezes, P.; Podgursky, V. Comparative Analysis of Two Methods for Evaluating Wear Rate of Nanocrystalline Diamond Films. *Key Eng. Mater.* **2017**, *721*, 345–350. [[CrossRef](#)]
33. Bogatov, A.; Viljus, M.; Raadik, T.; Hantschel, T.; Podgursky, V. Nanocrystalline diamond films deformation observed during sliding tests against Si<sub>3</sub>N<sub>4</sub> balls as a possible cause for ripple formation on wear scars. *Mater. Sci. (Medžiagotyra)* **2015**, *21*, 349–352.
34. Yashin, M.; Bogatov, A.; Podgursky, V. Comparative analysis of wear rates of microcrystalline diamond and diamond-like carbon coatings deposited on WC-Co substrates. *Key Eng. Mater.* **2017**, *721*, 436–440. [[CrossRef](#)]
35. Bogatov, A.; Traksmaa, R.; Podgursky, V. Changes in surface morphology, deflection and wear of microcrystalline diamond film observed during sliding tests against Si<sub>3</sub>N<sub>4</sub> balls. *Key Eng. Mater.* **2016**, *674*, 145–151. [[CrossRef](#)]
36. Bhushan, B. *Introduction to Tribology*; Wiley: New York, NY, USA, 2002; pp. 91–157.
37. Podgursky, V.; Bogatov, A.; Sedov, V.; Sildos, I.; Mere, A.; Viljus, M.; Buijnsters, J.G.; Ralchenko, V. Growth dynamics of nanocrystalline diamond films produced by microwave plasma enhanced chemical vapor deposition in methane/hydrogen/air mixture: Scaling analysis of surface morphology. *Diam. Relat. Mater.* **2015**, *58*, 172–179. [[CrossRef](#)]
38. Bogatov, A.; Podgursky, V.; Raadik, A.T.; Kamjula, A.R.; Hantschel, T.; Tsigkourakos, M.; Kulu, P. Investigation of morphology changes on nanocrystalline diamond film surfaces during reciprocating sliding against Si<sub>3</sub>N<sub>4</sub> balls. *Key Eng. Mater.* **2014**, *604*, 126–129. [[CrossRef](#)]
39. Brostow, W.; Hagg Lobland, H.E. *Materials: Introduction and Applications*; John Wiley & Sons: New York, NY, USA, 2017; pp. 391–427.
40. Desai, R.C.; Kapral, R. *Dynamics of Self-Organized and Self-Assembled Structures*; Cambridge University Press: Cambridge, UK; New York, NY, USA, 2009.
41. Myshkin, N.K.; Petrokovets, M.I.; Kovalev, A.V. Tribology of polymers: Friction, wear and mass transfer. *Tribol. Int.* **2005**, *38*, 910–921. [[CrossRef](#)]

42. Blau, P.J. Interpretation of the friction and wear break-in behavior of metals in sliding contact. *Wear* **1981**, *71*, 29–43. [[CrossRef](#)]
43. Mortazavi, V.; Nosonovsky, M. Wear-Induced Microtopography Evolution and Wetting Properties of Self-Cleaning, Lubricating and Healing Surfaces. *J. Adhes. Sci. Technol.* **2011**, *25*, 1337–1359. [[CrossRef](#)]



© 2018 by the authors. Licensee MDPI, Basel, Switzerland. This article is an open access article distributed under the terms and conditions of the Creative Commons Attribution (CC BY) license (<http://creativecommons.org/licenses/by/4.0/>).



**Publication II**

**M. Yashin;** A. Bogatov; V. Podgurski, Comparative Analysis of Wear Rates of Microcrystalline Diamond and Diamond-Like Carbon Coatings Deposited on WC-Co Substrates. *Key Engineering Materials*, 721 (2016) 436–440.



# Comparative Analysis of Wear Rates of Microcrystalline Diamond and Diamond-Like Carbon Coatings Deposited on WC-Co Substrates

Maxim Yashin<sup>a\*</sup>, Andrei Bogatov<sup>b</sup>, Vitali Podgurski<sup>c</sup>

Tallinn University of Technology, Department of Materials Engineering, 19086 Tallinn, Estonia

<sup>a</sup>mayash@ttu.ee, <sup>b</sup>andrei.bogatov@mail.ru, <sup>c</sup>vitali.podgurski@ttu.ee

**Keywords:** MCD, DLC, diamond coating deformation, wear rate, tribology

**Abstract.** The study investigates the wear of microcrystalline diamond (MCD) and diamond-like carbon (DLC) coatings. The MCD and DLC coatings were grown by plasma enhanced chemical vapor deposition (PECVD) method on WC-Co substrates. The sliding wear tests were performed on the ball-on-plate type of tribometer in reciprocating mode. The ball-cratering wear tests were carried out using Calo tester. The mechanical profilometer, optical and scanning electron microscopes (SEM) were used for investigation of the surface morphology of the wear scars. The wear of DLC coating is more intense in comparison to the MCD coating. In contrast to the MCD coating, no evidence of the DLC coating deflection was found.

## Introduction

Diamond and diamond like carbon (DLC) coatings are the well-known wear-resistant coatings. They have low coefficient of friction (COF), high hardness and chemical inertness [1, 2]. These coatings are widely used for protection of the cutting tools.

The tribological properties of diamond coatings deposited on Si substrates were investigated in our previous studies. It was shown that the surface morphology of the wear scars depends on load, frequency and tests duration [3, 4] of the sliding tests. In addition, formation of the ripple patterns on the wear scars surface and the deformation (deflection) of the coating were observed [5].

Hard metal (WC-Co) is important engineering materials for tooling and machining industry. Therefore, WC-Co was used as the substrate for the deposition of microcrystalline diamond (MCD) and DLC coatings. The main goals of the present study are to compare wear rates of MCD and DLC coatings in dry sliding and to investigate the phenomenon of coating deflection.

## Experimental

WC-Co substrates were polished on grinding machine (PHOEIX<sup>®</sup> 4000) to the average roughness  $R_a = 0.03 \mu\text{m}$ . Polished substrates were cleaned in ultrasonic bath with acetone and alcohol. MCD and DLC coatings were grown using plasma enhanced chemical vapor deposition (PECVD) method. Prior the deposition of MCD and DLC coatings a layer of CrN hard coating was deposited by physical vapor deposition (PVD) method. The thickness of DLC/CrN coating was 1.3/3.3  $\mu\text{m}$  and MCD/CrN one 3-5/2  $\mu\text{m}$ , respectively.

Sliding tests were carried out on the ball-on-plate tribometer (Bruker<sup>®</sup> CETER-UMT-2) in reciprocating regime.  $\text{Si}_3\text{N}_4$  balls  $\varnothing 3 \text{ mm}$  were used as a sliding counter body. The ball holder was fixed to the 1 kg sensor (DFM-1). The tests conditions were as following: the stroke length 1 mm,

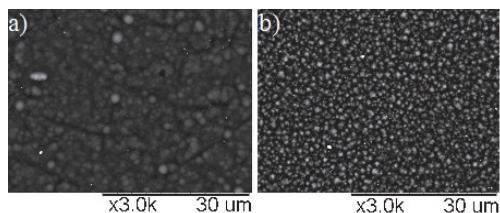


Fig. 1. Surface morphology of the DLC (a) and MCD (b) coatings.

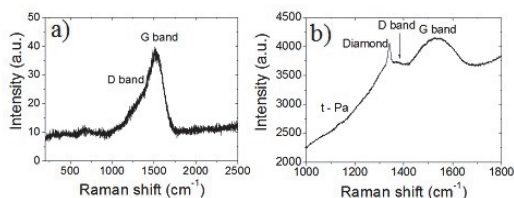


Fig. 2. Raman spectra of the DLC (a) and MCD (b) coatings.

the normal loads 0.5 N and 2 N and the number of cycles 18000, 36000 and 72000. Sliding tests were carried at room temperature and relative humidity of 35 %. The tribological properties of MCD coating were estimated in ball-cratering tests (calotests) using  $\varnothing$  20 mm steel ball. The rotational speed was 400 rpm. The calotest duration was 20 min and no diamond slurry was used.

The wear scars were investigated by mechanical profilometry (Mahr Perthometer<sup>®</sup> equipped with PGK 120 tracing arm). The wear rate was estimated using Eq. 1, where V - volume of worn material, F - normal load, L - sliding distance.

$$W = V / (F \times L) \quad (1)$$

The optical microscope and scanning electron microscope (SEM) (TM-1000 HITACHI<sup>®</sup>) were used for investigation of the surface morphology. The structure of MCD and DLC coatings was characterized by Raman spectroscopy (Horiba<sup>®</sup> LabRam HR 800).

## Results and discussions

Figure 1 shows the surface morphology of coatings. The grain size of DLC and MCD coatings is about 1-2  $\mu\text{m}$  and 0.5-1.5  $\mu\text{m}$ , respectively. The average roughness  $R_a$  of the DLC coating is 0.3  $\mu\text{m}$  and 0.2  $\mu\text{m}$  for the MCD coating.

The Raman spectra of the DLC and MCD coatings are shown in Fig. 2. In the case of the DLC coating, there are two main characteristic peaks corresponding to two bands: G band at 1500  $\text{cm}^{-1}$  and D band at 1300  $\text{cm}^{-1}$ . The Raman spectrum of the MCD coating has several peaks: at 1150  $\text{cm}^{-1}$  corresponding to t-Pa (trans-polyacetylene at the grain boundaries), at 1350  $\text{cm}^{-1}$  to diamond and the peaks at 1370  $\text{cm}^{-1}$  related to D-band, corresponding to the disordered graphite, and 1540  $\text{cm}^{-1}$  related to the G-band corresponding to the well-ordered graphite. There is a shift of diamond peak value from 1332  $\text{cm}^{-1}$  to a higher value of 1350  $\text{cm}^{-1}$  indicating a stress in the diamond film [6].

Figure 3 shows the COF versus number of cycles after sliding wear tests with 0.5 N and 2 N of normal load and test duration of 72000 cycles. In the case of DLC coating, after a short run-in

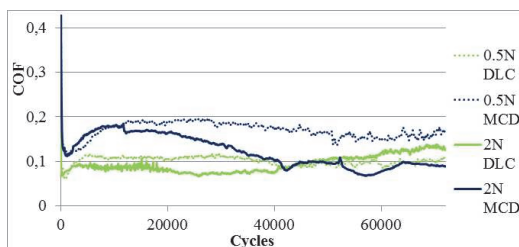


Fig. 3. COF versus number of cycles recorded on the DLC and MCD coatings.

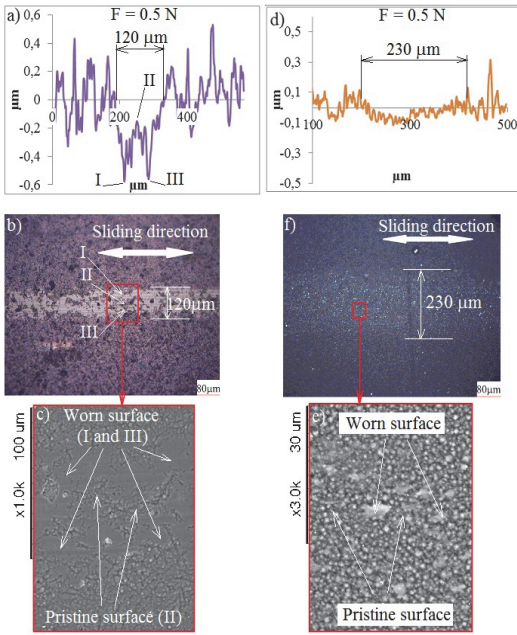


Fig. 4. Line scans, optical microscope and SEM images taken after sliding tests with 0.5 N (8000 cycles) on the DLC (a-c) and MCD (d-e) coatings.

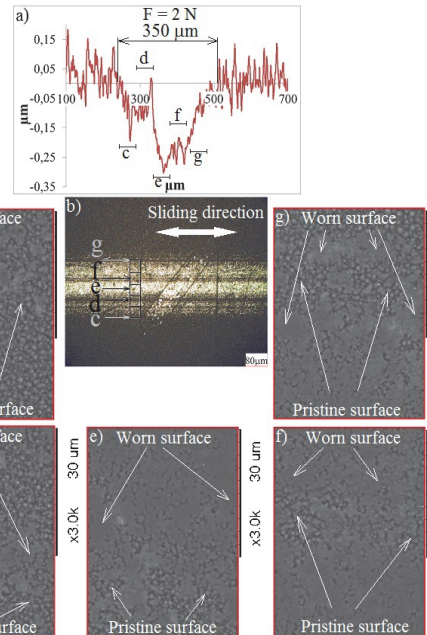


Fig. 5. Line scan (a) taken on the wear scar after the test with 2 N (72000 cycles) on the MCD coating. The optical microscope (b) and SEM (c-g) images taken on the same wear scar.

period, the COF value stabilizes about 0.1 for the test with 0.5 N. However, the COF value after 30000 cycles steadily increases to 0.14 for the test with 2 N. Run-in period for the MCD coating is longer than for DLC one. For instance, this period continues for 60000 and 40000 cycles for the tests with 0.5 and 2 N, respectively. The COF value is about 0.1 after run-in for the test with 2 N.

The depth profiles were taken at five different positions of each wear scar. The averaged depth profiles of the wear scars after the tests with 0.5 N (18000 cycles) are shown in Fig. 4 (DLC (a) and MCD (d)). Two valleys (I and III) correspond to brighter areas (worn surface) at the wear scar (Fig. 4b). The peak (II) corresponds to a darker area (either pristine or weakly polished surface) on the same image. The peak (II) is located at approximately the same height level as the level of the pristine surface, see the line scan outside of the wear scar. It is worth noting that, although the wear scar depth on the DLC coating is larger than on the MCD coating, the wear scar width on the DLC coating is about 160  $\mu\text{m}$ , in contrast to the MCD coating which is 230  $\mu\text{m}$ . In addition, no wear can be observed on the large area of the MCD surface (Fig. 4(f, e)), only very few islands can be characterized as polished areas (worn surface). However, a concave shape of the depth profile in Fig. 4d could suggest that there is a sizable wear of the MCD coating.

Figure 5a shows the line scan taken after the test with 2 N (72000 cycles) on the MCD coating. The wear scar depth is about 0.3  $\mu\text{m}$ . In analogy to Fig. 4, the darker areas in the optical microscope image (Fig. 5b) correspond to pristine or slightly polished coating surface and the brighter areas to the strongly polished surface of the MCD coating. The wear scar was scanned with SEM across the scar as it shown in Figs. 5b and 5(c-g). The locations of these SEM images are also shown on the

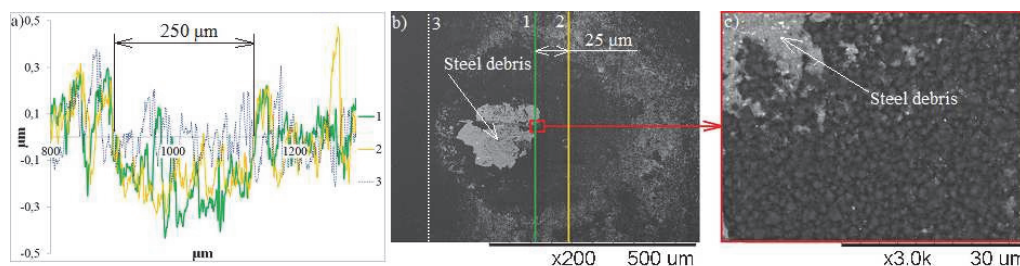


Fig. 6. Lines scan (a) and SEM images (b,c) taken on the crater after calotest on the MCD coating.

line scan (Fig. 5a) by small segments denoted with c-g. There is an interesting difference between the locations of segments d and f (or e), namely, the level of segment f (or e) is below the level of segment d, however pristine surface can be seen on both segments. The difference is about 0.15 - 0.2  $\mu\text{m}$ . This observation suggests that the MCD coating can be inhomogeneously deformed (deflected) during sliding, i.e. a part of coating can be deformed stronger than another one.

The results of calotests on the MCD coating are shown in Fig. 6. Two depth profiles were taken through the center (1) and the side (2) of the crater. For the sake of comparison, the line scan (3) taken on the pristine MCD surface is shown in Fig.6a,b. The crater depth is about 0.3  $\mu\text{m}$ . Steel debris can be observed on the crater surface (Fig. 6b, c). The wear of diamond grains located close to the center of the crater is negligible, however a concave shape of the line scan could suggest that there is the wear of MCD coating. The apparent contradiction can be resolved by assuming MCD coating deflection. This conclusion is also in good agreement with the above-mentioned results obtained after sliding tests, see Figs. 4 and 5 with corresponding text.

The wear rates were evaluated for DLC and MCD coatings after sliding tests. The wear rate of the DLC coating can be estimated only for short duration tests (for the tests with 2N), as the COF value increases after 30000 cycles, likely due to the fact that DLC layer was worn away (Fig. 3). The wear rate of the DLC coating is about  $2.3 \times 10^{-6}$  and  $1.0 \times 10^{-6}$   $\text{mm}^3/\text{Nm}$  after 18000 cycles at 0.5 and 2 N, respectively. In the case of MCD coating, the wear rate was about  $6.2 \times 10^{-7}$  and  $4.3 \times 10^{-7}$   $\text{mm}^3/\text{Nm}$  after 18000 cycles at 0.5 and 2 N, respectively. In other words, the wear resistance of MCD is one order higher than for DLC coating. However, this difference can be even higher because the effect of MCD coating deflection on the wear rate was not excluded.

It was shown that the tribological behavior of the MCD coating can be explained taking into account coating deflection. No clear signs of the DLC coating deflection were found. Indeed, as it was mentioned above, the peak (II) in Fig. 4a,b locates at the center of the wear scar, however the level of this peak height is coincided with the level of the pristine surface profile.

## Conclusions

The wear behavior of MCD coating can be explained based on the concept of MCD coating deflection. No clear evidence of the DLC coating deflection was found. The DLC coating shows lower wear resistance compared to MCD one in the reciprocating sliding tests. The wear rate of DLC coating measured in dry sliding tests is one order higher than for MCD one. The development of new methods for calculation of the wear rate of diamond coating is a challenge for further studies.

## Acknowledgments

This study was financially supported by the Estonian Ministry of Education and Research under target financing project IUT 19-29.

**References**

- [1] L. Pastewka, S. Moser, P. Gumbsch, M. Mosler, Anisotropic mechanical amorphization drives wear in diamond, *Nature Materials*. 10 (2011), 34-38.
- [2] A. Erdemir, C. Donnet, Tribology of diamond-like carbon films: recent progress and future prospects, *Journal of Physics D*. 39 (2006), 311-327.
- [3] A. Bogatov, V. Podgursky, A. T. Raadik, , A. R. Kamjula, T. Hantschel, M. Tsigkourakos, P. Kulu, Investigation of morphology changes on nanocrystalline diamond film surfaces during reciprocating sliding against Si<sub>3</sub>N<sub>4</sub> balls, *Key Engineering Materials*. 604 (2014), 126-129.
- [4] V. Podgursky, A. Bogatov, M. Freund, P. Kulu, Influence of surface morphology on the tribological behavior of diamond-like carbon coating, *Key Engineering Materials*. 527 (2013), 83-91.
- [5] A. Bogatov, M. Viljus, T. Raadik, T. Hantschel, V. Podgursky, Nanocrystalline diamond films deformation observed during sliding tests against Si<sub>3</sub>N<sub>4</sub> balls, *Materials Science (Medžiagotyra)*. 21 (2015), 349-352.
- [6] J. Michler, M. Mermouxb, Y. von Kaenela, A. Haounib, G. Lucazeaub, E. Blanka, Residual stress in diamond flms: origins and modelling, *Thin Solid Films*. 357 (1999), 189-201.



**Publication III**

V. Podgursky; A. Bogatov; **M. Yashin**; M. Viljus; A. P. Bolshakov; V. Sedov; O. Volobujeva; A. Mere; T. Raadik; V. Ralchenko, A comparative study of the growth dynamics and tribological properties of nanocrystalline diamond films deposited on the (110) single crystal diamond and Si (100) substrates. *Diamond and Related Materials*, 92 (2019) 159–167.10.1016.





Contents lists available at ScienceDirect

## Diamond &amp; Related Materials

journal homepage: [www.elsevier.com/locate/diamond](http://www.elsevier.com/locate/diamond)

# A comparative study of the growth dynamics and tribological properties of nanocrystalline diamond films deposited on the (110) single crystal diamond and Si(100) substrates



V. Podgursky<sup>a,\*</sup>, A. Bogatov<sup>a</sup>, M. Yashin<sup>a</sup>, M. Viljus<sup>a</sup>, A.P. Bolshakov<sup>b,c</sup>, V. Sedov<sup>b,c</sup>,  
O. Volobujeva<sup>d</sup>, A. Mere<sup>d</sup>, T. Raadik<sup>d</sup>, V. Ralchenko<sup>b,c</sup>

<sup>a</sup> Tallinn University of Technology, Department of Mechanical and Industrial Engineering, Ehitajate tee 5, 19086 Tallinn, Estonia

<sup>b</sup> Prokhorov General Physics Institute, Russian Academy of Sciences, Vavilova 38, 119991 Moscow, Russia

<sup>c</sup> National Research Nuclear University MEPhI, Kashirskoe shosse 31, Moscow 115409, Russia

<sup>d</sup> Tallinn University of Technology, Department of Materials and Environmental Technology, Ehitajate tee 5, 19086 Tallinn, Estonia

## ARTICLE INFO

## Keywords:

NCD  
Single crystal  
Tribology  
Wear

## ABSTRACT

Nanocrystalline diamond (NCD) films were grown on the High Pressure High Temperature (HPHT) (110) single crystal (SC) diamond substrates by Microwave Plasma Enhanced Chemical Vapor Deposition (MPCVD) in methane/hydrogen/nitrogen plasma. The thickness of the films was varied between 2.2 and 22.5  $\mu\text{m}$ . The cauliflower-like surface morphology was observed by means of Atomic Force Microscopy (AFM) and Scanning Electron Microscopy (SEM). The scaling behavior of NCD films growth was investigated. The relatively high value of the roughness exponent  $\alpha_s = 1.5\text{--}1.6$  was found indicating anomalous scaling. Therefore, shadowing and diffusional instabilities can affect the film growth. The tribological properties of the NCD films deposited on the SC(110) diamond were compared with the NCD films prepared on the Si(100) substrates. Both types of specimens were tested under similar Hertzian contact pressure. The lower wear volume losses were observed on the NCD/SC(110) specimens. Therefore, the influence of substrate and substrate/film interface properties on the tribological behavior of the NCD films grown on Si(100) can be expected to cause NCD films deflection.

## 1. Introduction

Diamond films have outstanding properties including high hardness, Young's modulus, chemical inertness and wear resistance. Therefore, diamond films are important engineering material for tooling industry, biomedical applications, etc. Tribological behavior of the diamond films can be characterized by different frictional and wear mechanisms. Wear on diamond is a load, velocity and sliding direction dependent process [1,2]. Material fracture, micro-ploughing and asperities polishing [3,4], chemical passivation of dangling carbon bonds by species from ambient atmosphere [5,6], formation of carbonaceous tribolayer [6–9] and morphological patterns [9] are among the most fundamental tribological mechanisms. The morphological adaptation of the contacting surfaces during run-in on diamond films can be considered as a process of self-organization initiated due to the coupling between friction and wear [10].

The influence of substrate on the coating properties is an important aspect of coatings tribology [11–16]. For instance, there is a difference

between the tribological behavior of the soft film on hard substrate and the hard film on soft substrate [12]. The load-carrying capacity of the film/substrate system is an ability to withstand pressure in the system without loss of the system functionality. In the past duplex coatings technology was developed to improve the tribological properties of coating/substrate system [14], including, for instance, diamond like coatings (DLC) prepared on the  $\text{Ti}_6\text{Al}_4\text{V}$  substrates [15]. However, the influence of substrate on tribological properties of the diamond films has not yet been thoroughly investigated. The deflection of the nanocrystalline diamond (NCD) films grown on the Si(100) and WC-Co substrates was observed after sliding tests [13,16]. The nature of this phenomenon remains unclear, likely the properties of the diamond film, substrate and interface between them must be taken into account to realize the mechanisms contributing to the film deflection. In practices, the NCD films are prepared on the Si(100) and WC-Co substrates using seeding with diamond particles prior deposition. The NCD/substrate interface consists of seeding particles, diamond grains and ballas-like nano-diamond material between the grains [17–19], which can

\* Corresponding author.

E-mail address: [vitali.podgurski@ttu.ee](mailto:vitali.podgurski@ttu.ee) (V. Podgursky).

<https://doi.org/10.1016/j.diamond.2018.12.024>

Received 18 September 2018; Received in revised form 14 November 2018; Accepted 25 December 2018

Available online 28 December 2018

0925-9635/ © 2019 Elsevier B.V. All rights reserved.

significantly affect tribological properties [20].

It is instructive to consider wear related phenomena on the different size scales, as wear and friction are multiscale phenomenon [12]. The Hertzian contact pressure is calculated on the macro level (i.e. mm) [12]. Different processes occurring on contact spots between the ball and surface asperities are aspects of the micro level asperity tribology (i.e.  $\mu\text{m}$ ) [12]. Diamond is a brittle material, thus the fracture of asperities can take place [21]. The deflection of diamond films occurs on the macro level, as a part of the film located within the wear scar becomes deformed [16,20].

Ashkinazi et al. [22] investigated the growth of NCD films on the single crystal (SC) diamond substrates with the different orientations. It was shown that NCD films can be grown on the (110), (111), (211) and (311) faces of SC diamond. Moore et al. [23] observed the NCD films growth on the SC (100) diamond.

The growth dynamics of diamond films was investigated using scaling concept [24–26]. The scaling is related to the properties of a fractal surface and shows high versatility and applicability to describe film growth [27]. In this method, the deposition process is characterized by a finite set of scaling exponents derived directly from experimental data. In the case of NCD films growth, different scaling regimes were found for cauliflower-like morphology of growing interface, namely Kardar-Parisi-Zhang (KPZ) [24,25] and Edwards-Wilkinson [25]. The growth dynamics of relatively thick Microcrystalline diamond (MCD) films is correlated with the KPZ model as well [26]. The KPZ regime is characterized by low sticking probability, conformal growth [28] and a large average surface gradient (local slope) [29]. It is worth mentioning that NCD and MCD films were grown on the Si(100) substrates using seeding of diamond particles prior deposition [24–26].

In the context of the present work, theoretical and experimental studies of the growth with the high value of roughness exponent ( $\alpha_s$ ) are of interest. High value of  $\alpha_s > 1$  corresponds to anomalous scaling regimes, i.e. local and global surface roughness fluctuations have different scaling exponents [30]. The anomalous scaling behavior of 1D Steppen model of the growth with faceting was investigated elsewhere [30,31]. There are two types A and B of Steppen model [31]. For type A, or a trivial case, the facets are formed by finite number of identical segments of constant slope, in this case  $\alpha_s = 1.5$ . In contrast, if facets are formed by not identical segments the value of  $\alpha_s$  differs from 1.5 [30]. The super-rough growth dynamics with the high value of  $\alpha_s = 1.6$  was found for cauliflower-like surface morphology in the case of growth of Ni on steel [29] and ZnO on glass [32]. On the other hand, unstable nonlocal interface dynamic was investigated by Nicoli et al. [33,34], it was found for superballistic interface diffusion (Lévy flight type)  $\alpha_s = 1.52 \pm 0.03$  and  $\alpha_s = 1.55 \pm 0.05$  for 1D and 2D models, respectively [33]. For elongated needle-like structures prepared by sputtering deposition of NiW on steel [29] and Nb on MgO (001) [35], the value of  $\alpha_s$  is equal to 1.35 and 1.38, respectively. The origin of anomalous scaling can be non-local effects including shadowing and diffusional instabilities during growth [32,36,37]. There is a relation between the local slope of surface segments and anomalous roughening [29,37], namely anomalous scaling can occur for smaller slopes [29]. To our knowledge, no growth dynamics with  $\alpha_s > 1$  was found for diamond films deposition.

In the present work the NCD films were deposited on High Pressure High Temperature (HPHT) SC (110) diamond substrates. A primary goal of the study is to compare tribological properties of NCD films prepared on the SC(110) diamond and Si(100) substrates, to understand an influence of the substrate on the tribological properties of the NCD films. Secondly, the study aims to compare the structure and the growth mechanisms of NCD films deposited on the SC(110) diamond and Si(100) [24].

## 2. Experimental

The HPHT (110) single crystal polished ( $R_a = 8 \pm 4 \text{ nm}$ )

$3 \times 4 \times 1.5 \text{ mm}$  in size diamond plates (Euro Superabrasives Limited®) were used as substrates. The NCD films were grown under next conditions: power 2.5 kW, pressure in chamber 80 Tr, temperature on the sample 1050–1100 °C. The gas mixture was as follows:  $\text{H}_2 - 460 \text{ sccm}$ ,  $\text{CH}_4 - 20 \text{ sccm}$  and  $\text{N}_2 - 20 \text{ sccm}$ . The growth time was 32, 54, 73 and 130 min. Two samples were prepared in each single deposition batch. Specimens were mechanically fractured and the thickness of the films was measured. The thickness of films was 2.2, 8, 10.5 and 22.5  $\mu\text{m}$ , which corresponds to the growth rates of 0.07, 0.15, 0.15 and 0.18  $\mu\text{m}/\text{min}$ , respectively.

Reciprocating sliding tests (normal load 0.5 and 2 N, displacement amplitude 1 mm, frequency 5 Hz, air relative humidity about 35%, ball diameter  $\varnothing 3 \text{ mm}$ ) were carried out by means of a CETR® UMT-2 tribometer. The test durations were 9000, 36,000 and 72,000 cycles.  $\text{Si}_3\text{N}_4$  balls (surface roughness  $R_a = 0.012 \mu\text{m}$ ) (REDHILL®) were used as counter bodies. According to the producer provided data, the hardness, Young's modulus and Poisson ratio of the  $\text{Si}_3\text{N}_4$  counter bodies were 1400–1700 HV, 310 GPa and 0.27, respectively. The properties of bulk diamond and Si(100) used for the calculation of Hertzian contact pressure were as follows: Young's modulus 1050 and 180 GPa [38] and Poisson ratio 0.2 and 0.278 [39], respectively. Monocrystalline Si (100) possesses a hardness of about 12 GPa [40] and the fracture strength is 6.1 GPa [41].

The max Hertzian contact pressure was calculated for the two types of specimens, namely flat diamond surface against  $\text{Si}_3\text{N}_4$  ball in the case of NCD/SC(110) and flat Si(100) surface against  $\text{Si}_3\text{N}_4$  ball in case of NCD/Si(100) for two normal loads 0.5 and 2 N. The Hertzian contact pressure was calculated following the method suggested by Erdemir et al. [42], i.e. between either SC(110) or Si (100) surfaces and  $\text{Si}_3\text{N}_4$  ball assuming that the same stress is within the NCD film. The max contact pressures for NCD/SC(110) samples are 1.4 and 2.3 GPa and for NCD/Si(100) ones 0.9 and 1.4 GPa under 0.5 and 2 N of load, respectively.

The surface roughness of the films was evaluated using Atomic Force Microscopy (AFM) (Bruker® MultiMode 8 AFM with Application Module based on Nanoscope V controller, J scanner) in non-contact mode with Si cantilevers and tips (PPP-NCHP tips, NanoAndMore GmbH®), with a tip radius of  $< 7 \text{ nm}$ . The AFM image sizes were  $20 \times 20$  and  $5 \times 5 \mu\text{m}^2$ . The root mean square roughness or interface width ( $S_q$ ) was evaluated.

Scanning Electron Microscopy (SEM) images were taken by a Zeiss EVO® MA - 15 system with LaB<sub>6</sub> cathode in secondary electron mode, applying an accelerating voltage of 10–15 kV and 6.5–8.5 mm working distance (WD). In addition, the surface morphology were investigated using high-resolution scanning electron microscope (HR-SEM Zeiss Merlin) equipped with an In-Lens SE detector for topographic imaging and In-Lens energy selective backscattered detector for compositional contrast. Measurements were carried out using accelerating voltage of 2–15 kV and WD was 2.5–9.3 mm.

Wear scars depth profiles were investigated by stylus profilometry (Mahr Perthometer).

The micro-Raman measurements were carried out on a Renishaw inVia micro-Raman setup equipped with an Ar<sup>+</sup> ion laser (514 nm wavelength).

X-ray Diffraction (XRD) patterns were recorded by a Rigaku Ultima IV diffractometer with Cu K $\alpha$  radiation ( $\lambda = 1.5406 \text{ \AA}$ , 40 kV at 40 mA) and using the silicon strip detector D/teX Ultra with a scan range of  $2\theta = 10.0\text{--}150^\circ$ , scan step  $0.02^\circ$ , scan speed  $5^\circ/\text{min}$ . The scan axes were  $\theta/2\theta$ .

## 3. Results and discussion

### 3.1. Structure characterization

Figs. 1 and 2 show the surface morphology of the NCD films investigated by means of AFM and SEM techniques. Secondary electron

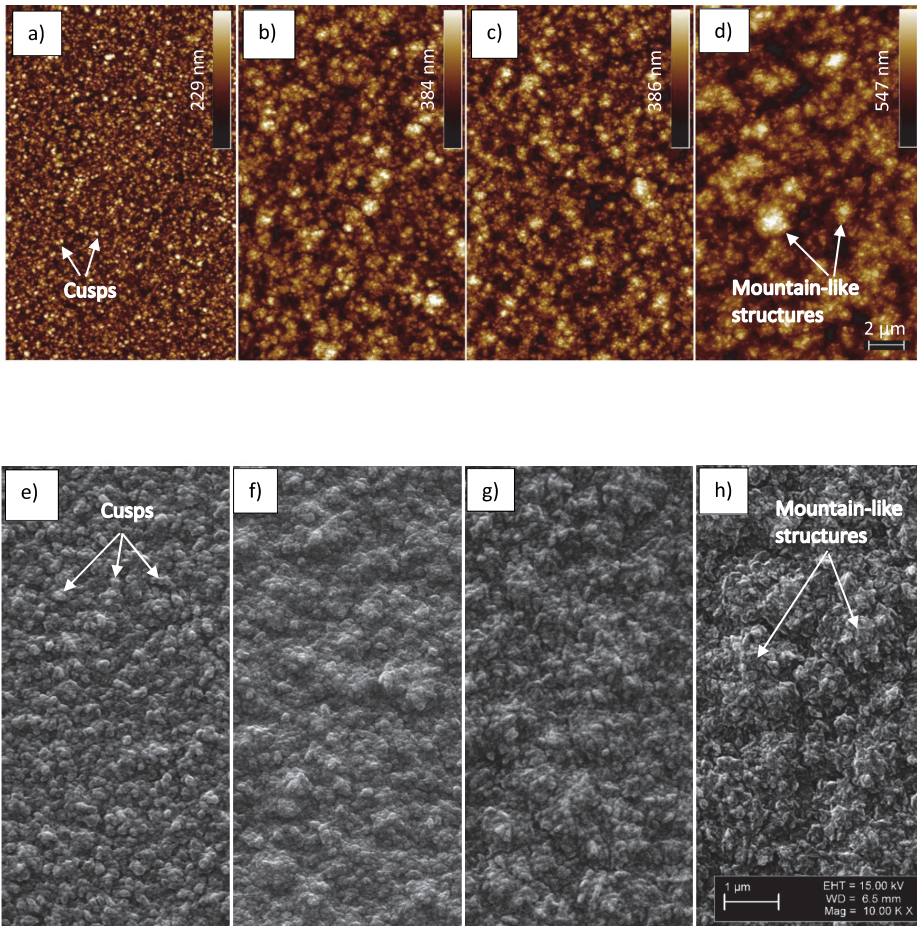


**Fig. 1.** AFM and SEM images taken on the NCD films grown on the SC(110) diamond. The thickness of the diamond films was as follows: (a) and (e) 2.2  $\mu\text{m}$ , (b) and (f) 8  $\mu\text{m}$ , (c) and (g) 10.5  $\mu\text{m}$  and (d) and (h) 22.5  $\mu\text{m}$ .

(SE) SEM and AFM images look differently, due to inherent difference between SEM and AFM techniques. The cauliflower-like surface morphology can be observed, which is similar to the surface morphology of the NCD films prepared on the Si(100) substrates [24]. The SEM investigation revealed changes in morphology with the increase of film thickness, namely, cusps can be observed on the thinner (Fig. 1e) and thicker films (Fig. 1f and g), but this is not evident in the case of 22.5  $\mu\text{m}$  thick film (Fig. 1h). Several morphological features can be observed on the images taken by both techniques. For instance, mountain-like structure with the size of islands about 1  $\mu\text{m}$  can be seen in Fig. 1d and h. The higher resolution AFM and SEM images were taken on the NCD films (Fig. 2). The AFM investigation revealed that the morphology of the 2.2 and 22.5  $\mu\text{m}$  thick films are apparently similar, i.e. they are formed by a coalescence of the cusps. The cusps on the SEM images look coarser than those on the AFM images, which look smoother due to probably tip convolution. Interesting that cusps can be observed on the AFM (Fig. 2a) and SEM (Fig. 2b) images for the 2.2  $\mu\text{m}$  thick film. However, in the case of 22.5  $\mu\text{m}$  thick film, in spite of regulation of accelerating voltage between 2 and 15 kV and WD between 2.5 and 9.3 nm, cusps can hardly be identified on the SEM image (Fig. 2d), although they can be seen on the AFM image (Fig. 2c).

Finally, well-formed chains of cusps can be found on the 22.5  $\mu\text{m}$  thick film (Fig. 2c). The cross section of 22.5  $\mu\text{m}$  thick film is shown in Fig. 3.

Fig. 4 shows Raman spectra of the NCD films grown on the SC(110) diamond surface. The Raman spectra are similar to ones taken on the NCD films prepared on Si(100) [24]. The diamond peak is at 1332  $\text{cm}^{-1}$  and peaks at 1134, 1190 and 1472  $\text{cm}^{-1}$  relate to *trans*-polyacetylene (t-PA). The peaks at 1358 and 1557  $\text{cm}^{-1}$  are the D and G bands correspond to six-fold ring breathing vibrations of  $\text{sp}^2$  sites and the in-plane stretching of  $\text{sp}^2$  bonds, respectively. The intensity of diamond peak tends to decrease with the thickness of NCD films, due to high absorption of NCD material. A reduction of the peak intensity corresponding to t-PA and G bands was observed for thicker films in both studies. In contrast to the present study, in the case of NCD films grown on Si(100) the stronger and broader G and t-PA peaks were observed [24]. A relatively strong 1332  $\text{cm}^{-1}$  peak for the 2.2  $\mu\text{m}$  thick film corresponds to the Raman emission from the SC(110) substrate surface and epitaxially grown film at the early stages of deposition. SEM and AFM images suggest that this film is fully formed. Indeed, the height bar on the AFM images is between 229 nm for  $20 \times 20 \mu\text{m}^2$  and 313 nm for  $5 \times 5 \mu\text{m}^2$  (Figs. 1a and 2a). These values are considerably smaller than the film thickness. Therefore, the 2.2  $\mu\text{m}$  thick film is

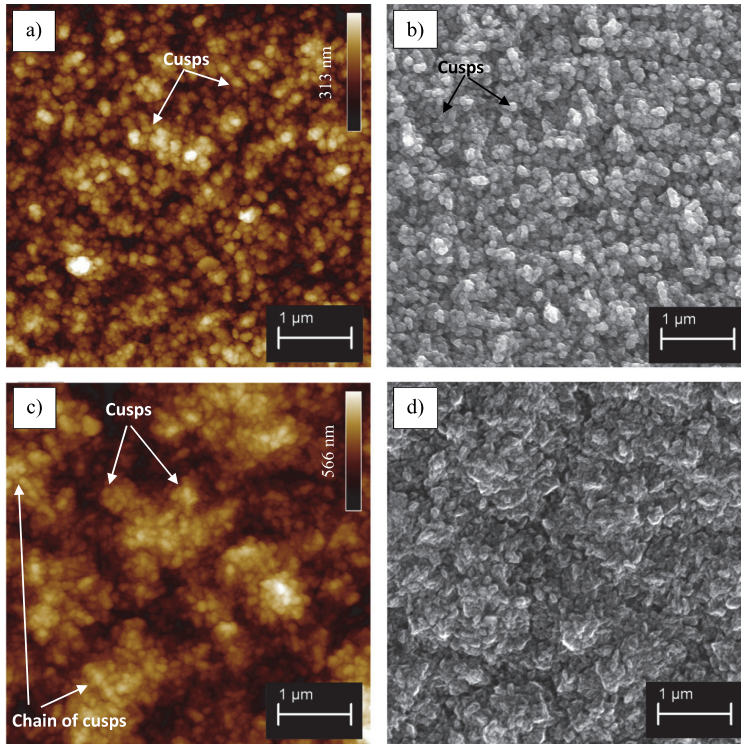


Fig. 2. AFM and SEM  $5 \times 5 \mu\text{m}^2$  images taken on the NCD films grown on the SC(110) diamond. The thickness of the diamond films was as follows: (a) and (b) 2.2  $\mu\text{m}$  and (c) and (d) 22.5  $\mu\text{m}$ .

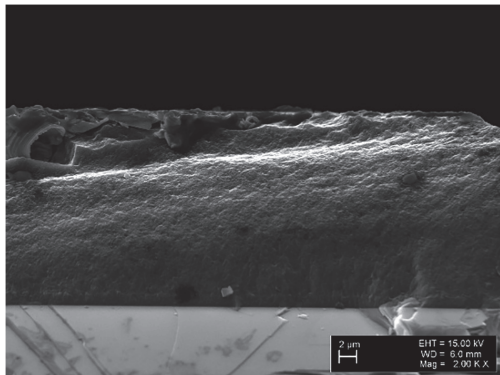


Fig. 3. Cross section of 22.5  $\mu\text{m}$  thick NCD film on SC(110).

continues. This conclusion is also supported by the fact that the film growth on the SC(110) diamond surface should homogeneously start along the whole surface area. An epitaxial growth is expected at the early stage of the growth followed by formation of the NCD films due to re-nucleation activated by deposition conditions [19,22]. In contrast, there are preferable growth centers located on the diamond grains in the case of deposition on the Si(100) substrate due to prior seeding.

Fig. 5a shows XRD pattern taken on the 22.5  $\mu\text{m}$  thick NCD film. The (111) peak at  $2\theta = 43.94^\circ$ , (220) at  $75.54^\circ$  and (311) at  $91.7^\circ$  correspond to diamond structure and indicate formation of well-ordered

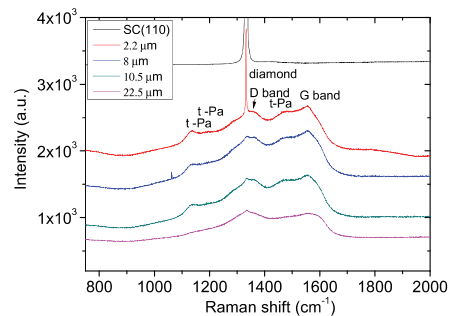


Fig. 4. Raman spectra taken on the clean SC(110) diamond and NCD/SC(110) samples.

crystallites. Strong (220) peak reflects the structure of SC(110) HPHT substrate, as well as could correspond to the orientation of diamond crystallites in the NCD film. Fig. 5b shows the ratio of (220) and (111) peaks intensities, i.e. a fraction of the (111) oriented crystallites increases with the film thickness. Similar behavior was observed in the case of NCD films growth on Si(100) [24].

The NCD films growth kinetics was investigated within scaling concept. Figs. 6 and 7 show the interface width and roughness exponent  $\alpha_s$ , respectively. It was unable to draw a straight line across data points in Fig. 6 to estimate the growth exponent ( $\beta$ ). A varying growth rate between 0.07 and 0.18  $\mu\text{m}/\text{min}$  was found (see Experimental part) indicating an unstable growth [34]. The unstable growth rate in the case

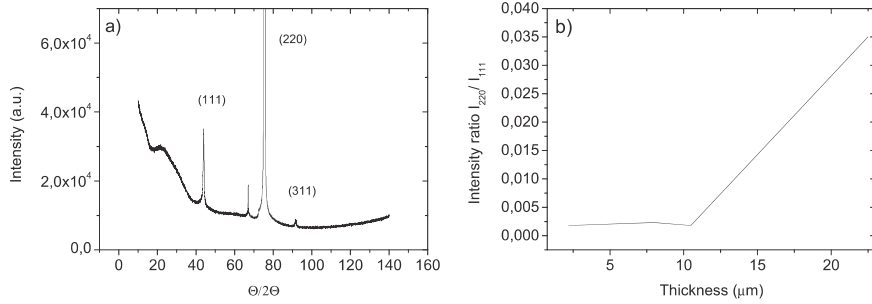


Fig. 5. XRD pattern measured on (a) 22.5 μm thick NCD film grown on the SC(110) diamond and (b) intensity ratio between (220) and (111) XRD reflections for different films.

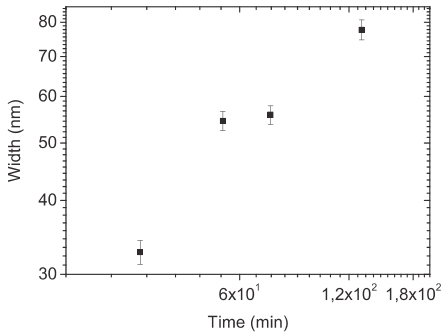


Fig. 6. Interface width  $S_q$  versus deposition time in logarithmic scale.

of growth of NCD on the SC(100) diamond during 3 h of deposition was reported as well [23]. The roughness exponent can be calculated from power spectral density (PSD) function using linear regression method. The value of  $\alpha_s$  changes from 1.5 to 1.6 at the length scale of about 100 nm (Fig. 7a and b) indicating unstable growth as well. At the larger length scale,  $\alpha_s$  changes to 1.0 in case of the 8.0 μm thick film, however no region with  $\alpha_s = 1.0$  was found for the 2.2 μm thick film (Fig. 7a). The region of the PSD curve with  $\alpha_s = 1.0$  can be related with the formation of cauliflower-like structure [24,29] and the length of this region increases with the increase in film thickness. The Raman and XRD measurements revealed alterations in the structure of the films and orientation of diamond crystallites, depending on the film thickness. In conclusion, nonlocal effects like shadowing and diffusional instabilities [32,36,37] and transition from the epitaxial to re-nucleation type of growth determine the NCD films surface morphology.

Finally, it is instructive to compare the growth kinetics of the NCD films prepared on the Si(100) and SC(110) diamond substrates. The

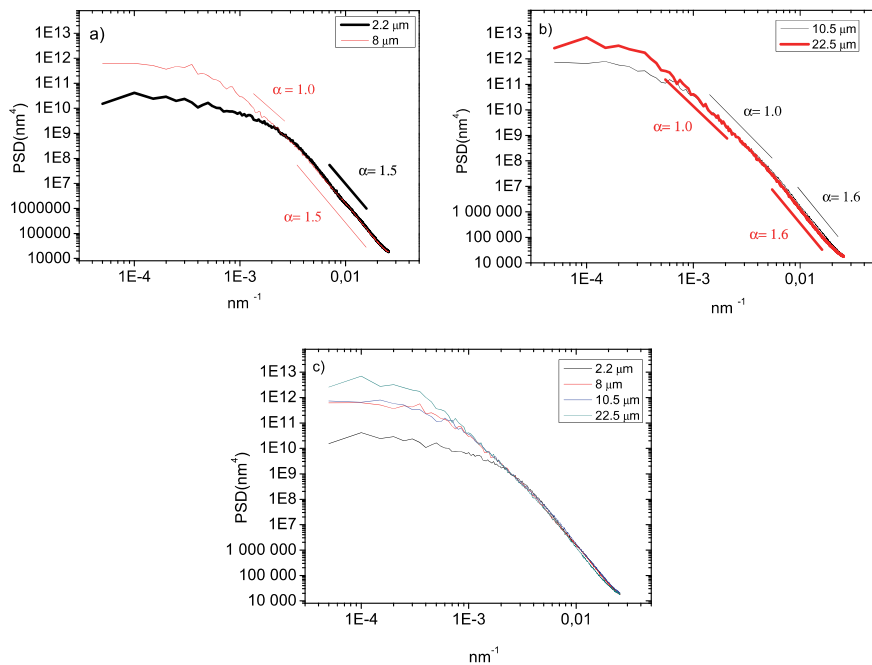


Fig. 7. PSD versus  $k$  for NCD/SC(110) samples: (a) 2.2 and 8 μm, (b) 10.5 and 22.5 μm thick films and (c) collapse of the data shown in (a) and (b).

deposition rate is higher on the SC(110) diamond ( $\sim 0.07\text{--}0.18\ \mu\text{m}/\text{min}$ , see *Experimental part*), than that on Si(100), which was  $\sim 0.03\ \mu\text{m}/\text{min}$  [24]. NCD films deposited on the SC(110) diamond were smoother ( $S_q$  varied between 33 and 78 nm for the 2.5–22.5  $\mu\text{m}$  thick films), than those deposited on Si(100) ( $S_q$  varied between 55 and 99 nm for the 2.7–22  $\mu\text{m}$  thick films) [16,24]. Due to the seeding of Si(100) wafers prior the deposition, the growth of diamond film is precipitated on the seeded diamond grains, which likely leads to the higher surface roughness. Raman and X-ray diffraction measurements confirmed that the structure of the NCD films grown on both types of substrates is relatively similar. The formation of cauliflower-like structure was observed on both types of specimens, this structure can be associated with  $\alpha_s = 1.0$ . In contrast, the KPZ regime of growth was established only on the 22  $\mu\text{m}$  thick film prepared on Si(100), as well as relatively high value of  $\alpha_s$  (within the range 1.5–1.6) was only found for the films grown on SC(110) diamond. Further research is needed to evaluate  $\beta$  and  $z$  exponents in the case of growth NCD films on SC(110) substrates. The cusp-like granular structures with characteristic length of 30–200 and 80–500 nm were found on the NCD/SC(110) and NCD/Si(100) [24] samples, respectively.

### 3.2. Tribological properties characterization

The tribological properties of the NCD films deposited on the SC(110) diamond were investigated in reciprocating sliding tests against  $\text{Si}_3\text{N}_4$  balls and compared with the properties of the NCD films prepared on the Si(100) substrates [16]. Fig. 8 shows COF versus number of cycles curves for the tribological tests taken on the NCD/SC(110) samples (a) and pristine SC(100) diamond (b). The run-in period is shortest for the tests taken on the pristine SC(100) diamond (Fig. 8b), as well as run-in is shorter for the NCD/SC(110) in comparison with the NCD/Si(100) samples [16]. The surface roughness is an important factor influencing friction and wear on diamond films, the friction tests start from higher COF value due to interlocking between asperities on the rubbing surfaces of the counterbodies [43]. Likely, due to smaller roughness of SC(110) diamond surface the run-in period is shortest for these samples, as well as the longest run-in period is for the NCD/Si(100) samples possessing highest roughness. The COF value is smallest for the pristine SC(110) diamond surface, which is equal to 0.12 (Fig. 8b), in contrast to the COF value of 0.14 for the NCD/SC(110) samples (Fig. 8a). The COF value for the NCD/Si(100) samples was also about 0.14 [16], i.e. similar to the COF values observed on the NCD/SC(110) samples. In other words, in spite of the different roughness of NCD films prepared on different substrates no notable difference in COF value for steady state regime of sliding was found. This finding demonstrates that the structures of the NCD films deposited on the different substrates are relatively similar. Noisy COF curves were observed in the tests at low load on the pristine SC(110) diamond, in the tests under higher load the COF curves look smoother (Fig. 8b). The tests

with different loads were carried out on two SC(110) diamond samples. Probably, the hard and soft polishing directions were accidentally selected in tribological tests on different samples [2].

The apparent wear loss volumes measured on the NCD/Si(100) and NCD/SC(110) samples and  $\text{Si}_3\text{N}_4$  balls increases with the increasing of the contact pressure (Fig. 9a,b and d). Fig. 9c shows the average of data presented in Fig. 9a and b with the error bars representing standard deviation. The analysis only apparent wear loss volume (no wear rate) is presented due to expected bending of the diamond films on the Si(100) substrates [16,20]. The wear loss volume on the NCD films increases with increasing of the number of cycles (Fig. 9). However, the wear loss volumes measured on the balls weakly depend on the sliding distance, i.e. do not follow behavior on the respective NCD films (Fig. 9d).

The wear loss volumes measured on the NCD/Si(100) samples are larger than those on the NCD/SC(110) samples under contact pressure equal to 1.4 GPa (Fig. 9c), in spite of possible variation in Hertzian contact pressure due to the film thickness (see *Introduction*). Therefore, the NCD films deposited on the different substrates show different tribological behavior. We believe that the deflection of the NCD films prepared on the Si(100) takes place, thus the wear loss volume can be divided into two parts, due to wear and deflection of the film. Under the load, a stress concentration on a single diamond particle seeded on the Si(100) surface before deposition may result in local fracture of the Si substrate and the NCD film can be impressed into the substrate [20]. Worth to mention that the wear loss volumes measured on the pristine SC(100) diamond and NCD/SC(110) samples are similar (Fig. 9b and c), therefore no deflection is expected for the NCD films grown on the SC(110) diamond. The wear loss volumes measured on the  $\text{Si}_3\text{N}_4$  balls are slightly smaller after the tests on the SC(110) diamond in comparison with the NCD/SC(110) samples (Fig. 9d), which can be linked to smaller COF value for the pristine SC(110) diamond (i.e. 0.12) in contrast to 0.14 for the NCD/SC(110) samples.

The wear scars depth profiles are shown in Fig. 10. The relatively smooth and symmetrical profiles were observed for the 2.2–10.5  $\mu\text{m}$  thick NCD films on the SC(110) diamond independent of contact pressure. The characteristic wear scar profiles for 8  $\mu\text{m}$  thick film is shown in Fig. 10a. However, the profile for the 22.5  $\mu\text{m}$  thick film taken after 72,000 cycles is relatively rough and asymmetric including a peak within the wear scar (Fig. 10b). Such profile shape resembles the shape of wear scars profiles observed on the NCD/Si(100) samples [16]. The depth profiles taken on the NCD/Si(100) samples were generally rough and asymmetric often with the peaks formed within the wear scars [16]. The unstable sliding resulting in inhomogeneous wear can be induced due to variation in surface roughness, chemical composition, film/substrate interface structure, etc. [10,16].

The depth profiles observed on the pristine SC(110) diamond surface after the tests with the low load are rough (Fig. 10c), which correlates with the very noisy COF curve (Fig. 8b). However, smoother

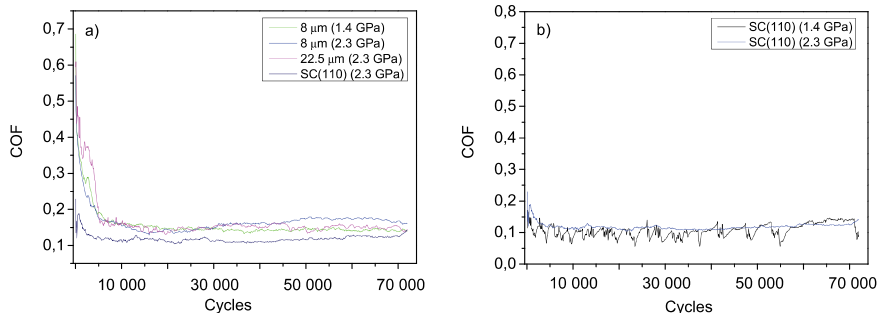
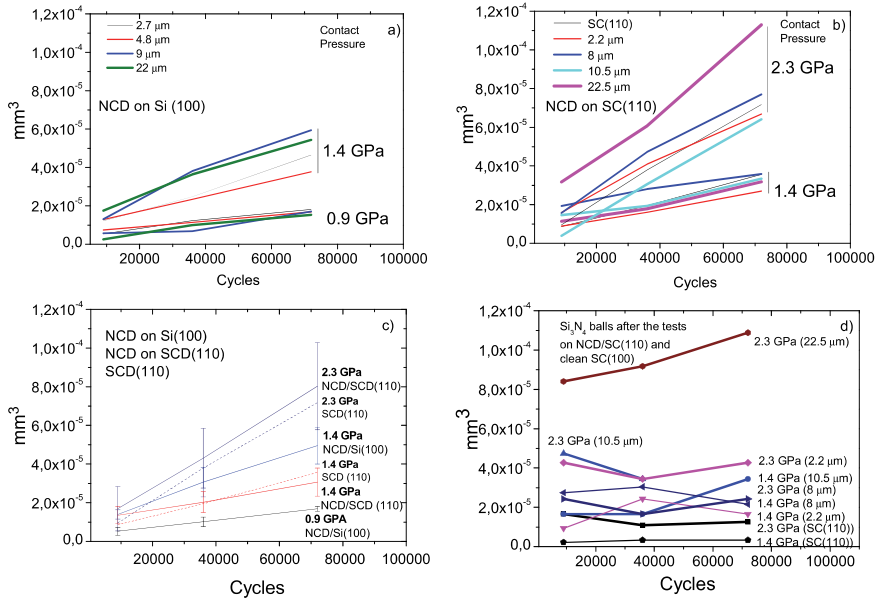


Fig. 8. COF versus number of cycles curves taken on (a) the NCD/SC(110) samples and (b) the pristine SC(110) diamond.



**Fig. 9.** Wear loss volumes measured on the NCD films: (a) NCD/Si(100) from Ref. [16], (b) NCD/SC(110) present study and (c) averaged results shown in (a) and (b) with standard deviation, finally, (d) shows wear volumes measured on the Si<sub>3</sub>N<sub>4</sub> balls.

wear scars profiles were observed after the tests with higher load (Fig. 10d) in agreement with the smoother COF curve (Fig. 8b).

Fig. 11 shows surface morphology of the 8 μm thick NCD film

deposited on the SC(110) diamond after the test with the contact pressure of 2.3 GPa and the sliding distance of 72,000 cycles. The surface morphology is similar to the morphology of the NCD films

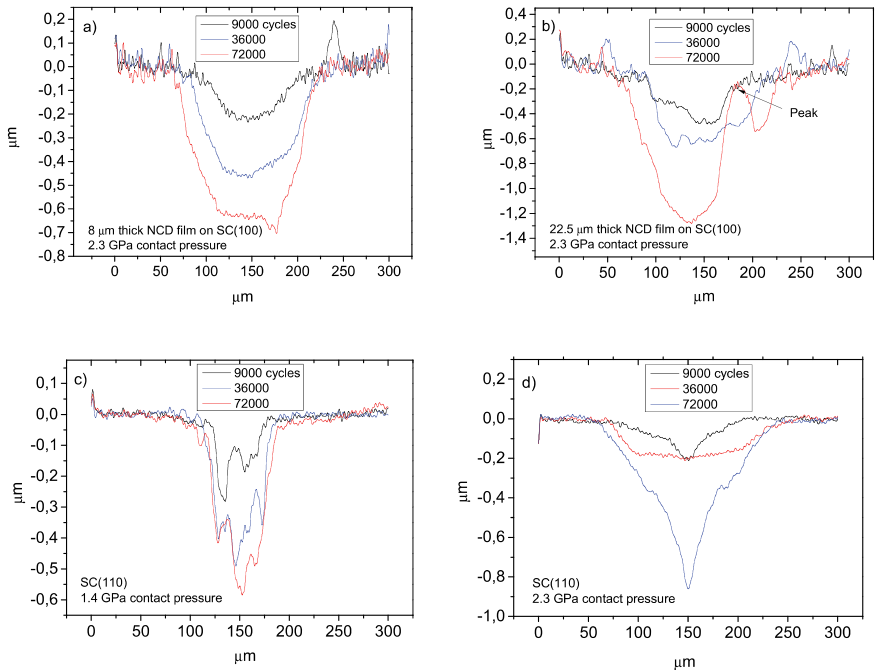


**Fig. 10.** Depth profiles of the wear scars taken after the sliding tests on (a) 8 μm and (b) 22.5 μm thick NCD films prepared on the SC(110) diamond, and (c,d) on the pristine SC(110) diamond.

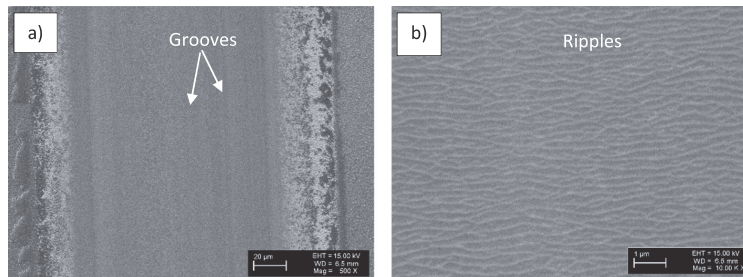


Fig. 11. Morphological peculiarities (a) grooves and (b) ripples observed on the wear scar after the test with contact pressure of 2.3 GPa and distance of 72,000 cycles on the 8 µm thick NCD film prepared on the SC(110) diamond.

prepared on the Si(100) substrates and tested in similar tribological tests, namely transversal ripples and longitudinal grooves can be seen on the wear scar surface [9,16]. The mechanical properties of the counterparts like elastic modulus and fracture strength and structural changes within the amorphous layer formed between the counterparts likely play a key role in the ripple pattern formation under high shear stress [9].

#### 4. Conclusions

The growth dynamics and tribological properties of the NCD films deposited on the SC(110) diamond were compared with the NCD films prepared on the Si(100) substrates. The similarity of chemical composition and crystal structure between the both types of specimens was revealed by Raman and XRD measurements. The growth on SC(110) diamond was unstable, probably due to the fact that the early epitaxial stage of growth follows by re-nucleation type of growth characteristic for NCD films. Shadowing and diffusional instabilities can influence during film growth as well. The COF value equal to 0.14 was found for NCD-Si<sub>3</sub>N<sub>4</sub> tribo-pair, independent of the type of specimens. The apparent wear loss volumes in the case of NCD/SC(110) were smaller than those for NCD/Si(100) samples after the tests with similar contact pressure equal to 1.4 GPa. The wear loss volumes on the NCD/SC(110) samples were compared with ones on the pristine SC(110) diamond after the tests with 1.4 and 2.3 GPa contact pressure. No difference was observed. Therefore, the tribological properties of the NCD films can depend on the substrate and film/substrate interface properties.

#### Prime novelty statement

For the first time the relatively high value of the roughness exponent  $\alpha_s = 1.5\text{--}1.6$  was found on diamond films indicating anomalous scaling. The lower wear volume losses were observed on the NCD/SC(110) in comparison with the NCD/Si(100) samples, thus the influence of substrate and substrate/film interface properties on the tribological behavior of the NCD films can be expected.

#### Acknowledgments

This study was financially supported by the Estonian Ministry of Education and Research under financing projects PUT 1369, IUT 19-28, IUT19-4 and by the European Regional Development Fund project TK141 “Advanced materials and high-technology devices for energy recuperation systems”.

#### References

- [1] J.R. Hird, J.E. Field, Diamond polishing, *Proc. R. Soc. Lond. A* 460 (2004) 3547–3568.
- [2] S.E. Grillo, J.E. Field, F.M. Van Bouwelen, Diamond polishing: the dependency of friction and wear on load and crystal orientation, *J. Phys. D* 33 (2000) 1–6.
- [3] A. Erdemir, C. Donnet, Tribology of diamond, diamond-like carbon, and related films, in: B. Bhushan (Ed.), *Modern Tribology Handbook*, 2 (24) CRC Press LLC, Boca Raton, 2001, pp. 871–909.
- [4] B. Bhushan, V.V. Subramanian, A. Malshe, B.K. Gupta, J. Ruan, Tribological properties of polished diamond films, *J. Appl. Phys.* 74 (6) (1993) 4174–4180.
- [5] A.R. Konicek, D.S. Grierson, A.V. Sumant, T.A. Friedmann, J.P. Sullivan, P.U.P.A. Gilbert, W.G. Sawyer, R.W. Carpick, Influence of surface passivation on the friction and wear behavior of ultrananocrystalline diamond and tetrahedral amorphous carbon thin films, *Phys. Rev. B* 85 (2012) 155448–1–155448-13.
- [6] W. Qin, W. Yue, C. Wang, Understanding integrated effects of humidity and interfacial transfer film formation on tribological behaviors of sintered polycrystalline diamond, *RSC Adv.* 5 (2015) 53484–53496.
- [7] R.R. Chromik, A.L. Winfrey, J. Lüning, R.J. Nemanich, K.J. Wahl, Run-in behavior of nanocrystalline diamond coatings studied by in situ tribometry, *Wear* 265 (2008) 477–489.
- [8] L. Pastewka, S. Moser, P. Gumbsch, M. Moseler, Anisotropic mechanical amorphization drives wear in diamond, *Nat. Mater.* 10 (2011) 34–38.
- [9] V. Podgursky, T. Hantschel, A. Bogatov, E. Kimmari, M. Antonov, M. Viljus, V. Mikli, M. Tsigkourakos, W. Vandevorst, J.G. Buijnsters, A.T. Raadik, P. Kulu, Rippling on wear scar surfaces of nanocrystalline diamond films after reciprocating sliding against ceramic balls, *Tribol. Lett.* 55 (2014) 493–503.
- [10] V. Podgursky, A. Bogatov, M. Yashin, S. Sobolev, I.S. Gershman, Relation between self-organization and wear mechanisms of diamond films, *Entropy* 20 (2018) 279–295.
- [11] K. Holmberg, H. Ronkainen, A. Laukkanen, K. Wallin, Friction and wear of coated surfaces - scales, modeling and simulation of tribomechanisms, *Surf. Coat. Technol.* 202 (2007) 1034–1049.
- [12] H. Ronkainen, J. Koskinen, S. Varjus, K. Holmberg, Load-carrying capacity evaluation of coating/substrate systems for hydrogen-free and hydrogenated diamond-like carbon films, *Tribol. Lett.* 6 (1999) 63–73.
- [13] M. Yashin, A. Bogatov, V. Podgursky, Comparative analysis of wear rates of microcrystalline diamond and diamond-like carbon coatings deposited on WC-Co substrates, *Key Eng. Mater.* 721 (2017) 436–440.
- [14] T. Bell, H. Dong, Y. Sun, Realising the potential of duplex surface engineering, *Tribol. Int.* 31 (1998) 127–137.
- [15] A.F. Yetim, A. Celik, A. Alasaran, Improving tribological properties of Ti<sub>6</sub>Al<sub>4</sub>V alloy with duplex surface treatment, *Surf. Coat. Technol.* 205 (2010) 320–324.
- [16] V. Podgursky, A. Bogatov, S. Sobolev, M. Viljus, V. Sedov, E. Ashkinazi, V. Ralchenko, Effect of nanocrystalline diamond films deflection on wear observed in reciprocating sliding tests, *J. Coat. Sci. Technol.* 3 (2016) 109–115.
- [17] A.N. Obratzov, P.G. Kopylov, A.L. Chuvilin, N.V. Savenko, Production of single-crystal diamond needles by a combination of CVD growth and thermal oxidation, *Diam. Relat. Mater.* 18 (2009) 1289–1293.
- [18] P. Setasuwon, T. Metanawin, Study of diamond film interface structure and contacting area, *Mater. Res.* 12 (1) (2009) 89–94.
- [19] O.A. Williams, O. Douheret, M. Daenen, K. Haenen, E. Osawa, M. Takahashi, Enhanced diamond nucleation on monodispersed nanocrystalline diamond, *Chem. Phys. Lett.* 445 (2007) 255–258.
- [20] A. Bogatov, M. Yashin, M. Viljus, P. Menezes, V. Podgursky, Comparative analysis of two methods for evaluating wear rate of nanocrystalline diamond films, *Key Eng. Mater.* 721 (2017) 345–350.
- [21] M. Nosonovsky, B. Bhushan, Multiscale Dissipative Mechanisms and Hierarchical Surfaces Friction, Superhydrophobicity and Biomimetics, Springer, Berlin/Heidelberg, Germany, 2008, pp. 13–47.
- [22] E.E. Ashkinazi, R.A. Khmelitskii, V.S. Sedov, A.A. Khomich, A.V. Khomich, V.G. Ralchenko, Morphology of diamond layers grown on different facets of single crystal diamond substrates by a microwave plasma CVD in CH<sub>4</sub>-H<sub>2</sub>-N<sub>2</sub> gas mixtures, *Crystals* 7 (2017) 166.
- [23] S.L. Moore, G.K. Samudrala, S.A. Catledge, Y.K. Vohra, Rapid growth of nanocrystalline diamond on single crystal diamond for studies on materials under extreme conditions, *Sci. Rep.* 8 (2018) 1402.
- [24] V. Podgursky, A. Bogatov, V. Sedov, I. Sildos, A. Mere, M. Viljus, J.G. Buijnsters, V. Ralchenko, Growth dynamics of nanocrystalline diamond films produced by microwave plasma enhanced chemical vapor deposition in methane/hydrogen/air

- mixture: scaling analysis of surface morphology, *Diam. Relat. Mater.* 58 (2015) 172–179.
- [25] J.G. Buijnsters, L. Vazquez, Growth dynamics of nanocrystalline diamond films deposited by hot filament chemical vapor deposition: influence of low sticking and renucleation processes, *J. Phys. Chem. C* 115 (2011) 9681–9691.
- [26] M.C. Salvadori, M.G. Silveira, M. Cattani, Roughness and critical exponents analysis of diamond films by AFM imaging, *Thin Solid Films* 354 (1999) 1–4.
- [27] A.-L. Barabasi, H.E. Stanley, *Fractal Concepts in Surface Growth*, Cambridge University Press, Cambridge, 1995.
- [28] R. Cuerno, M. Castro, Transients due to instabilities hinder Kardar-Parisi-Zhang Scaling: a unified derivation for surface growth by electrochemical and chemical vapor deposition, *Phys. Rev. Lett.* 87 (23) (2001) 236103-1–236103-4.
- [29] P.A. Orrillo, S.N. Santalla, R. Cuerno, L. Vázquez, S.B. Ribotta, L.M. Gassa, F.J. Mompean, R.C. Salvarezza, M.E. Vela, Morphological stabilization and KPZ scaling by electrochemically induced co-deposition of nanostructured NiW alloy films, *Sci. Rep.* 7 (2017) 17997.
- [30] J.J. Ramasco, J.M. López, M.A. Rodríguez, Generic dynamic scaling in kinetic roughening, *Phys. Rev. Lett.* 84 (10) (2000) 2199–2202.
- [31] K. Sneppen, Self-organized pinning and interface growth in a random medium, *Phys. Rev. Lett.* 69 (24) (1992) 3539–3542.
- [32] B.C. Mohanty, H.R. Choi, Y.S. Cho, Fluctuations in global surface scaling behavior in sputter-deposited ZnO thin films, *Europhys. Lett.* 93 (2011) 26003-p1–26003-p6.
- [33] M. Nicoli, R. Cuerno, M. Castro, Unstable nonlocal interface dynamics, *Phys. Rev. Lett.* 102 (2009) 256102-1–256102-4.
- [34] M. Nicoli, M. Castro, R. Cuerno, Unified moving-boundary model with fluctuations for unstable diffusive growth, *Phys. Rev. E* 78 (2008) 021601-1–021601-17.
- [35] D. Beringer, W.M. Roach, C. Clavero, R.A. Lukaszew, Anomalous morphological scaling in epitaxial niobium thin films on MgO (001), *Proceedings of SRF2011*, 2011, pp. 883–885.
- [36] M.A. Auger, L. Vázquez, R. Cuerno, M. Castro, M. Jergel, O. Sánchez, Intrinsic anomalous surface roughening of TiN films deposited by reactive sputtering, *Phys. Rev. B* 73 (2006) 045436-1–045436-7.
- [37] J.M. Lopez, M. Castro, R. Gallego, Scaling of local slopes, conservation laws, and anomalous roughening in surface growth, *Phys. Rev. Lett.* 94 (2005) 166103-1–166103-4.
- [38] E.J. Boyd, D. Uttamchandani, Measurement of the anisotropy of Young's modulus in single-crystal silicon, *J. Microelectromech. Syst.* 21 (1) (2012) 243–249.
- [39] L. Gan, B. Ben-Nissan, A. Ben-David, Modelling and finite element analysis of ultramicrohardness indentation of thin films, *Thin Solid Films* 290–291 (1996) 362–366.
- [40] B. Bhushan, X. Li, Micromechanical and tribological characterization of doped single-crystal silicon and polysilicon films for microelectromechanical systems devices, *J. Mater. Res.* 12 (1) (1997) 54–63.
- [41] F. Ericson, J.-A. Schweitz, Micromechanical fracture strength of silicon, *J. Appl. Phys.* 68 (1990) 5840–5844.
- [42] A. Erdemir, M. Halter, G.R. Fenske, C. Zuiker, R. Csencsits, A.R. Krauss, D.M. Gruen, Friction and wear mechanisms of smooth diamond films during sliding in air and dry nitrogen, *Tribol. Trans.* 40 (1997) 667–675.
- [43] R. Rami, N. Kumar, A.T. Kozakov, K.A. Googlev, K.J. Sankaran, P. Kr, S. Das, A.K. Tyagi Dash, I-Nan Lin, Superlubrication properties of ultrananocrystalline diamond film sliding against a zirconia ball, *RSC Adv.* 5 (2015) 100663–100673.



**Publication IV**

**M. Yashin;** J. Baronins; P. Menezes; M. Viljus; T. Raadik; A. Bogatov; M. Antonov; V. Podgursky, Wear Rate of Nanocrystalline Diamond Coating under High Temperature Sliding Conditions. *Solid State Phenomena*, 267 (2017) 219–223.



## **Wear Rate of Nanocrystalline Diamond Coating under High Temperature Sliding Conditions**

Maxim Yashin<sup>1,a\*</sup>, Janis Baronins<sup>1,b</sup>, Pradeep L. Menezes<sup>2,c</sup>, Mart Viljus<sup>1,d</sup>,  
Taavi Raadik<sup>3,e</sup>, Andrei Bogatov<sup>1,f</sup>, Maksim Antonov<sup>1,g</sup>  
and Vitali Podgursky<sup>1,h</sup>

<sup>1</sup>Tallinn University of Technology, Department of Mechanical and Industrial Engineering,  
19086 Tallinn, Estonia

<sup>2</sup>University of Nevada Reno, Department of Mechanical Engineering, Reno, NV 89557, USA

<sup>3</sup>Tallinn University of Technology, Department of Materials and Environmental Technology,  
19086 Tallinn, Estonia

<sup>a</sup>maysh@ttu.ee, <sup>b</sup>jbaronins@gmail.com, <sup>c</sup>pmenezes@unr.edu, <sup>d</sup>mart.viljus@ttu.ee,  
<sup>e</sup>taavi.raadik@ttu.ee, <sup>f</sup>andrei.bogatov@mail.ru, <sup>g</sup>maksim.antonov@ttu.ee, <sup>h</sup>vitali.podgurski@ttu.ee

**Keywords:** NCD; high temperature; wear rate; tribology.

**Abstract.** The present study deals with the tribological behavior of nanocrystalline diamond (NCD) coatings under high temperature sliding conditions. The NCD coatings were grown by plasma enhanced chemical vapor deposition (PECVD) method on hard metal (WC-Co) substrates. Friction and wear tests were performed on ball-on-disc tribometer using a high-temperature chamber with a rotary drive. The tests were carried out at room temperature, 300, 450 and 600 °C. Scanning electron microscopy (SEM), optical microscopy, mechanical profilometry and Raman spectrometry were used for investigation of the morphology and the chemical composition of the wear scars and the pristine surface. The depth and width of the wear scars measured after the high temperature sliding tests are larger in comparison with room temperature tests. It was observed that coefficient of friction (COF) increased with increasing temperature. The wear rate of NCD coatings tested at 300–450 °C was about 10 times higher than that at room temperature. The mechanisms responsible for these variations are discussed.

### **Introduction**

Diamond coatings have a wide range of tribological applications due to high Young's modulus and hardness [1]. Different types of diamond coatings are used for protection of cutting tools in engineering and mining industry [2].

High temperature wear resistance is important for cutting tools. Therefore, the study of tribological behavior of diamond coatings at high temperatures is of special interest. Hard metal (WC-Co) is widely used as material for manufacturing of cutting tools, thus WC-Co plates were selected as a substrate for deposition of nanocrystalline diamond (NCD) coatings.

The reported values of coefficient of friction (COF) of NCD coatings were 0.2 and 0.4 in sliding tests at 200 and 500 °C, respectively [3]. Oxidation and structural phase transformation of NCD coatings were observed in sliding tests at temperatures between 627–1000 °C [4,5].

The main goal of the present study is the investigation of wear of NCD coating at high temperature under dry unidirectional sliding conditions.

### **Experimental**

Hard metal substrates were cleaned by sandblasting and polished on grinding machine (Buehler PHOENIX® 4000) to the average roughness  $R_a < 0.05 \mu\text{m}$ . Polished substrates were cleaned in an ultrasonic bath with acetone and alcohol. Initially, CrN coating was deposited using physical vapor deposition (PVD) method for better adhesion of the NCD coating. The NCD coating (3 samples)

was grown using plasma enhanced chemical vapor deposition (PECVD) method (PECVD UPISA-100 unit). The thickness of CrN and NCD coatings was 2  $\mu\text{m}$  and 3 – 5  $\mu\text{m}$ , respectively.

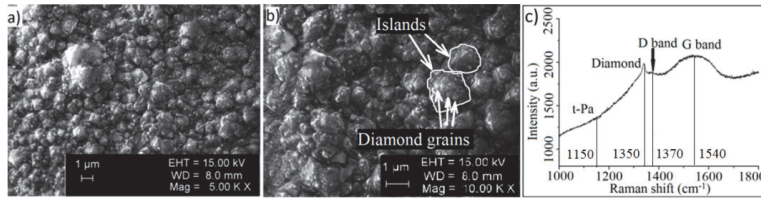


Fig. 1. SEM image of surface morphology (a, b) and Raman spectrum (c) of the NCD coating

The tribological behavior of the NCD coating during sliding tests was estimated using a ball-on-disk tribometer (Bruker® CETR UMT-2), equipped with a high-temperature chamber with rotary drive (S21ME-1000).  $\text{Si}_3\text{N}_4$  ball was selected as a counter body, as it possesses good high temperature resistance and high hardness [6]. The sliding tests were carried out at room temperature on three samples. After that, the first sample was tested at 300 °C, the second at 450 °C and the third at 600 °C. For each condition, the experiments were repeated three times at different places on each sample. Test conditions were as follows: normal load 10 N, rotation speed 300 rpm, sliding track diameter 3 mm and tests duration 3 hours. The structure of the NCD coating was characterized by Raman spectroscopy (Horiba® LabRam HR 800) before and after the test on the pristine surface and within the wear scars after each test. The surface morphology and roughness of the NCD coating was characterized by optical microscopy, scanning electron microscopy (SEM) (TM-1000 HITACHI®) and mechanical profilometry (Mahr Perthometer® equipped with PGK 120 tracing arm). Five line scans were taken across each wear scar, and the averaged line scan was calculated. A volume of wear scar was estimated using Eq. 1, where the cross-section area is  $S$  and the wear scar length is  $l$ .

$$V = S \times l \quad (1)$$

The wear rate was estimated using Eq. 2, where  $V$  is the volume of wear scar,  $F$  is normal load and  $L$  is sliding distance.

$$W = V / (F \times L) \quad (2)$$

The average wear rate with the corresponding standard deviation for each temperature was calculated using results of three repeated tests carried out at the same temperature.

## Results and Discussion

Fig. 1 a and b shows the surface morphology of NCD coatings at different magnifications. The NCD coating has cauliflower-like morphology. The diamond grains size is about 0.1 – 0.15  $\mu\text{m}$ . The size of islands is about 1 – 2  $\mu\text{m}$ . The average roughness  $R_a$  of surface is 0.22  $\mu\text{m}$ . It should be noted, that the structure of obtained diamond coating can be characterized as transition structure between MCD (microcrystalline diamond) and NCD.

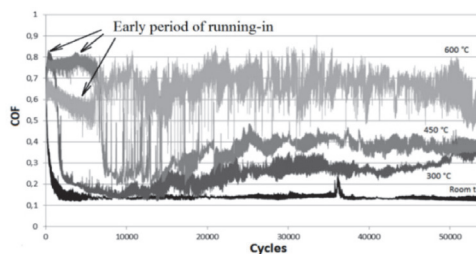


Fig. 2. COF versus number of cycles recorded on the NCD coating at room and elevated temperatures

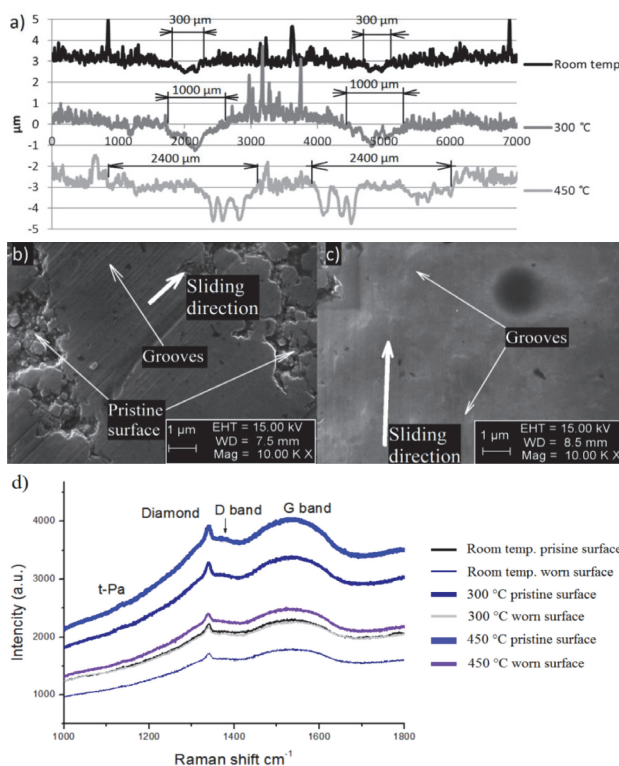


Fig. 3. Line scans taken on wear scars (a), SEM images of wear scars after the tests at room temperature (b) and 300 °C (c), and Raman spectra of the wear scars after the tests at room temperature, 300 and 450 °C (d)

By definition, the roughness  $R_a$  and diamond grains size of the MCD coatings is 0.4 – 1 and 0.5 – 10 μm respectively, and the values of the same parameters for NCD coatings are typically 0.05 – 0.1 and 0.05 – 0.1 μm [7]. In this research NCD notation is used because cauliflower-like morphology is a very characteristic property of NCD coatings [8]. The Raman spectrum is shown in Fig. 1 c.

The peak at 1150 cm<sup>-1</sup> corresponds to t-Pa (trans-polyacetylene at the grain boundaries) and one at 1350 cm<sup>-1</sup> to diamond. The peaks at 1370 cm<sup>-1</sup> and 1540 cm<sup>-1</sup> correspond to D band (disordered graphite) and G band (well-ordered graphite), respectively [9]. The height and shape of diamond peak can be an additional confirmation of the transition structure of obtained coatings, if compared with the diamond peak corresponding to NCD [10] and MCD [11] coatings.

Fig. 2 shows COF versus number of cycles curves recorded during wear tests at room temperature, 300, 450 and 600 °C. For the early period of running-in for all tests, COF is equal to about 0.8.

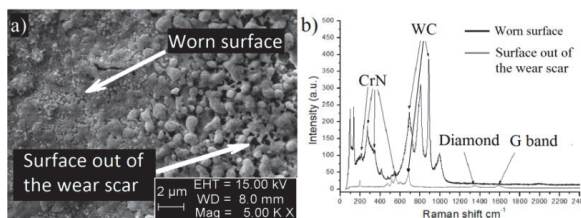


Fig. 4. Surface morphology (a) and Raman spectra (b) of NCD coating after the test at 600 °C

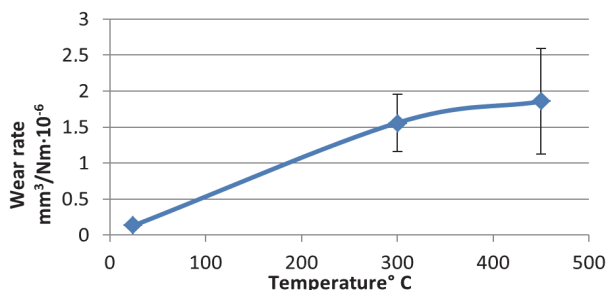


Fig. 5. Average value of wear rates versus temperature of NCD coatings. Standard deviation is shown on the graph

After this period, COF value recorded at room temperature, 300 and 450 °C decreases to 0.13, 0.15 and 0.2, respectively. COF for the test at room temperature stabilizes at 0.13, but at 300 and 450 °C, the COF increases after 15000 cycles and stabilize at 0.3 and 0.4, respectively. These results are in good agreement with another study [3]. The duration of the early period of running-in varies depending on temperature, it increases with increase of temperature. The highest COF value of 0.7 was observed for sliding at 600 °C. Noise curves can be seen in Fig. 2, however, amplitude of noise increases with increasing of temperature.

The line scans were taken on the wear scars (Fig. 3 a). The averaged depth and width of the wear scar after the test at room temperature is 0.35 and 300  $\mu\text{m}$ , respectively. Fig. 3 b shows the surface morphology of NCD coating after the sliding test at room temperature. Concentric grooves can be observed on the wear surface. Islands of pristine surface can be seen as well. Wear scars after the sliding tests at 300 °C have a larger depth and width, than that of the tests at room temperature 1.5 and 1000  $\mu\text{m}$ . The SEM image was taken after sliding test at 300 °C (Fig. 3 c). The grooves are less visible than after sliding at room temperature. The pristine surface is not observed. The wear track after sliding test at 450 °C has the depth and width of 2 and 2400  $\mu\text{m}$ , respectively. The surface morphology was similar to the wear scar after the test at 300 °C (not shown). Raman spectra taken on the wear scars and pristine surface are shown in Fig. 3 d. A height, position and shape of the peaks did not strongly change under the influence of high temperature.

A significant difference in tribological behavior was observed after the test at 600 °C. The surface morphology within and out of wear scar can be seen in Fig. 4 a. Depth of wear scar was about 7.5  $\mu\text{m}$  (not shown). The roughness  $R_a$  of the surface located out of wear scar was about 0.11  $\mu\text{m}$ , i.e. the NCD surface becomes smoother after heating up to 600 °C. Raman spectra was taken after the test at 600 °C (Fig. 4 b). The spectrum of worn surface of NCD coating has several peaks: the peaks at 215, 267, 284 and 586  $\text{cm}^{-1}$  correspond to CrN [12] and at 688 and 885  $\text{cm}^{-1}$  to WC [13]. The Raman spectrum of the surface out of wear scar has the same peaks at 215 (CrN), 586 (CrN) and 688  $\text{cm}^{-1}$  (WC), and two additional peaks at 1350 and at 1540  $\text{cm}^{-1}$  corresponding to diamond and to G band, respectively. In other words, the NCD coating was worn away in area of wear scar, and pristine NCD coating undergone structural phase transformation.

Evolution of wear rates versus temperature is shown in Fig. 5. Wear rate can be estimated only for the tests carried out at room temperature, 300 and 450 °C, as the NCD coating was worn away during the test at 600 °C. The wear rate at room temperature is about 10 times lower than that for tests at higher temperatures. Standard deviations were calculated for tests carried out at different temperatures (Fig. 5). Standard deviation of wear rate is increased with increase of temperature, indicating higher variation of results, probably, due to increased vibrations during sliding (it can be seen in Fig. 2).

## Summary

NCD coating was investigated at different temperatures in sliding tests. Strong phase transformation of the surface was observed after the test at 600 °C. The COF and size of wear scars increased with increase of temperature. The wear resistance of NCD coatings at 300 – 450 °C was about 10 times lower than at room temperature. However, no significant structural transformations of NCD coating were observed in Raman spectra after the tests at 300 – 450 °C. Explanation of such behavior is a challenge for the next studies.

## Acknowledgments

This study was financially supported by the Estonian Ministry of Education and Research under target financing project IUT 19-29.

## References

- [1] L. Pastewka, S. Moser, P. Gumbsch, M. Mosler, Anisotropic mechanical amorphization drives wear in diamond, *Nature Materials* 10 (2011) 34-38.
- [2] I. Reineck, M.E. Sjöstrand, Diamond coated cutting tools, *International Journal of Refractory Metals and Hard Materials* 14 (1996) 187-193.
- [3] Y. Qiao, X. Sun, B. Xu, S. Ma, High temperature tribological behaviors of nano-diamond as oil additive, *Journal of Central South University of Technology* 12 (2005) 181-184.
- [4] A.P. Semenov, M.M. Khrushchov, Influence of environment and temperature on tribological behavior of diamond and diamond-like coatings, *Journal of Friction and Wear* 31 (2010) 195-218.
- [5] S. Shimada, H. Tanaka, M. Higuchi, T. Yamaguchi, S. Honda, K. Obata, Thermo-chemical wear mechanism of diamond tool in machining of ferrous metals, *CIRP Annals – Manufacturing Technology* 53 (2004) 57-60.
- [6] R.A. Andrievskii, Silicon nitride: synthesis and properties, *Russian Chemical Reviews* 64 (1995) 291-308.
- [7] A.R. Krauss, O. Auciello, D.M. Gruen, A. Jayatiss, A. Sumant, J. Tucek, D.C. Mancini, N. Moldovan, A. Erdemir, D. Ersoy, M.N. Gardose, H.G. Busmann, E.M. Meyer, M.Q. Ding, Ultrananocrystalline diamond thin films for MEMS and moving mechanical assembly devices, *Diamond and Related Materials* 10 (2001) 1952-1961.
- [8] M. Marton, T. Izak, M. Vesely, M. Vojs, M. Michalka, J. Bruncko, Effect of argon and substrate bias on diamond thin film surface morphology, *Vacuum* 82 (2008) 154-157.
- [9] A.C. Ferrari, J. Robertson, Resonant Raman spectroscopy of disordered, amorphous, and diamond like carbon, *Physical Review B* 64 (2001) 075414-1 – 075414-13.
- [10] V. Podgursky, A. Bogatov, V. Sedov, I. Sildos, A. Mere, M. Viljus, J.G. Buijnsters, V. Ralchenko, Growth dynamics of nanocrystalline diamond films produced by microwave plasma enhanced chemical vapor deposition in methane/hydrogen/air mixture: Scaling analysis of surface morphology, *Diamond & Related Materials* 58 (2015) 172-179.
- [11] A. Bogatov, R. Traksmaa, V. Podgursky, Changes in surface morphology, deflection and wear of microcrystalline diamond film observed during sliding tests against Si<sub>3</sub>N<sub>4</sub> balls, *Key Engineering Materials* 674 (2016) 145-151.
- [12] A. Barata, L. Cunha, C. Moura, Characterisation of chromium nitride films produced by PVD techniques, *Thin Solid Films* 398-399 (2001) 501-506.
- [13] M. Uysal, H. Akbulut, M. Tokur, H. Algül, T. Çetinkaya, Structural and sliding wear properties of Ag/Graphene/WC hybrid nanocomposites produced by electroless Co-deposition, *Journal of Alloys and Compounds* 654 (2016) 185-195.

# Curriculum vitae

## Personal data

Name: Maxim Yashin  
Date of birth: 9.08.1992  
Place of birth: Moscow  
Citizenship: Russian

## Contact data

E-mail: mayash@taltech.ee

## Education

2015–2019 Tallinn University of Technology, PhD  
2009–2015 Bauman Moscow State Technical University, Specialist  
2002–2009 State educational institution of secondary school № 283

## Language competence

Russian – Native  
English – Fluent

## Professional employment

2013–2015 Open Joint Stock Company "Moscow Mechanical Plant Avangard"

## Projects in progress

IUT19-29 "Multi-scale structured ceramic-based composites for extreme applications (1.01.2014–31.12.2019)", Jakob Kübarsepp, Tallinn University of Technology, Faculty of Mechanical Engineering, Tallinn University of Technology, School of Engineering, Department of Mechanical and Industrial Engineering.

PUT1369 "Adaptation mechanisms of diamond films in dry sliding wear (1.01.2017–31.12.2020)", Vitali Podgurski, Tallinn University of Technology, School of Engineering, Department of Mechanical and Industrial Engineering.

## Industrial property

Invention: Method to protect diamond films at high temperature to preserve tribological properties; Owners: Tallinn University of Technology, University of Tartu; Authors: Vitali Podgurski, Andrei Bogatov, Maxim Yashin, Heinar Vagiström, Taivo Jõgiaas; Priority number: P201900008; Priority date: 26.02.2019.

## Elulookirjeldus

### Isikuandmed

Nimi: Maxim Yashin  
Sünniaeg: 9.08.1992  
Sünnikoht: Moskva  
Kodakondsus: Venemaa

### Kontaktandmed

E-post: mayash@taltech.ee

### Hariduskäik

2015–2019 Tallinna Tehnikaülikool, PhD  
2009–2015 Baumani-nimeline Moskva Riiklik Tehnikaülikool, Spetsialist  
2002–2009 Keskkooli riiklik õppeasutus № 283

### Keelteoskus

Vene keel – Emakeel  
Inglise keel – Kõrgtase

### Teenistuskäik

2013–2015 Avatud aktsiaselts "Moskva mehaaniline tehas Avangard"

### Projektid

IUT19-29 "Mitmeastmeliselt struktureeritud keraamika-baasil komposiitmaterjalid kasutamiseks ekstreemtingimustes (1.01.2014–31.12.2019)", Jakob Kübarsepp, Tallinna Tehnikaülikool, Mehaanikateaduskond, Tallinna Tehnikaülikool, Inseneriteaduskond, Mehaanika ja tööstustehnika instituut.

PUT1369 "Teemantpinnete adaptatsioonimehhanismid kuiv hõõrdekulumise (1.01.2017–31.12.2020)", Vitali Podgurski, Tallinna Tehnikaülikool, Inseneriteaduskond, Mehaanika ja tööstustehnika instituut .

### Tööstusomand

Patentne leiutis: Teemantpinde triboloogiliste omaduste parandamine kõrgel temperatuuril õhu käes; Omanikud: Tallinna Tehnikaülikool, Tartu Ülikool; Autorid: Vitali Podgurski, Andrei Bogatov, Maxim Yashin, Heinar Vagiström, Taivo Jõgiaas; Prioriteedi number: P201900008; Prioriteedi kuupäev: 26.02.2019.